2022

ELUCIDATING THE ROLE OF POLYCOMB REPRESSIVE COMPLEX 2 IN LUNG STEM CELL FATE AND LUNG DISEASE

Aria Byrd
University of Kentucky, aby224@g.uky.edu
Author ORCID Identifier:
https://orcid.org/0000-0002-0681-0384
Digital Object Identifier: https://doi.org/10.13023/etd.2022.212

STUDENT AGREEMENT:

I represent that my thesis or dissertation and abstract are my original work. Proper attribution has been given to all outside sources. I understand that I am solely responsible for obtaining any needed copyright permissions. I have obtained needed written permission statement(s) from the owner(s) of each third-party copyrighted matter to be included in my work, allowing electronic distribution (if such use is not permitted by the fair use doctrine) which will be submitted to UKnowledge as Additional File.

I hereby grant to The University of Kentucky and its agents the irrevocable, non-exclusive, and royalty-free license to archive and make accessible my work in whole or in part in all forms of media, now or hereafter known. I agree that the document mentioned above may be made available immediately for worldwide access unless an embargo applies.

I retain all other ownership rights to the copyright of my work. I also retain the right to use in future works (such as articles or books) all or part of my work. I understand that I am free to register the copyright to my work.

REVIEW, APPROVAL AND ACCEPTANCE

The document mentioned above has been reviewed and accepted by the student's advisor, on behalf of the advisory committee, and by the Director of Graduate Studies (DGS), on behalf of the program; we verify that this is the final, approved version of the student's thesis including all changes required by the advisory committee. The undersigned agree to abide by the statements above.

Aria Byrd, Student

Christine F. Brainson, Major Professor

Isabel Mellon, Director of Graduate Studies

ELUCIDATING THE ROLE OF POLYCOMB REPRESSIVE COMPLEX 2 IN LUNG STEM CELL FATE AND LUNG DISEASE

DISSERTATION

A dissertation submitted in partial fulfillment of the requirements for the degree of Doctor of Philosophy in the College of Medicine
at the University of Kentucky

By
Aria Lynn Byrd
Lexington, Kentucky
Director: Dr. Christine Fillmore Brainson, Professor of Toxicology and Cancer Biology
Lexington, Kentucky
2022

ABSTRACT OF DISSERTATION

ELUCIDATING THE ROLE OF POLYCOMB REPRESSIVE COMPLEX 2 IN LUNG STEM CELL FATE AND LUNG DISEASE

The average human lungs take ~22,000 breaths and inhale ~2,000 gallons of air each day. This organ is the primary conduit for the transfer of oxygen to the internal organs, making it crucial for the sustainment of life. Consequently, mechanical malfunction of the lungs and/or pollution of inhaled air negatively impact internal organ function and ultimately put survival in jeopardy. Epigenetics, by nature, is a plastic phenomenon in which environmental stimuli influence short term, long term, and generational gene expression patterns. Chronic exposure of harmful stimuli to the lung epithelium has also been shown to alter epigenetic pathways, engender aberrant lung cell differentiation, and manifest into long term diseases. Chronic Obstructive Pulmonary Disease (COPD) is a progressive, incurable lung disorder that is pathologically rooted in chronic inflammation and aberrant lung cell differentiation. Polycomb Repressive Complex 2 (PRC2) is a key epigenetic regulator of lung stem cell fate during development, but little is understood of its role in adult lung. In the following chapters, I will expound on how I utilized human patient samples, ex vivo lung organoids, and murine in vivo models to better elucidate how PRC2 controls lung cell biology and offer insight into potential therapeutic avenues to combat lung disease. To understand the role of PRC2 in COPD, we first analyzed patient and control lung tissues. Using quantitative immunohistochemistry and immunofluorescence, we observed a very significant decrease in the Polycomb Repressive Complex 2 catalytic mark, histone H3 lysine 27 tri-methylation (H3K27me3) in bronchiolar epithelium of COPD patients. Furthermore, H3K27me3 staining was strongly inversely correlated with markers of basal and goblet cells in patient samples. Next, we developed a new mouse model of conditional deletion of the Polycomb Repressive Complex 2 enzyme, EZH2, and used this model to interrogate lung stem cell function in organoid cultures and in vivo. Single cell RNA-sequencing of organoid cultures revealed the appearance of *Krt17*-negative basal cells and loss of the newly identified *Krt8*-positive progenitor cells in Ezh2-null cultures. Gene signatures associated with immune response were increased is Ezh2-heterozygous cultures, and genes enriched in EZH2 deficient organoids were enriched in human emphysemic lung. Furthermore, when we used this *Ezh2* conditional knock-out mouse to interrogate the role of EZH2 in lung homeostasis and allergen response in vivo, we found that Ezh2-heterozygous mice had increased response to ovalbumin allergen and showed hallmarks of COPD including bronchiolar epithelial thickening and club to goblet cell transdifferentiation. Lastly, we sought to learn the mechanism of decreased PRC2 activity in COPD patients. We used human bronchiolar epithelial cells to interrogate the role of the redox-sensitive enzyme, cystathionine beta synthase (CBS), in controlling EZH2 levels and gene expression modulation. In the patient samples, we found that CBS was significantly higher in COPD lung. Excitingly, we identified shared transcriptional profiles between human bronchiolar epithelial cells that over-express CBS and mouse organoids with *Ezh2* loss, offering insight into how redox stress may drive aberrant epigenetic reprogramming. Taken together, these findings suggests that PRC2 is integral to facilitating proper lung stem cell differentiation in adult humans and mice.

KEYWORDS
Epigenetics, COPD, PRC2, EZH2, H3K27me3, CBS

Aria Lynn Byrd

04/13/2022

ELUCIDATING THE ROLE OF POLYCOMB REPRESSIVE COMPLEX 2 IN LUNG STEM CELL FATE AND LUNG DISEASE

By
Aria Lynn Byrd

Dr. Christine Fillmore Brainson
Director of Dissertation

Dr. Isabel Mellon
Director of Graduate Studies

04/13/2022
Date

DEDICATION

This work is firstly dedicated to my mother and late father, Veronica Lynn and Thomas Jefferson Byrd, who have greatly influenced and guided me to chase after my dreams with passion and sincere intention. Secondly, to my siblings Carmen, Desaree, Shannon, Thomas, and Kalah, who have inspired me to embody the legacy of greatness with the same style and fervor that they have. Thirdly, to my lifelong friends, Jasmine T., Jazzmyn C., Sesyli, Jakia, and Trey, whose love and support has sustained me through this long and arduous journey. Finally, to my bonus mom, Hope Thompson, whose endless nurturing has bolstered me throughout my entire post-secondary educational career. It is because of you all that I have arrived at this place of self-actualization, intelligence, and wisdom. I love you

Acknowledgements

This work was supported in part by NCI K22 CA201036, Kentucky Lung Cancer Research Program, V Foundation Scholar Award, American Cancer Society Institutional Research Grant IRG-85-001-25, NIGMS P20 GM121327-03, NCI R01 CA237643, American Cancer Society Research Scholar Grant 133123-RSG-19-081-01-TBG and American Association for Cancer Research-Bayer Innovation and Discovery Grant, Molecular Mechanisms of Toxicity Training Grant T32ES07266, and Ruth L. Kirschstein National Research Service Award (NRSA) 5F31HL151111-02. This research was also supported by the Biostatistics & Bioinformatics Shared Resource Facility, Oncogenomics Shared Resource Facility, Biospecimen Procurement & Translational Pathology Shared Resource Facility and Flow Cytometry & Immune Monitoring Shared Resource Facility of the University of Kentucky Markey Cancer Center (P30CA177558). We thank Donna Gilbreath from the Markey Cancer Center Research Communications Office for assisting with graphic designs.

TABLE OF CONTENTS

LIST OF TABLES

LIST OF FIGURES

LIST OF MANUSCRIPTS

Jian Han, Justin Plummer, Lumei Liu, **Aria Byrd**, Michael Aschner & Keith M. Erikson. (2017). **The impact of obesity on brain iron levels and α-synuclein expression is regionally dependent**. Nutritional Neuroscience, 0,0. PMID: 29034829

Ji Won Park, **Aria Byrd**, Choon-myung Lee, Edward T. Morgan. (2017). **Nitric oxide stimulates cellular degradation of human CYP51A1, the highly conserved lanosterol 14α-demethylase**. Biochemical Journal, 747,19. PMID: 28830911

Liu, L., **Byrd, A**., Plummer, J., Erikson, K. M., Harrison, S. H., & Han, J. (2016). **The Effects of Dietary Fat and Iron Interaction on Brain Regional Iron Contents and Stereotypical Behaviors in Male C57BL/6J Mice**. Frontiers in Nutrition, 3, 20. PMID: 29034829

Fan Chen, Xiulong Song, Tanner J. DuCote, **Aria L. Byrd**, Christine F. Brainson. **EZH2 inhibition confers PIK3CA-driven lung tumors enhanced sensitivity to PI3K inhibition**. Cancer Letters June 2021.

Fan Chen, **Aria L. Byrd**, Jinpeng Liu, Robert M. Flight, Tanner J. DuCote, Xiulong Song, Abigail R. Edgin, Alexsandr Lukyanchuk, Danielle T. Dixon, Stuart H. Orkin, Hunter N.B. Moseley, Chi Wang, Christine F. Brainson. **–Polycomb Deficiency Drives a FOXP2-high Metastatic State Targetable by Epigenetic Inhibitors**

-under revision for Nature Communications

Aria L. Byrd, Xufeng Qu, Alexsandr Lukyanchuk , Fan Chen, Jinpeng Liu, Xiulong Song, Stuart H. Orkin, Chi Wang, Jinze Liu, Christine F. Brainson **Dysregulated Polycomb Repressive Complex 2 contributes to chronic obstructive pulmonary disease by rewiring stem cell fate**

-under revision for Stem Cell Reports. This manuscript is the one presented in the body of the thesis.

CHAPTER 1. INTRODUCTION

1.1 Normal Lung Function

The average human lung is composed of five lobes. There are two lobes on the left side of the body that are anatomically denoted as superior and inferior, and three lobes on the right side that are denoted as superior, middle, and inferior. The lungs are further organized into proximal and distal regions which also inform their mechanical functions. The conducting zone is positioned closer to the proximal region of the body and facilitates airflow from the external environment and deeper into the body. Conversely, the respiratory zone is positioned closer to the distal regions and facilitates the transport of oxygen into and carbon dioxide out of the bloodstream [1].

The mechanical functions of the lungs inform its physiological structure, which can be described as an inverted tree with numerous branches. The distal lung begins in the trachea, also known as the windpipe. It is made of descending cartilage rings that connect to a posteriorly positioned, thick band of smooth muscle known as the trachealis muscle [2]. The tracheal lumen is lined with a mucous membrane that, along with a number of epithelial cells which will be discussed later in the text, assists with maintaining moisture and protecting against harmful xenobiotics [2]. At the base of the trachea is a ridge of cartilage called the carina that serves as the branching point where the lungs divide into the left and right bronchi, appropriately denoted as the primary bronchi [2]. As these passageways extend closer to the proximal regions of the lung, the bronchi subdivide into more numerous and gradually narrower passageways [3]. The secondary bronchi encompass the middle portion of the lung, while the tertiary bronchi encompass the outermost regions of the lung [3, 4], In order to optimize mechanical expansion and contraction of

the lungs, as these channels progress deeper into the body, the amount of cartilage decreases while the airway smooth muscle remains stalwart [5]. The end of the conducting zone is marked by the final airway subdivisions known as the terminal bronchioles [4]. Consequently, the beginning of the respiratory zone is marked by the final airway canals called respiratory bronchioles, which lead into cylindrically oriented alveolar cells called alveolar ducts, and open into spherically oriented alveolar cells which make up the alveolar sacs [4]. The alveolar sacs are the locations where oxygen gathers and gas exchange occurs, via simple diffusion.

1.2 Normal Lung Epithelium

To deliver sufficient amounts of oxygen to the bloodstream, the lung epithelium must also be sufficiently populated with stem cells that possess indefinite self-renewal and differentiation capabilities, progenitor cells that possess finite self-renewal and varying differentiation capabilities, and differentiated cells that have neither self-renewal nor differentiation capabilities.

The differentiated cells of the lung airways are goblet and ciliated cells [6]. Goblet cells are colloquially termed as being simple columnar, meaning that they typically resemble an upright column (columnar) and are positioned in a single layer (simple) along the basal lamina; a sheath of connective tissue that line the airways. These cells produce and secrete mucins into the bronchial lumen in order to bind and sequester inhaled pathogens, debris, and other small particles that don't belong in the lungs [6]. Ciliated cells, on the other hand, are pseudostratified columnar epithelial cells, meaning that they're positioned in a single cell layer along the basal lamina, but they appear to be stacked atop one another. Ciliated cells are equipped with over 300 apically protruding cilia that whip back and forth to move mucous and other debris up and out of the lungs [6, 7]. Ciliated

cells are present throughout the airways, including the respiratory bronchioles, but the number of goblet cells gradually decreases as the lungs deepen [6, 8]. The differentiated cells in the lung parenchyma are known as type I pneumocytes or alveolar type 1 (AT1) cells. These are squamous cells (meaning they're thin and flat) that interconnect to form a net-like configuration to make up the alveolar sacs [4, 9]. Moreover, these sacs are enveloped in a labyrinth of capillaries to create an air-blood barrier; effectively preventing the formation of air bubbles in the vasculature and the transfer of blood into the lungs [9].

The progenitor cells in the lung airways are club (formerly known as Clara) cells; simple columnar epithelial, secretory cells that play an essential role in lung detoxification [6, 10]. Their primary secretion is the bioactive compound, secretoglobin 1A1 also known as club cell secretory protein (CCSP), which have been shown to suppress inflammation, protect against xenobiotic damage, and defend against bacterial infections [10]. Additionally, these cells express large amounts of cytochrome P450 metabolizing enzymes, which function to increase the solubility, and thereby excretion of harmful compounds like ozone, naphthalene, and elements of tobacco smoke [10, 11]. The progenitor cells of the lung parenchyma are type II pneumocytes or alveolar type 2 (AT2) cells; cuboidal epithelial cells that secrete surfactants to reduce lung surface tension at the air-water interface of alveolar sacs [12]. The progenies of AT2 cells are AT1 cells, while the progeny of club cells are AT2, ciliated, and goblet cells.

Finally, the lung stem cells, from which all the aforementioned cells descended, are basal stem cells (BSC) and bronchioalveolar stem cells (BASC). BSC are undifferentiated, simple cuboidal epithelial cells that are capable of differentiating into club and goblet cells [6]. These cells are typically enriched in the upper airways and decrease in number as the lungs deepen [13].

Alternatively, BASC are nonspecific, simple cuboidal epithelial cells that express both surfactant (specifically, surfactant protein C [SP-C]) and CCSP [13]. Having only been characterized in mouse lung, these unique cells reside at the junction between the respiratory bronchioles and the alveolar ducts, appropriately coined the Bronchioalveolar-duct junction (BADJ) [13]. Intuitively, their location and co-expression enable them to repopulate the bronchiolar airways with club cells and the alveolar sac with AT2 cells.

1.3 Abnormal Lung Function and Epithelium

Due to the prevalence of harmful xenobiotics in the air and common respiratory infections, the lung epithelium is primed for efficient self-repair. However, if the lungs are under chronic stress, abnormal epithelial cell functioning ensues.

1.3.1 Lung Cancer

Lung cancer is the leading cause of cancer deaths in the world; killing more than 1.80 million people in 2020 [14]. Non-small cell lung cancers (NSCLC) accounts for 80-85% of all cases while small cell lung cancer (SCLC) accounts for the remaining 10-15%. Cigarette smoke exposure is the number 1 risk factor for all lung cancers; primarily attributable to the presence of more than 60 carcinogens [15]. SCLC originates in lung neuroendocrine cells (epithelial cells that receive neuronal input from the local environment and consequently secrete hormones into the blood) and are typically found in the proximal bronchi [16]. It is also generally more aggressive than NSCLC due to its high proliferative rate and strong predilection for metastasis [17]. Squamous cell carcinoma is a type of NSCLC that originates from the transformation of squamous

cells that line the airways, such as the trachea and main bronchi [18]. Adenocarcinoma is another type of NSCLC that typically occurs in the proximal lung and develops in secreting epithelial cells, such as goblet cells [19]. Finally, large cell carcinoma is an undifferentiated malignant tumor that can develop in any part of the lung [20].

1.3.2 Pulmonary Fibrosis

Pulmonary Fibrosis (PF) is a fatal lung disease in which fibrotic tissue replaces the alveoli, ultimately hindering ventilation and oxygen delivery to the bloodstream [21]. This disease affects about 200,000 people nationwide [22], but it is often subject to late stage diagnosis, as the symptoms are shared with other lung diseases [23]. Decades of research suggests that the pulmonary fibrotic response is endorsed in three general stages- injury, inflammation and repair [24]. Regardless of the various potential causes of PF [25, 26], the initial injury elicits production of metal metalloproteinase (MMP) 2 and 9 from the epithelia and inflammatory cells, respectively [27-29]. MMPs degrade surrounding ECM and enable leukocyte influx to- and efflux from the damaged site [30-32]. Additionally, damaged epithelial cells and leukocytes up-regulate chemokine production in an effort to stimulate the immune response. During the inflammatory stage, there is a complex network of inflammatory cascades underway. Among these, Transforming Growth Factor (TGF) β and Interleukin (IL) 4 dominate the fibrotic response by directly activating myofibroblast transdifferentiation [33-35] and collagen deposition, respectively [36, 37]. IL-4 also indirectly promotes myofibroblast transdifferentiation by activating TGFβ production in M2 macrophages [38-40] and eosinophils [41]. The repair stage is the hallmark of PF. It involves unrelenting myofibroblast transmigration to the alveolar space, collagen deposition, and contraction [24].

1.3.3 Chronic Obstructive Pulmonary Disease

Chronic Obstructive Pulmonary Disease (COPD) claims over 3 million lives annually, making it the third leading cause of worldwide deaths [42]. This progressive and irreversible condition is presented as two, often overlapping, diseases; chronic bronchitis, a disease of long-term inflammation of the bronchi, and emphysema, a disease of persistent damage to and destruction of the lung parenchyma. Cigarette smoke is the primary risk factor for COPD development, as it promotes reactive oxygen species (ROS) production and subsequent inflammation [43-45]. Nevertheless, respiratory infections [46] and long term exposure to chemical fumes [47] air pollution [48, 49], and particulate matter [50] also promote its development and progression. Individuals with COPD typically have multiple comorbidities [51], with the largest contributors to death being respiratory failure [52], cardiovascular disease [53], and lung cancer [54]. Cigarette smoke-induced ROS production, low grade inflammation, and abnormal epithelial cell differentiation are all shared features between COPD and lung cancer [55]. Smokers with COPD are 3.5 times more likely to develop squamous lung cancer than smokers with pathologically normal lung epithelium [56]. In a normal injury response, inflammation eventually subsides, which allows for the initially hyperplastic epithelium to revert back to pseudostratified columnar epithelium. However, in COPD lung, continual exposure to noxious agents perpetuates inflammation and hinders epithelial resolution, so that even after the agent is removed, reversion still does not occur [57]. The major epithelial changes observed in the COPD airway are basal and goblet cell hyperplasia, squamous metaplasia, and mucin hypersecretion [58, 59]. Most recently, scRNA sequencing technology has allowed for the discovery of rare stromal, immune and epithelial cell subpopulations present in diseased lungs [60-65].

1.4 Epigenetic Principles and Remodeling Factors

A genome is an organism's complete set of DNA, and an epigenome is a set of chemical compounds and proteins that influence genomic activity without changing its DNA sequence. In the nucleus, DNA is highly coiled and organized into chromatin. Histones are basic proteins that enable this coiling by serving as net-positively charged spools for the net-negatively charged DNA to wrap around. When DNA is wrapped around a histone octamer (made of two H2A, H2B, H3 and H4 histones) and held in place by a histone H1 protein, it is called a "nucleosome". This structure is plastic, allowing its components to be loosely or tightly associated based on particular stimuli. The four ways to epigenetically, manipulate DNA is through independent or interdependent RNA-mediated regulation, nucleosome remodeling, DNA methylation, and histone modifications. RNA-mediated regulation occurs through a range of activities by small and long non-coding (lnc) RNA [66]. For example, microRNA (miRNA) inhibit gene expression by degrading genetic transcripts [67], and lncRNA influence gene expression by recruiting additional epigenetic factors to particular chromosomal regions [68]. Nucleosome remodeling is facilitated by the BRG1-Associated Factor (BAF) complex. This multimer functions by either sliding or transporting histone octamers to effectively "activate" (allow transcription factor access) or "silence" (prohibit transcription factor access) genes [69]. DNA methylation silences genes and typically occurs at the 5'C of cytosines at CpG islands (a short stretch of DNA in which the cytosine-guanine sequence is higher than other regions) within promotor regions. DNA methyltransferase (DNMT) facilitates DNA methylation [70] while teneleven translocation (TET) enzymes facilitate DNA de-methylation [71]. Finally, histones are post-translationally modified at specific amino acids located on the N-terminal domain. The addition and/or removal of functional groups essentially serve as tags to signal the recruitment of additional activating or silencing proteins [72]. Methyl groups can serve as both an activating and silencing tag [73]. Histone methylation and demethylation is carried out by histone methyltransferases (HMT) and histone demethylases (HDM), respectively. Moreover, these enzymes are

capable of mono- (me1) di- (me2) and tri- (me3) methylating/demethylating histones. While all histone tails are capable of methylation [74-77] and all basic amino acids (histidine, arginine, and lysine) can be methylated [78-80], lysine methylation on histone H3 (H3K) has been broadly studied. As a result, extensive characterization of these alterations has led to strong associations between specific modification patterns and transcriptional profiles. For example, mono-methylation of histone H3 on lysine 4 (H3K4me1) is an activating mark that is commonly found at transcriptional enhancers [81], H3K9me2 is a repressive mark commonly associated with silenced genomic regions [82], and H3K27me3 is a repressive mark that is commonly associated with temporary control of developmental regulators [83] and often found in facultatively repressed genes [84]. Most H3K targets have redundant HMTs [73], but H3K27me3 has only been linked to one highly conserved HMT; Enhancer of Zeste Homolog 2 (EZH2) [85]. EZH2 is a 746 amino acid-long protein that works alone or with other proteins to influence transcription. As a single entity, this enzyme acts as a transcriptional activator by physically linking transcription factors with one another and their promoters [86, 87]. On the other hand, EZH2 acts as a transcriptional repressor by serving as the catalytic subunit that facilitates H3K27me3 [13, 88, 89]. To carry out this repressive function, EZH2 interacts with two additional proteins-EED and Suz12. EED serves as the scaffold protein that holds histone H3 and EZH2 together [13, 88, 89], and Suz12 has been implicated in serving as the "homing" subunit, which recognizes particular nucleosomes for downstream action [90-93]. These three components make up what is called the Polycomb Repressive Complex 2 (PRC2); an epigenetic multimer that maintains cellular specificity via repression of unassociated genes. This complex is integral to homeostasis, as it maintains spatial and temporal gene expression throughout an organism's life. During embryonic development, the complex is crucial to stem cell fate decisions, as it regulates repression of homeotic genes [94]. With age, EZH2 expression typically decreases [95] and usually only increases to enable cell proliferation and survival [96]. Alternatively, PRC2 malfunction can bring about incongruous gene expression and result in diseases rooted in aberrant cell

development [97-101]. Numerous cancers, for example, have been associated with repression of tumor suppressor genes, as a consequence of increased EZH2 activity [96-102]. Conversely, loss of EZH2 activity stifles lung endoderm development in mice due to its role in repressing lung stem cell-associated genes [103, 104]. Furthermore, recent unpublished data from the Brainson lab suggests that EZH2 activity underlies chronic obstructive pulmonary disease (COPD), as a significant decrease in its function is associated goblet cell hyperplasia in human lung. These findings suggest that improper PRC2/EZH2 activity is important for cell development, fate, and function. They also warrant further investigation into EZH2's role in disease development and propagation, particularly those involving lung functions.

1.5 Role of Polycomb Repressive Complex 2 in Chronic Obstructive Pulmonary Disease Pathology

Methyl group availability is integral to PRC2 activity, suggesting metabolic pathways could influence PRC2 activity levels. Cystathionine Beta Synthase (CBS) is an enzyme that condenses serine and homocysteine to produce cystathionine, an upstream precursor of glutathione (GSSH). GSSH has been implicated in the mitigation of ROS production in COPD lung [105]. Post-translational modification analysis on mouse and human cells treated with cigarette smoke showed the unique presence of mono- and di-methylated histone H3 lysine 27 that was not seen in controls, suggesting that cigarette smoke could lead to decreased PRC2 activity [106]. However, a separate immunohistochemistry analysis of normal and COPD lung showed a significantly higher number of tri-methylated histone H3 lysine 27 regardless of smoking status [107].

1.6 Technical Advances for 3-Dimendional Organoid Cultures

We are the first lab to use scRNA-seq to characterize the transcriptome of 3D cultured, *Ezh2* knockout mouse lung organoids. In the past, genome wide location analysis was employed to characterize the transcriptome of 2D cultured, human embryonic fibroblasts following *Ezh2* siRNA transfection [94]. Our choice to use the 3D spheroid model is based on previous literature that demonstrates more physiologically relevant results compared to 2D cultures; specifically regarding noticeable differences in differentiation and proliferation patterns, cell cross talk, and comparable gene expression patterns to *in vivo* experiments [108].

CHAPTER 2. MATERIALS AND METHODS

2.1 Mouse Cohorts

Mouse cohorts of *Ezh2*$^{flox/flox}$,*Ezh2*$^{flox/+}$, *and Ezh2*$^{+/+}$ [109, 110] were all maintained in virus-free conditions and bred to *Teto:H2B-GFP*, *Rosa26:rtTA* and *Teto:Cre* mice [111-113]. All care and treatment of experimental animals were in accordance with University of Kentucky Institutional Animal Care and Use Committee (IACUC) guidelines.

2.2 Ovalbumin Inhalation Model

Mice that ingested doxycycline water at 1mg/mL for approximately 4 months were used for the following experiments. One mouse that did not receive doxycycline was included in the *Ezh2*$^{+/+}$ no-challenge cohort and was indistinguishable from the mice receiving doxycycline. After 4 months, cohorts were sensitized to ovalbumin by administering two doses of 20µg of ovalbumin (SIGMA) in Imject Alum (#7761, Thermo Scientific) by intraperitoneal injection 3-5 days apart. Approximately three weeks later, cohorts were challenged with either saline (control) or 2% ovalbumin in saline (OVA) by aerosolizer for 30 minutes. Exactly 7 days after challenge, cohorts were sacrificed and lungs were inflated with neutral buffered 10% formalin at 25cm gravity pressure, tied off at the trachea, and allowed to incubate for at least 24 hours at room temperature in 10% formalin. In the case that the gravity inflation did not work, lungs were carefully hand inflated with formalin using a 27g needle and immediately placed into 10% formalin. After full fixation, lungs were dissected by lobes, placed in cassettes, transferred to 70% ethanol, embedded in paraffin, and sectioned at 4µm. Genotyping revealed that one non OVA challenged mouse,

initially identified as *Ezh2* wild type, had the presence of the *Ezh2* floxed excised band, suggesting the mouse had undergone heterozygous recombination in the germline, and was thus excluded from the final analysis. Another non OVA challenged mouse was excluded from final analysis due to advanced age relative to the rest of the cohort.

2.3 Patients Samples

Patient slides were provided by the Markey Cancer Center Biospecimen Procurement & Translational Pathology Shared Resource Facility (BPTP SRF) of University of Kentucky. The COPD tissue (n=10) was from routine lung reduction surgeries and the normal tissue (n=9) was from biopsies of suspected lung cancers that were found to be non-cancerous. Patient tissues used in this study were fully de-identified and do not constitute human subjects research. Samples were initially selected for presence of enough intact bronchiolar tissue then sectioned at 4µm for analysis.

2.4 Sorting of Murine Lung Cells

Mice were euthanized via intraperitoneal avertin or ketamine/xylazine injection followed by thoracectomy, and lungs were injected with 2mL of dispase. All five lung lobes from one or two genotype-matched donor mice were dissected from trachea and other tissues, were minced with scissors and incubated in PBS, collagenase and dispase for 45 minutes. Tissues were strained through 100- and 40 µm filters, then the cells were spun down and red cells were lysed in red blood cell lysis buffer (0.15M NH_4Cl, 10mM $KHCO_3$, and 0.1mM Ethylenediaminetetraacetic acid). Single cell suspensions were stained using rat-anti-mouse antibodies including anti-mouse-Sca1-

APCCy7 (Fisher Scientific BDB560654), anti-mouse-EpCAM-PECy7 (BioLegend 118216), anti-mouse-CD31-APC (Fisher Scientific BDB551262) and anti-mouse-CD45-APC (Fisher Scientific BDB559864). Live cells were gated by exclusion of 4',6-diamidino-2-phenylindole (DAPI) positive cells (SIGMA). Cell sorting was performed with a Sony iCyt with a 100µm nozzle. Following the sort, cells were subject to cytospin and immunofluourescent staining in order to quantify the distribution of bronchiolar and alveolar cells (**Figure 2.1**). From this analysis, it was revealed that a majority of the Sca1- cells were pro-SPC positive and lacked CCSP expression, indicating their alveolar type 2 identity. The Sca1+ cells were a mixture of pro-SPC+, CCSP+ and acetylated tubulin+ cells, with some cells co-expressing pro-SPC and CCSP. The number of CCSP+ cells was significantly higher in Sca1+ cells compared to Sca1- ($p=0.04$).

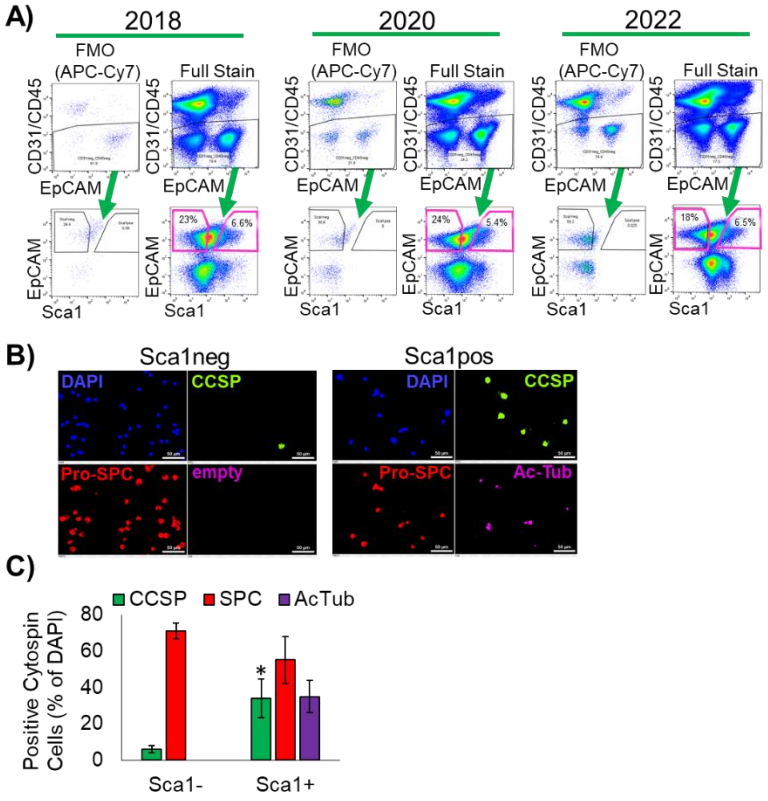

Figure 2.1 Murine-derived Sca1- and Sca1+ cell sort and quantification

A) Representative flow cytometry gating strategies for lung samples over time. After gating for DAPIneg live cells and singlets, hematopoietic and endothelial cells were excluded and then EpCAM+/Sca1- and EpCAM+/Sca1+ cells were gated for sorting. **B)** Cytospin images of EpCAM+/Sca1- and EpCAM+/Sca1+ cells stained for the indicated cell lineage markers. Note that speckles and blotches of non-specific stain (not associated with a DAPIpos nucleus) were edited from images because they were artifacts of cytospin that would interfere with quantification of cell types. Scale bar = 50µm. **C)** Graphs of percentages of DAPIpos cells that had staining for each marker. Acetylated tubulin was only stained for in the EpCAM+/Sca1+ fraction. Mean ± sem is graphed for n=4 independent lungs sorted. 9-11 4x images of the cytospins were used for quantifications with the Nikon AR bright spot detection module. * indicates p=0.04 using 2-tailed t- test with equal variance comparing Sca1- club cells to Sca1+ club cells.

2.5 Murine Bronchiolar Organoid Culture

Bronchioalveolar stem (EpCAM+/Sca1+) and alveolar type 2 cells (EpCAM+/Sca1-) were sorted from doxycycline naïve *Ezh2*-floxed mice. Cells were plated with neonatal mouse lung endothelial cells in air-liquid-interface Matrigel cultures [114]. 3D media was composed of DMEM-F12, fetal bovine serum (FBS), and insulin-transferrin-selenium (ITS). Doxycycline (100-200 ng/mL) was added to the cultures approximately 5 days after plating. Cultures were passaged as needed. Cultures with sufficient bronchiolar organoids were then dispased, collected, trypsinized, sorted for GFP+ cells, and then seeded at equal densities to grow for an additional 2.5-4 weeks based on the growth rate of the cultures in each experiment. This experiment was repeated 5 times. Due to COVID19, the fifth experiment was not sorted, but rather the organoids were allowed to sink by gravity in 1x PBS and the supernatant was removed in order to deplete the endothelial cells prior to trypsinization. For the final analysis, one *Ezh2* heterozygous culture that was clearly cross-contaminated with an unknown GFP-negative cell type, and one *Ezh2* null outlier, that was determined through the ROUT method on GraphPad Prism graph 9, was excluded. After the final 4-week growth period, fixed or fresh organoids were counted by eye on a fluorescence microscope. Cultures were fixed with 10% neutral buffered formalin overnight at room temperature (Experiments 1, 2, 3, and 5) or dispased to collect cells for GFP+ sorting for scRNAseq (Experiment 4). For fixed cultures, after rinsing with 70% ethanol, fixed Matrigel plugs containing the organoids were immobilized with Histogel (Thermo Scientific) on 10cm dishes, counted again, and imaged at 4x magnification for size quantification prior to paraffin embedding. For scRNA-seq, organoids were pooled by genotype prior to GFP resort. There were initially two wild type donors, but further genotyping later revealed that one donor likely underwent heterozygous recombination in germline. However, it is important to note that this particular cohort

only accounted for 3% of total harvested wild type organoids, and the loxP recombination site junction was undetectable in the 'wild-type' cells captured, but was detectable in the *Ezh2* null and heterozygous samples.

2.6 Single Cell RNA-sequencing

The sequencer produced Chromium single-cell data and then the Cell Ranger toolkit version 3.1 (10X Genomics) was used to de-multiplex samples from raw sequencing reads to gene-count matrices with alignment to the mm10 genome (v93). In order to perform the downstream analysis, such as cell type identification and differential gene expression analysis, Seurat (V3) R package [115] was employed to aggregate the gene-counts matrices from all samples and provide the analytical insight. A five-step process was performed using Seurat package: (1) For quality control and data pre-processing, we discarded genes expressed in fewer than three cells and discarded the low-quality cells that had less than 100 genes expressed. We also assessed the percentage of mitochondrial transcripts for each sample, and each of them indicated a low level of expression (below 10%). The count matrices were then log-transformed. (2) For sample merging and feature selection, we combined the log-transformed matrices of each sample and applied the variance-stabilizing transformation (vst) method to remove cell-to-cell variation. The top 2000 genes were selected for downstream analysis. (3) For dimension reduction and clustering, we applied "PCA" to reduce the dimensionality of the merged data to 50 principle components and then performed a shared nearest neighbor (SNN) modularity optimization-based algorithm to identify clusters of cells. We utilized the UMAP [116] technique to visualize the clustering results as shown in **Figure 3A**. (4) For cell type identification, we created a dot plot (**Figure 3B**) using 42 cell type specific marker genes to understand the cell identities of each cluster. Cell cluster

identities were also validated by examining highly expressed genes in each cell cluster as shown in the heatmap (**Figure S3**). (5) For differential gene expression analysis for each cell population, we used a DEG (Differential Expressed Gene) identification method in Seurat, namely "MAST" [117], to identify the up/down-regulated sets of genes between a pair of *Ezh2* genotypes within each cell population. Other analytical results from Seurat were visualized in **Figure 4 and S4**. In **Figure 4A**, the UMAP plot depicted a combined perspective of the three genotypes, and the violin plots in **Figure 4B** showed how the expression of six gene markers varied across the three genotypes. Furthermore, trajectory inference was performed on each genotype using Slingshot (v2.0) [118] and the results were illustrated in **Figure S4A**. The UMAP plot illustrated a split view of the three genotypes in contrast to the group view in **Figure 3A**. The nodes in the figure represent centers of clusters and connections between these nodes are called lineages. The lineages of adjacent cell populations indicated these cell populations were biologically relevant. In the **Figure 4C**, the distribution of cell clusters across genotypes was assessed by z-test and p values were adjusted for multiple hypothesis testing.

2.7 RNA-sequencing

Human Bronchiolar Epithelial Cell RNA was extracted by Agilent Absolutely RNA kit with a DNAse step performed on the columns. Library preparation and sequencing were performed by the Beijing Genomics Institute (BGI Group) using DNBseq and 50bp single end reads. Sequencing reads were trimmed and filtered using Trimmomatic (V0.39) [119] to remove adapters and low quality reads. Reads from human samples were mapped to Ensembl GRCh38 transcripts annotation (release 98), respectively, using RSEM [120]. Gene expression data normalization and

differential expression analysis were performed using the R package edgeR [121]. Significantly up/downregulated genes were determined as fold change ≥ 2 and q-value < 0.05.

2.8 Gene Set Enrichment Analysis

GSEA was performed with GSEA version 4.0.3 (Broad Institute) with rank-ordered gene lists generated using all log-fold change values. Mouse_Gene_Symbol_Remapping_Human_Orthologs_MSigDB.v7.4.chip was used to map mouse genes to human orthologs. Databases queried included Hallmarks (h.all.v7.4), Curated (c2.all.v7.4), BioCarta (c2.cp.biocarta.v7.4), KEGG (c2.cp.kegg.v7.4), Reactome (c2.cp.reactome.v7.4), Gene Ontology (c5.all.v7.4), Oncogenic Signatures (c6.all.v7.4), and Immunologic Signatures (c7.all.v7.1). Gene signatures that converged on common themes were selected for further analysis and graphing of enrichment scores and FDRs for specific contrasts. CBS overexpression vs empty vector HBEC gene list was generated based on adjusted p value <0.05 and LFC >1. Null vs wild type, and heterozygous vs wild type *Krt17*- basal cell gene lists were generated based on adjusted p value <0.05. For comparison to the emphysema signatures, data were accessed from GEO under accession number GSE1650 and processed using R with affy and limma packages and rma normalization. The moderated t-statistic was used to produce the rank ordered gene list comparing emphysemic smokers to healthy smokers, noting that emphysema is one of the hallmarks of COPD.

2.9 Immunofluorescence and Quantification

All sections were deparaffinized and subjected to antigen retrieval in citrate buffer pH 6.0 with the Lab Vision™ PT module (Thermofisher) machine. Patient derived tissue sections were blocked with 10% Donkey serum (Jackson ImmunoResearch, #017-000-121) in PBS-TritonX and immunostained with antibodies for CCSP (R&D systems, #MAB4218,1:150), Keratin 5 (Biolegend, #905501,1:200), and MUC5AC (AbCAM, #AB3649,1:100) in a humid chamber overnight at 4°C. Secondary Antibody staining included donkey anti-rat Alexa Fluor 488 (#A21208), donkey anti-rabbit Alexa Fluor 647 (#A31573), and donkey anti-mouse Alexa Fluor 594 (#A21203) (Invitrogen,1:200). Nuclei were stained with ProLong Gold with DAPI (Invitrogen, #P36935). Mouse organoids and whole lung tissue sections were immunostained with antibodies for CCSP (Millipore, #ABS1673,1:100), KRT5 (Biolegend, #905501,1:200), Acetylated tubulin (SIGMA, #T7451,1:1000), and pro-SPC (Millipore, #AB3786,1:200). Secondary antibody staining included donkey anti-goat Alexa Fluor 488 (#A11055), donkey anti-rabbit Alexa Fluor 647 (#A31573), donkey anti-mouse Alexa Fluor 594 (#A21203) (Invitrogen,1:200). Nuclei were stained with ProLong Gold with DAPI (Invitrogen, #P36935).

Stain imaging was conducted on Nikon Eclipse inverted microscope using 20x objective and quantification was conducted with the Nikon NIS-Elements AR software, respectively. For quantification of lungs, blinded 20x images were obtained on one exposure and NIS-Elements was used to quantify each batch using equivalent settings. For quantification of organoids, 20x images were matched to H&E stains and LUTs were set by image batch due to differing staining intensities. Organoid type and cell number quantifications were done blinded by eye. Organoids with characteristics difficult to interpret on the original image were further analyzed by microscopy

to ensure correct classification. Squamous types were classified as such if morphological characteristics were present in at least part of the organoid.

2.10 Alcian Blue Staining and Quantification

Alcian Blue staining of whole mouse lung was performed by the Biospecimen Procurement & Translational Pathology Shared Resource Facility of the University of Kentucky Markey Cancer Center. Representative images of bronchus from each mouse stained were captured in a blinded fashion and were used to measure Alcian Blue cell number and area and epithelium lengths with the HALO® 3.2 software (Indica Labs).

2.11 Immunohistochemistry and Quantification

Antigen retrieved patient derived tissues were blocked with 3% hydrogen peroxide for 10 minutes at room temperature, washed with PBS, then blocked with goat serum (Vectastain® ABC Kit, PK-6101) in PBS-TritonX. Tissues were immunostained with antibodies for H3K27me3 (Cell Signaling, #9733,1:500), EZH2 (Cell Signaling, #5246S,1:300), and CBS (Novus, #NBP1-83255,1:250) in a humid chamber overnight at 4°C. Secondary antibody, biotinylated rabbit antibody (Vectastain® ABC Kit, PK-4001), was incubated for 30 minutes at room temperature. Tissues were incubated in ABC reagent (Vectastain® ABC Kit, PK-4001) for 30 minutes at room temperature, washed in PBS, then submerged in DAB (Vectastain® ABC Kit, SK-4100) solution and counter-stained with Harris' Hematoxylin (Electron Microscopy Science, #26754-01) prior to mounting. Scoring of H3K27me3 (Cell Signaling, #9733) and EZH2 (Cell signaling, #5246S) nuclear staining was performed with Nikon NIS-Elements AR software. 20x magnification images

were captured of bronchiolar epithelial regions. The bronchiolar regions were gated by hand, prior to using the NIS dot detection module to quantify stained nuclei with increasing stringency on the blue channel. The user confirmed the correct counting of nuclei and the cutoffs for DAB signal for each set of images prior to running the macro on all batched images. Percentage of positive nuclei were quantified and graphed for each cutoff.

2.12 Western Blotting

Whole cell extracts were made in RIPA buffer (0.5% Deoxycholate, 1% IGEPAL-CA630, 0.1% sodium dodecyl sulfate, 150mM NaCl, 50mM Tris-8.1) with Halt™ Protease and Phosphatase Inhibitor (Thermo) and with or without additional 1mM DTT, lysates were cleared by centrifugation, and protein concentrations were quantified with the Pierce BCA Protein Assay Kit (Thermo Fisher, #23225). For Western blotting, concentration matched samples were denatured with heat and reducing agents, split into identically loaded lanes, separated on a 4-15% acrylamide gel (BioRad) and transferred to nitrocellulose membranes (GE Healthcare, #10600002). Antibodies used for Western blotting were: EZH2 (Cell Signaling, #5246s, 1:1000), H3K27me3 (Cell Signaling, #9733s, 1:1,000) and CBS (Cell Signaling, #14782s, 1:1,000) all incubated at least 18 hours at 4ºC. Histone H3 (Abcam, #ab1791, 1:5,000) was used as loading control run on a blot with 1/3 the concentration of the primary blot diluted from the same samples and run simultaneously. Secondary anti-rabbit IgG, HRP-linked antibody (Novus, #NB7160, 1:10,000) was incubated for 1 hour at room temperature. After washing, chemiluminescence was visualized with Super-signal West Pico PLUS Chemiluminescent Substrate (Thermo) and exposure onto Hyperfilm (Amersham). Western Blot quantification was performed with the Gel Analysis tools in ImageJ.

2.13 Human Bronchiolar Epithelial Cultures

Human Bronchial Epithelial Cell (HBEC) lines were donated from the David Orren Lab at the University of Kentucky and were authenticated by IDEXX laboratories using CellCheck9. HBECs were initially grown in PneumaCult™-EX media, on gelatin coated plates and transduced with viral supernatant for 4-6 hours, then maintained in PneumaCult™-EX media for 4-5 days. Cells were then transferred onto gelatin coated 10cm plates and selected for with PneumaCult™-EX media + 1µg/mL Blasticidin (Gibco, A1113903) for 4-5 days and then passaged for experiments.

2.14 Viruses

The human CBS open reading frame (ORF) was purchased from Origene (RC201755). The ORF was amplified by PCR with proof reading polymerase (Agilent 600385-51) and cloned into pENTR™/D-TOPO™ Vector (Thermo) and then flipped into pLenti6⁄V5-DEST® Gateway® (Thermo). Vectors were maintained and amplified in One Shot® Stbl3™ Chemically Competent *E. coli* (Thermo). pLenti6-CBS lentivirus or pLenti6 were packaged in HEK293T cells with a lipofectamine, VSVG, VPRΔ8.2 vector system [122].

2.15 Statistical Analysis

Statistical analyses were carried out using GraphPad Prism or Microsoft Excel. Unless otherwise stated, all numerical data are presented as mean ± standard error of the mean. To compare continuous outcomes between two experimental groups, data with sufficient n were tested for normality using Kolmogorov-Smirnov test. For normally distributed data and data with small

n, an unpaired 2-tailed t-test with equal variance was used, and for data that failed the normality test, a Mann-Whitney *U* test was used as indicated in the figure legends. For grouped analyses, simple one-way ANOVA with Holm's multiple comparison correction was used when all the values of one group were the same, while Brown-Forsythe and Welch ANOVA tests with Games-Howell's multiple comparison correction was used for all other tests. Pearson's Correlation was used to test the linear relationship between markers. A p value (or adjusted p value) less than 0.05 was considered statistically significant.

2.16 Data Availability

The single cell RNA-sequencing data for study are available at the NCBI GEO database under GSE184347, the bulk RNA-sequencing are available at the NCBI GEO database under GSE183858. The data that support the findings of this study are available from the corresponding author upon reasonable request.

CHAPTER 3. PATIENT DERIVED TISSUES SHOW DRAMATIC REDUCTION IN H3K27ME3 IN COPD BRONCHIOLAR CELLS

Chronic Obstructive Pulmonary Disease (COPD) is a progressive, lethal disease that hinders respiration at the lung's conducting and respiratory zones. This disease is characterized by chronic bronchitis, excessive airway mucus deposition, and profuse inflammatory cell infiltration into the lung airway and alveoli [123]. Given these deleterious effects, it is important to elucidate the molecular mechanisms that drive COPD, and to understand why, even when environmental factors such as cigarette smoke are removed, COPD persists. EZH2 is the subunit within the PRC2 complex that tri-methylates histone H3 at lysine 27 (H3K27me3), marking DNA for transcriptional silencing and allowing expression of a single transcriptional profile [124]. Furthermore, loss of PRC2 leads to aberrant basal cell gene expression in distal airways of embryonic mouse lungs, suggesting its role in determining proper bronchiolar cell differentiation [103, 104].

3.1 COPD bronchiolar epithelium exhibit significant reduction in H3K27me3

To understand the relationship between PRC2 activity and the COPD phenotype, we obtained 10 COPD and 9 normal lung tissue samples **(Tables 3.1-3.2)** and stained sections for EZH2, the catalytic mark of EZH2, histone H3 lysine 27 trimethylation (H3K27me3), KRT5, a basal cell marker, MUC5AC, a goblet cell marker, and CCSP, a club cell marker **(Figure 3.1; 3.3)**. Using quantitative measurement of immunostaining intensity, there was a striking and very significant reduction of H3K27me3 mark in the nuclei of bronchiolar epithelial cells in COPD lung relative to normal controls **(p=0.003, Figure 3.2B-C)**. This finding was supported by results from an independent immunohistochemistry experiment conducted on cross-sections from a

different level of the tissue blocks **(Figure 3.2A)**. In these same tissues, there were no differences in EZH2 expression between the normal and disease state **(Figure 3.2D)**.

Table 3.1 Patient Derived Tissue Demographics

Patient-Derived Tissue Demographics			
	Normal Cases (%)	**COPD Cases (%)**	*P* Value†
Sex			**0.6285**
Female	2 (22.2)	4 (40.0)	
Male	7 (77.8)	6 (60.0)	
Smoking Status			**0.3698**
Unknown/Never	6 (66.7)	4 (40.0)	
Former/Current	3 (33.3)	6 (60.0)	
	Mean +/- SD	**Mean +/- SD**	*P* Value#
Age	55 (±13.2)	61 (±9.9)	**0.7473**
IHC Results			
H3K27me3-high	77.4 (±5.4)	50.3 (±5.7)	**0.003**
CBS-pos	2.6 (±1.1)	13.4 (±2.7)	**0.0024**

† p indicates Fisher's exact test
# p indicates Two-tailed Student's t-test with equal variance

Table 3.2 Extended Patient Demographics

Extended Patient Demographics					
Patient ID	**Age**	**Sex**	**Race**	**Hispanic**	**Appalachian**
Normal 1	34	F	White	Non-Hispanic	no
Normal 2	56	M	Asian	Non-Hispanic	yes
Normal 3	61	M	White	Non-Hispanic	unknown
Normal 4	63	M	Black	Non-Hispanic	no
Normal 5	80	F	White	Non-Hispanic	no
Normal 6	55	M	Black	Non-Hispanic	no
Normal 7	54	M	White	Non-Hispanic	yes
Normal 8	52	M	White	Non-Hispanic	no
Normal 9	40	M	Black	Hispanic	no
COPD 1	59	M	White	Non-Hispanic	yes
COPD 2	51	M	White	Non-Hispanic	yes
COPD 3	50	M	White	Non-Hispanic	no
COPD 4	63	F	White	Non-Hispanic	yes
COPD 5	39	M	White	Non-Hispanic	no
COPD 6	61	F	White	Non-Hispanic	yes
COPD 7	28	F	White	Non-Hispanic	no
COPD 8	60	F	White	Non-Hispanic	yes
COPD 9	68	M	White	Non-Hispanic	yes
COPD 10	52	M	White	Non-Hispanic	no

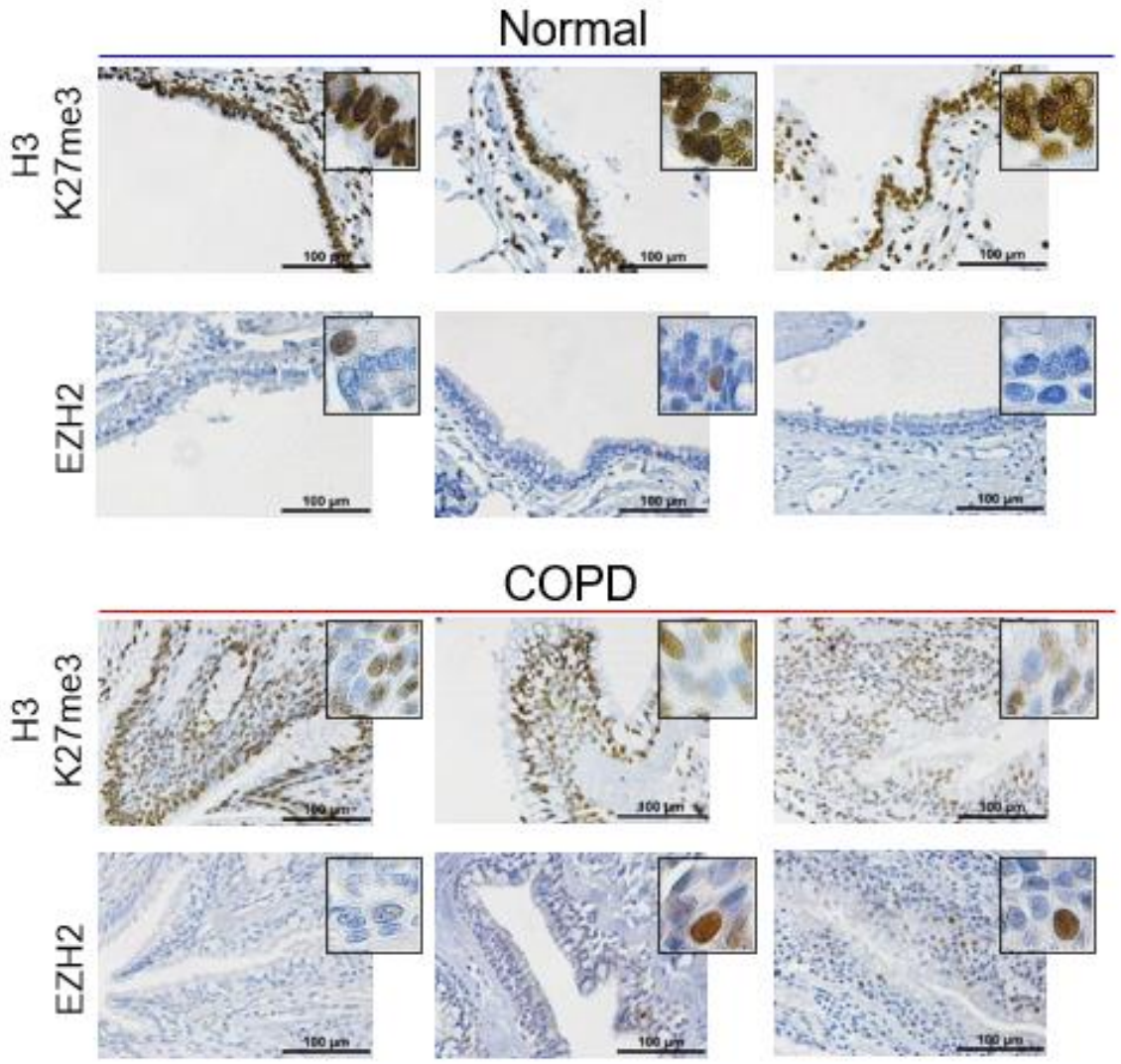

Figure 3.1 Representative images of H3K27me3 and EZH2 immunohistochemistry stains of normal and COPD lung, scale bar = 100µm.

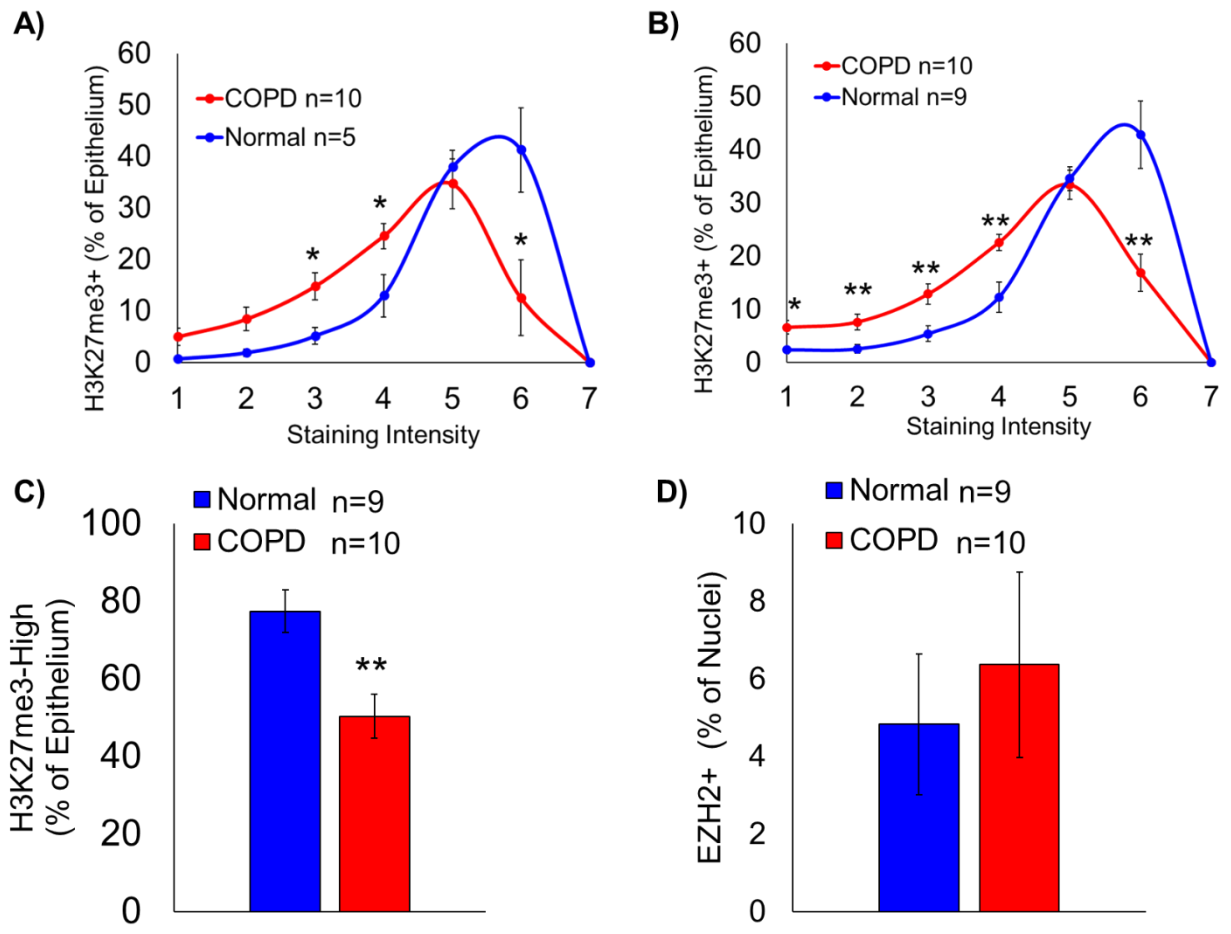

Figure 3.2 H3K27me3 and EZH2 Immunohistochemistry Analysis

A) Average percentage of epithelial cells expressing varying levels of H3K27me3 in normal (n=5) and COPD (n=10) patient derived lung tissues, * indicates $p<0.05$ using 2-tailed t- test with equal variance. **B)** Average percentage of epithelial cells expressing varying levels of H3K27me3. * indicates $p<0.05$ and ** indicates $p<0.01$ with a 2-tailed Mann-Whitney U with equal variance comparing Normal to COPD. **C)** Average percentage of epithelial cells expressing high levels of H3K27me3, ** indicates $p<0.01$ with a 2-tailed t-test with equal variance comparing Normal to COPD. **D)** Average percentage of epithelial cells expressing EZH2 in human lung.

3.2 Reduced lung H3K27me3 significantly correlate with increased basal cell hyperplasia and club-goblet cell transdifferentiation

Next, we quantified several parameters of the KRT5, MUC5AC and CCSP immunofluorescence staining and correlated these results with H3K27me3 expression levels. There was a strong negative correlation between the percentage of epithelial cells with high H3K27me3 and the area of KRT5 expression (Pearson's Correlation=-0.57, p=0.01 **Figure 3.5A**). Similarly, the area of MUC5AC+ epithelia were also significantly negatively correlated with the percentage of H3K27me3-high cells (Pearsons's Correlation=-0.53, p=0.02, **Figure 3.5B**). Evaluation of co-localized CCSP/MUC5AC expression showed that the percentage of double positive cells were strongly inversely correlated with the percentage of H3K27me3-high cells (Pearson's Correlation=-0.50, p=0.03, **Figure 3.5C**).

3.3 COPD bronchiolar epithelium exhibit dramatic increase in basal, club and goblet cell lineage genes

Analysis between disease states revealed that more than 70% of MUC5AC+ cells in COPD lung had co-localized CCSP expression, whereas only 30% of MUC5AC+ cells in normal lungs co-expressed CCSP (p=0.01, **Figure 3.4B**). Furthermore, COPD lung exhibited a significantly higher numbers of MUC5AC+ cells compared to normal **(Figure 3.4A)**. Together these data show that EZH2 function is significantly diminished in COPD lung, and this loss correlates with aberrant lung cell fate.

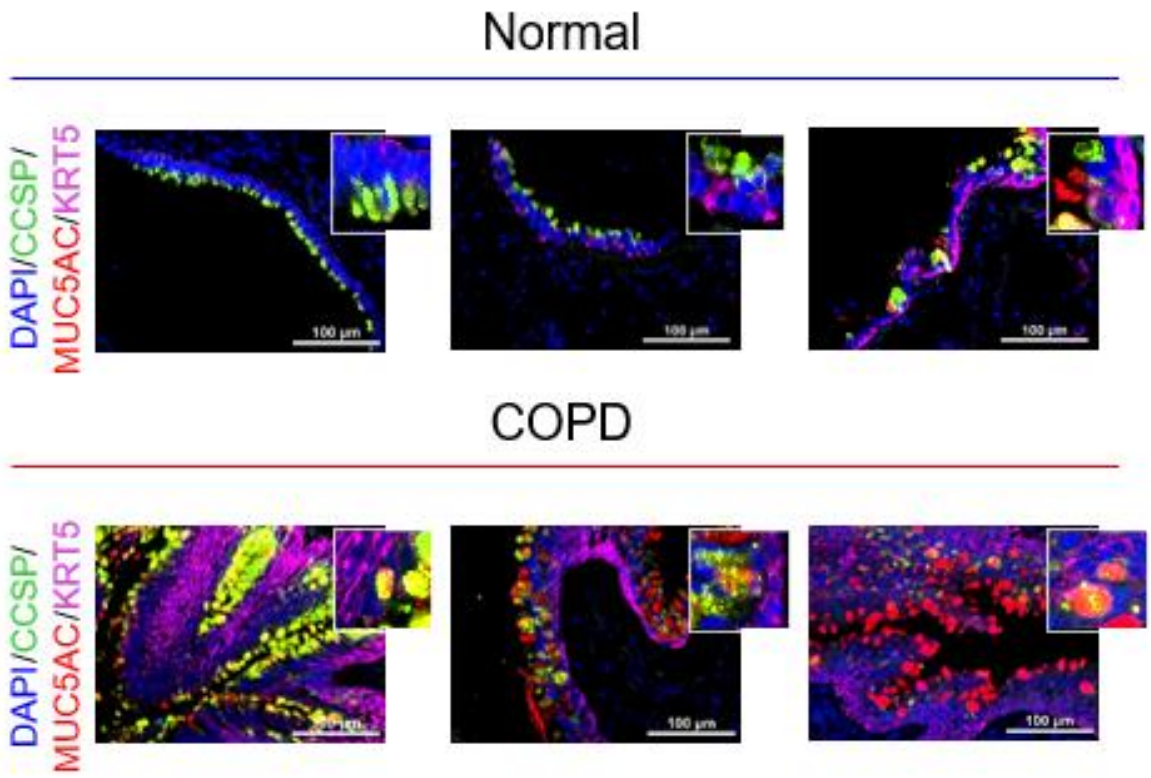

Figure 3.3 Representative images of immunofluorescent stains of normal and COPD lung from three different patients, scale bar = 100µm.

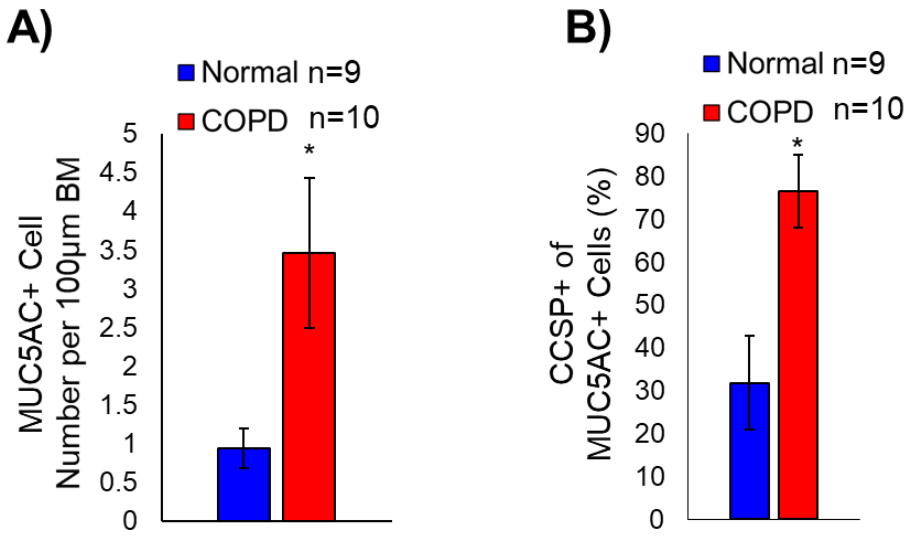

Figure 3.4 Immunofluourescence analysis of normal and COPD lung

A) Average number of epithelial cells expressing MUC5AC * indicates p=0.03 using 2-tailed t-test with equal variance. Analysis was performed on at least 4 separate, 20x images. **B)** Average percentage of epithelial cells that co-express MUC5AC and CCSP, * indicates p=0.01 with a 2-tailed Mann-Whitney *U* with equal variance.

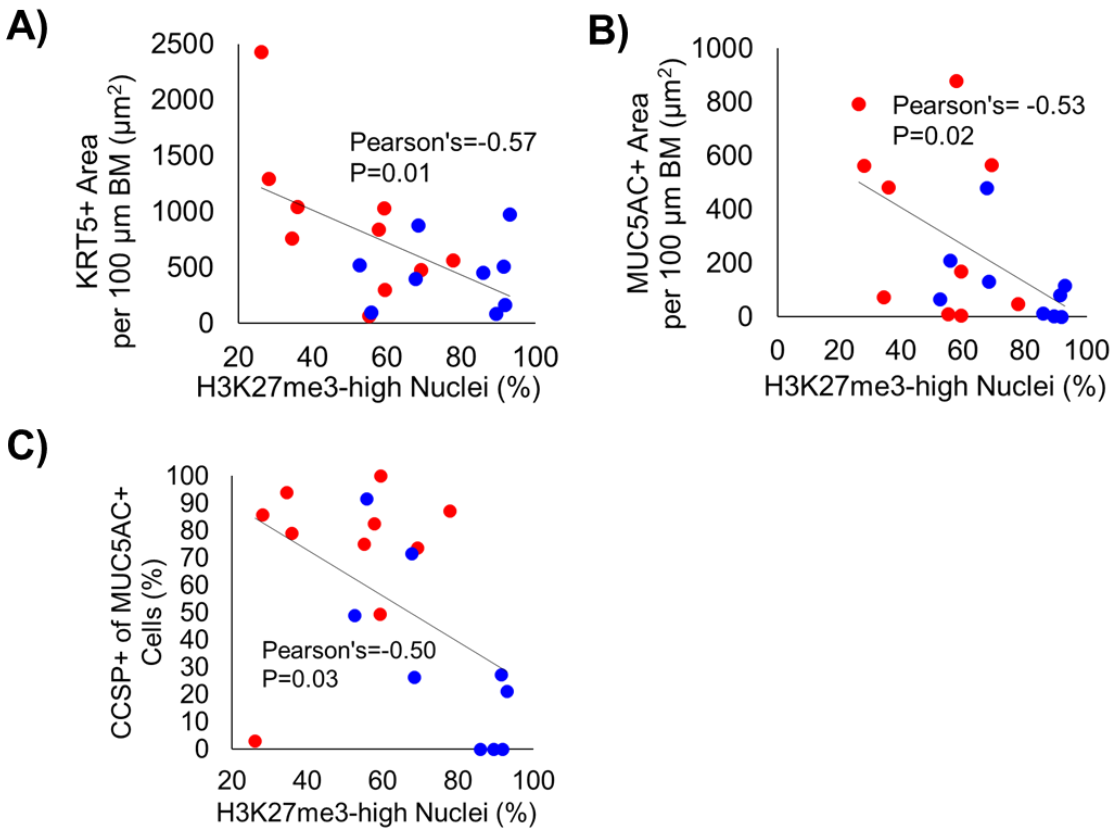

Figure 3.5 Correlation analysis of H3K27me3 immunohistochemistry and immunofluorescences stains on normal and COPD lung.

A) Correlation between high H3K27me3 expression and KRT5+ area within the epithelium (Pearson's Correlation= -0.57, p=0.01). **B)** Correlation between high H3K27me3 expression and MUC5AC+ area within the epithelium (Pearson's Correlation= -0.53, p=0.02). **C)** Correlation between high H3K27me3 expression and the percentage of cells that co-express MUC5AC and CCSP (Pearson's Correlation= -0.50, p=0.03). Correlation Analysis was conducted by Alexsandr Lukyanchuk.

3.4 Increased lung CBS significantly correlates with increased club-goblet transdifferentiation

Both Cystathionine Beta Synthase (CBS) and PRC2 activity are modulated in the wake of cigarette smoke-induced reactive oxygen species production [105, 125]. To elucidate if CBS is a potential upstream modulator of PRC2 activity, we conducted immunohistochemistry stains on COPD and normal human tissues **(Figure 3.6)**. We found that COPD bronchiolar epithelial cells exhibited significantly more CBS expression compared to normal bronchiolar cells, and that COPD cells often showed nuclear staining of CBS (p=0.002, **Figure 3.7**). Next, we conducted correlation analysis between CBS expression and the immunofluorescence stains for MUC5AC, CCSP and KRT5. We observed a significant positive correlation between the percentage of CBS+ cells and the percentage of CCSP+/MUC5AC+ cells (Pearson's Correlation=0.63, p=0.004, **Figure 3.8**). Next, to determine if CBS expression was a direct upstream target for PRC2 inhibition, we overexpressed CBS in Human Bronchial Epithelial Cells (HBECs) and grew them as 2D cultures. Western Blot analysis showed that significant overexpression of CBS (P=0.0001) led to a significant decrease in both EZH2 and H3K27me3 expression (P=0.001, p=0.0003, **Figure 3.9**). These data demonstrate that CBS may alter lung epithelial cell fate towards a more PRC2-depleted state, leading to the aberrant cellular differentiation seen in COPD patients.

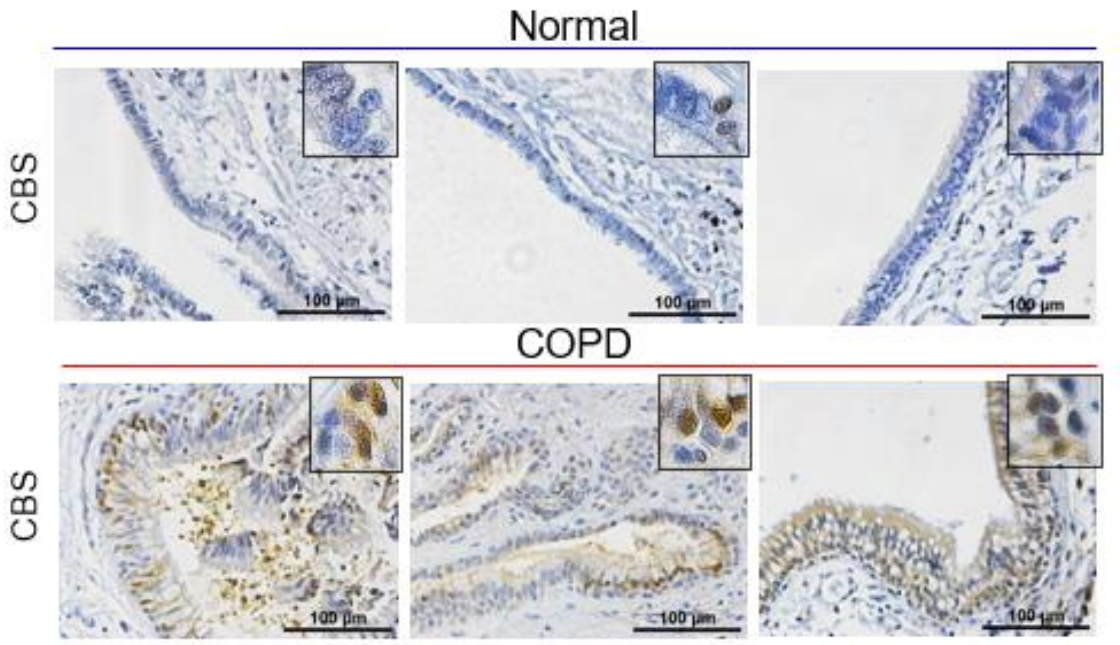

Figure 3.6 Representative images of Cystathionine Beta Synthase (CBS) immunohistochemistry stains on normal and COPD lung.

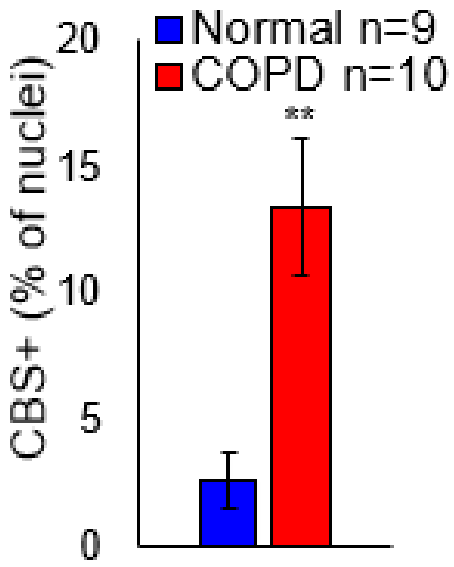

Figure 3.7 Analysis of Cystathionine Beta Synthase (CBS) immunohistochemistry stains on normal and COPD lung. * indicates p=0.0024 using 2-tailed t-test with equal variance

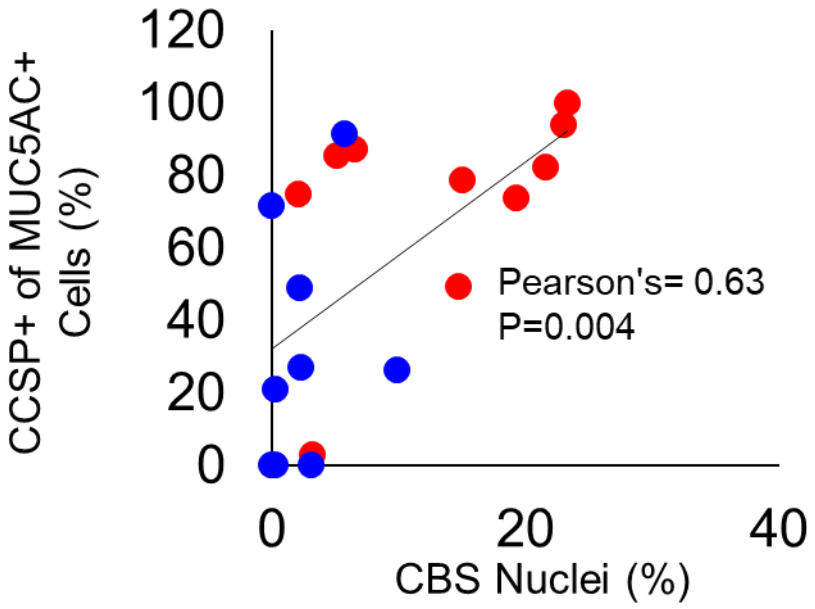

Figure 3.8 Correlation analysis of Cystathionine Beta Synthase (CBS) immunohistochemistry and immunofluorescence stains on normal and COPD lung. Correlation Analysis was conducted by Alexsandr Lukyanchuk.

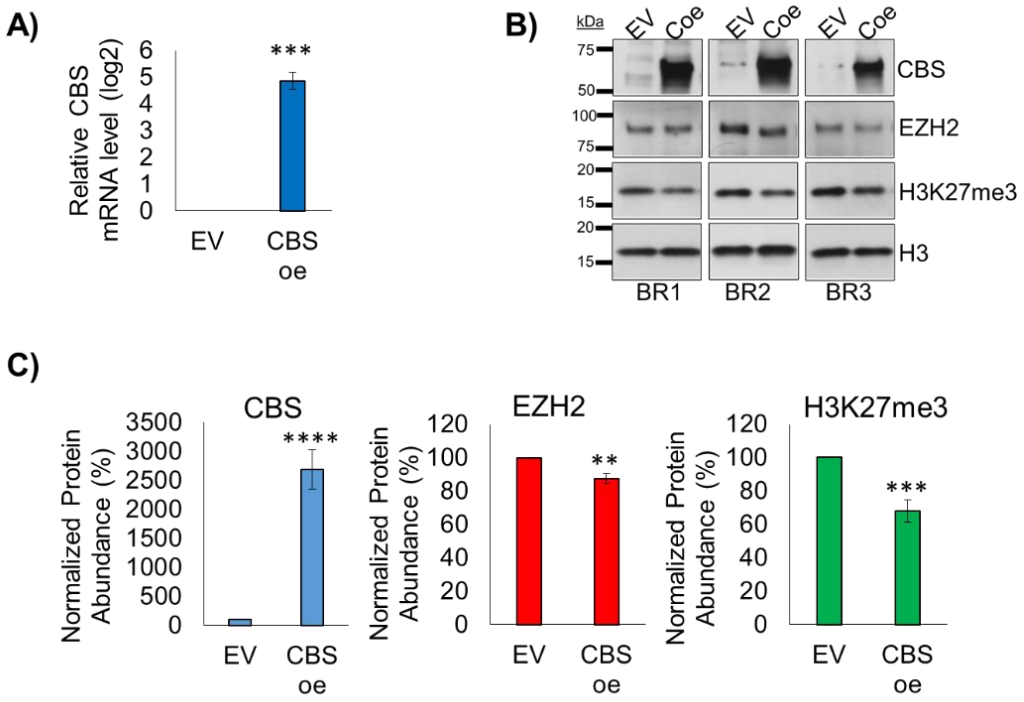

Figure 3.9 Cystathionine beta synthase western blot analysis

A) RT-qPCR for CBS transcript in the three biological replicate HBEC3KT cultures, n=3. *** indicates p=0.0001 using 2-tailed t- test with equal variance. **B)** Western blot images from three biological replicate experiments (new infection and selection) of HBEC3KT with control virus (EV) or virus over-expressing CBS. H3 is the loading control. **C)** Quantification of three independent Western blots for each biological replicate, n=9. **** indicates p<0.00001 using 2-tailed t- test with equal variance. ** indicates p=0.001 using 2-tailed t- test with equal variance. *** indicates p=0.0003 using 2-tailed t- test with equal variance. Western blot analysis was conducted by Kassandra Naughton.

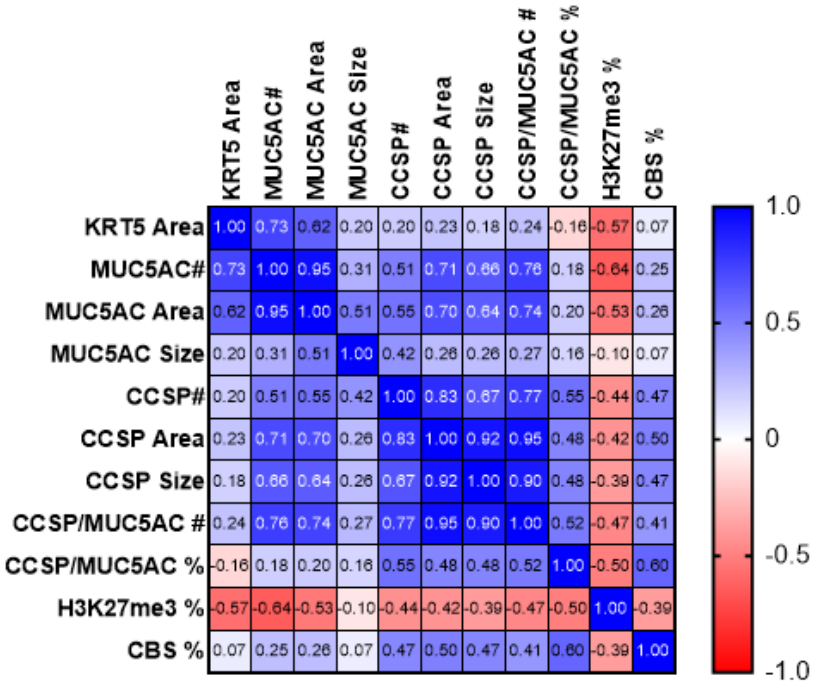

Figure 3.10 Correlation Plots of normal and COPD patient derived tissues

Pearson's Correlation table showing the relationship between varying bronchial epithelial cell IF stains and expression of H3K27me3 and CBS in normal (n=9) and COPD (n=10) lung.

CHAPTER 4. EZH2 DEPLETED ORGANOIDS HAVE DECREASED SELF-RENEWAL AND INCREASED SQUAMOUS MORPHOLOGY

EZH2 is a 746 amino acid-long protein that works alone or with other proteins to influence transcription. Within the Polycomb Repressive Complex 2 (PRC2), EZH2 acts as a transcriptional repressor by facilitating H3K27me3 [13, 88, 89]. PRC2 is integral to homeostasis, as it maintains spatial and temporal gene expression throughout an organism's life. During embryonic development, this complex is crucial to stem cell fate decisions, as it regulates repression of homeotic genes [94]. With age, EZH2 expression typically decreases [95] and usually only increases to enable cell proliferation and survival [96]. Alternatively, PRC2 malfunction can bring about incongruous gene expression and result in diseases rooted in aberrant cell development [97-101]. Conversely, loss of EZH2 activity stifles lung endoderm development in mice due to its role in repressing lung stem cell-associated genes [103, 104]. These findings suggest that improper PRC2/EZH2 activity is important for cell development, fate, and function.

4.1 3-Dimensional organoid culture analysis elucidates the effects of dose dependent gene expression in vitro

In order to have temporal control over *Ezh2* expression in adult mice, we bred mice that possessed conditional floxed alleles of *Ezh2* with mice that possessed a tetracycline response element followed by *Cre* gene (**Figure 4.1**). These mice also have a reversible tetracycline trans-activator under the control of the ubiquitously and constitutively expressed *Rosa26* promoter. With this model, *Ezh2* was intact until doxycycline was administered via tissue culture media.

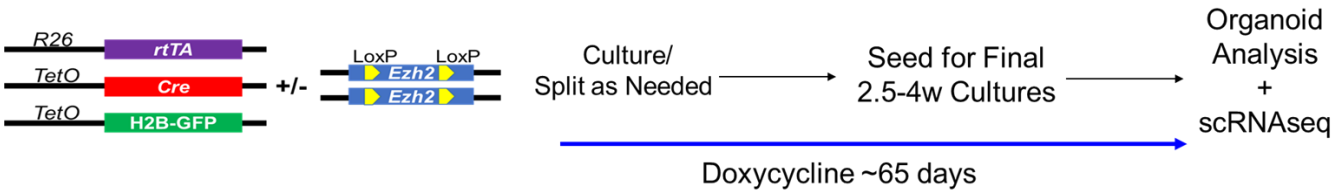

Figure 4.1 Mouse organoid treatment schematic

Schematic: Mouse bronchioalveolar stem cells (BASC) and alveolar type 2 cells were isolated, using fluorescence activated cell sorting (FACS), from doxycycline naïve mice that had no, one or two floxed alleles of *Ezh2*. Cells were cultured in air-liquid-interface Matrigel with neonatal mouse lung endothelial support cells. After organoids were established, the cells were switched to doxycycline media. Organoids were grown and passaged for approximately 5 weeks, then seeded at equal densities to grow for an additional 2.5-4 weeks based on the growth rate of the cultures in each experiment.

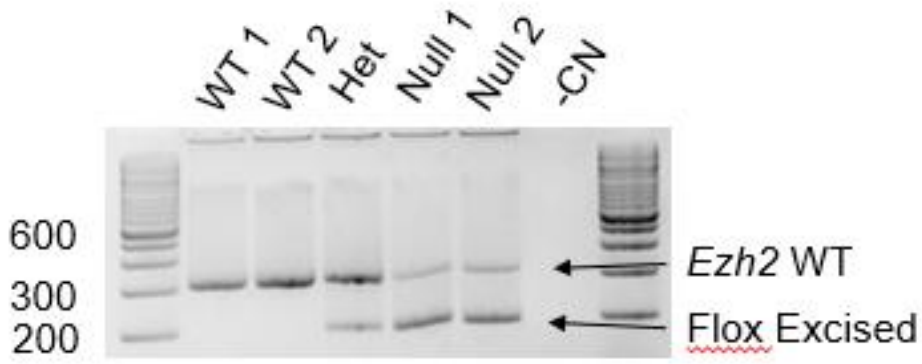

Figure 4.2 Mouse organoid genotype verification

Gel electrophoresis of *Ezh2* wild-type, heterozygous, and null organoids showing efficient recombination of *Ezh2* expression after doxycycline treatment. The *Ezh2* wild type bands present in the null lanes are from the co-cultured, mouse lung endothelial support cells which are *Ezh2* wild-type.

4.2 *Ezh2* null organoids lose self-renewal and replication capabilities

To understand how *Ezh2* expression alters mouse stem cell fate in culture, doxycycline was added to the media several days after cell seeding when primitive organoids had formed. Organoids were grown and passaged as needed in 3D culture, and at approximately 5 weeks of culture were seeded at equal densities to grow for an additional 2.5-4 weeks (**Figure 4.1**). We reasoned that this was sufficient time for loss of PRC2 activity to influence lineage fate decisions. We confirmed that *Ezh2* was excised in these cultures by PCR (**Figure 4.2**). From these final cultures, the number of *Ezh2* null organoids were significantly lower compared to *Ezh2* wild-type cultures ($p=0.0047$) (**Figure 4.3**). The diameter of *Ezh2* null organoids were significantly smaller than wild type when each organoid was considered a biological replicate, but not when averaged sizes per donor were compared (**Figure 4.4**).

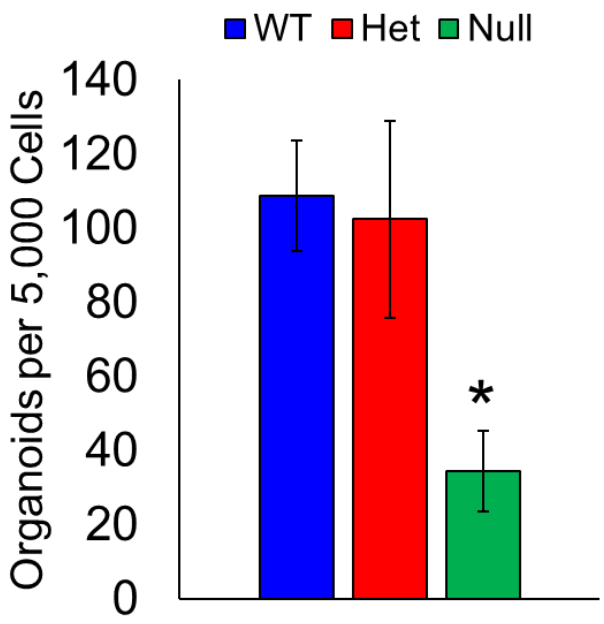

Figure 4.3 Mouse organoid count analysis

Average number of organoids represented of *Ezh2* wild type (n=7), heterozygous (n=10) and null (n=9) mouse donors, ** indicates p=0.0047 between *Ezh2* wild-type and *Ezh2* null organoids using ANOVA.

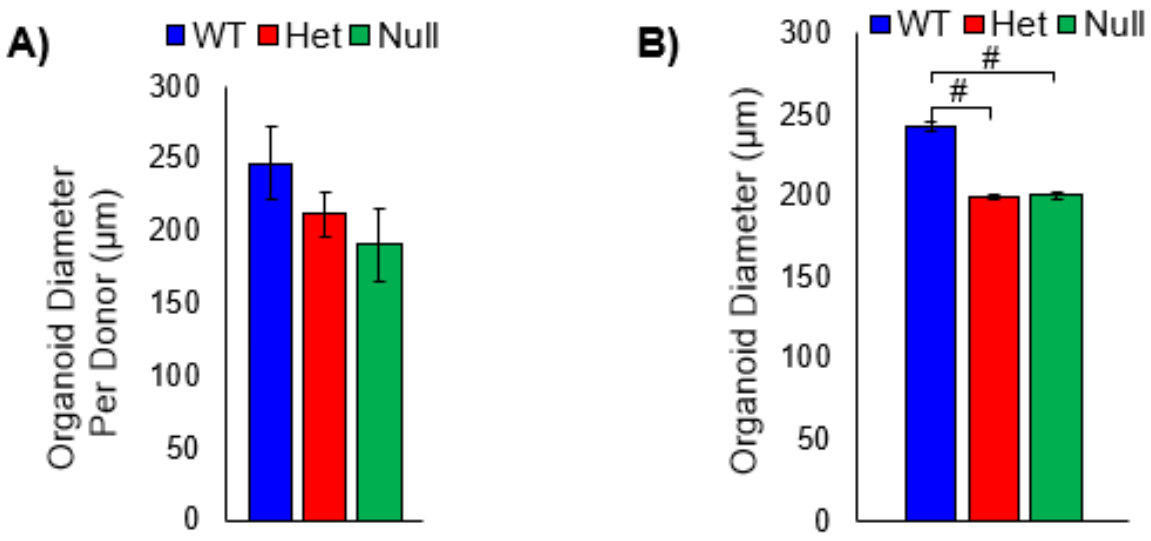

Figure 4.4 Mouse organoid diameter analysis

A) Average diameter of *Ezh2* wild-type (n=6), heterozygous (n=5), and null (n=4) organoids per donor. **B)** Average diameter of *Ezh2* wild type (n=1093), heterozygous (n=1452), and null (n=517) organoids per measured genotype. # indicates $p<0.0001$ using ANOVA.

4.3 Ezh2 null organoids gain squamous morphology

Organoid cultures were fixed, sectioned and stained for hematoxylin and eosin, CCSP, KRT5, Acetylated tubulin (ciliated cell marker), Pro-SPC (alveolar type 2 cell marker), EZH2, or H3K27me3 (**Figure 4.5;4.7**). When compared to wild-type, there was a significant increase in *Ezh2* null organoids with squamous morphology, characterized by stratified layers of KRT5+ cells (p=0.0124, **Figure 4.8B**). *Ezh2* null cells tended to form mixed organoids, while wild-type cells trended more towards a bronchiolar phenotype. However, due to heterogeneity among the organoid cultures, these results did not meet significance.

By quantitative nuclear immunohistochemistry, EZH2 and H3K27me3 expression levels were depleted in *Ezh2* null organoids compared to wild type (**Figure 4.5-4.6**). We also quantified the number of positively stained cells within each organoid and found that *Ezh2* null organoids had fewer acetylated tubulin positive cells, likely due to the decreased numbers of bronchiolar organoids (**Figure 4.8A**). These results suggests that *Ezh2* deletion could perturb lung cell differentiation and self-renewal, leading to decreased self-renewal and skewing of organoid subtype distributions.

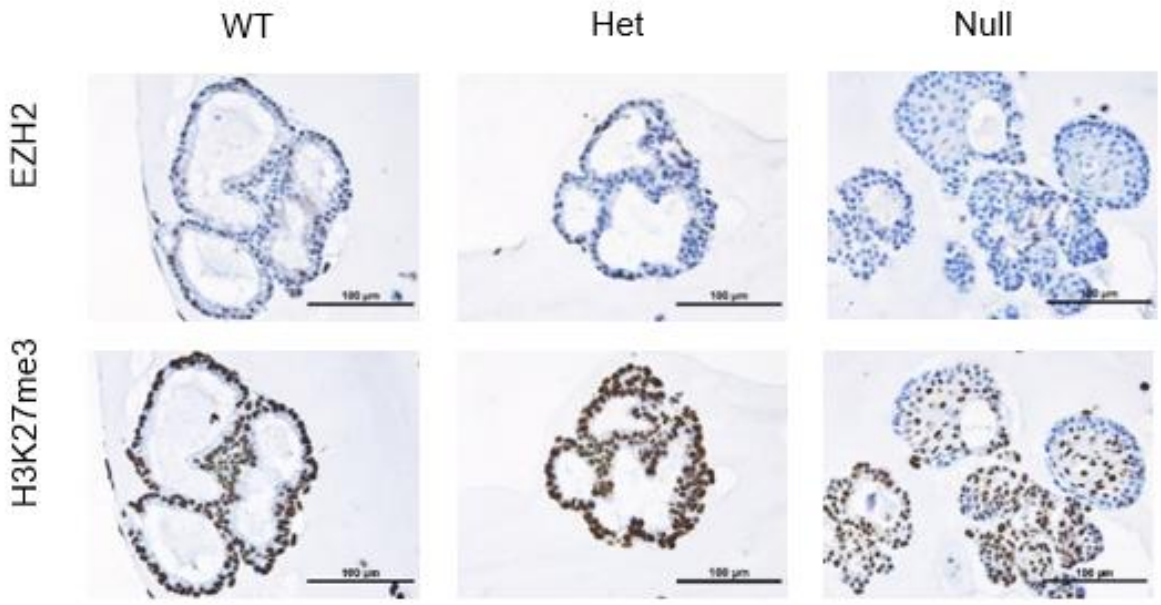

Figure 4.5 Mouse EZH2 and H3K27me3 immunohistochemistry representative images, scale bar = 100µm.

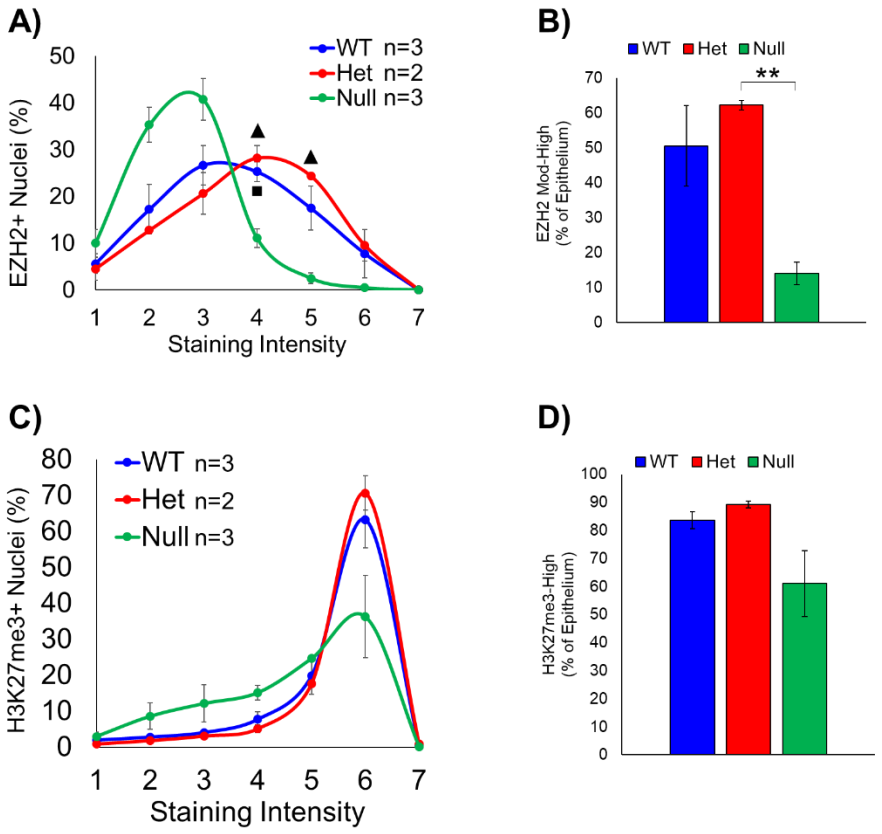

Figure 4.6 Mouse EZH2 and H3K27me3 immunohistochemistry analysis.

A) Average percentage of organoid nuclei expressing varying levels of EZH2 from *Ezh2* wild-type (n=3), heterozygous (n=2), and null (n=3) mouse donors. ■ indicates p=0.016 with a ANOVA comparing *Ezh2* wild-type to *Ezh2* null, and ▲ indicates p=0.0012 with a ANOVA comparing *Ezh2* heterozygous to *Ezh2* null. **B)** Average percentage of organoid cells expressing mod-high levels of EZH2, ** indicates p<0.0032 using ANOVA. **C)** Average percentage of organoid nuclei expressing varying levels of H3K27me3 from *Ezh2* wild-type (n=3), heterozygous (n=2), and null (n=3) mouse donors. **D)** Average percentage of organoid cells expressing high levels of H3K27me3. Mod-high expression is constituted as staining intensities 4-7, while high levels are staining instensities 5-7.

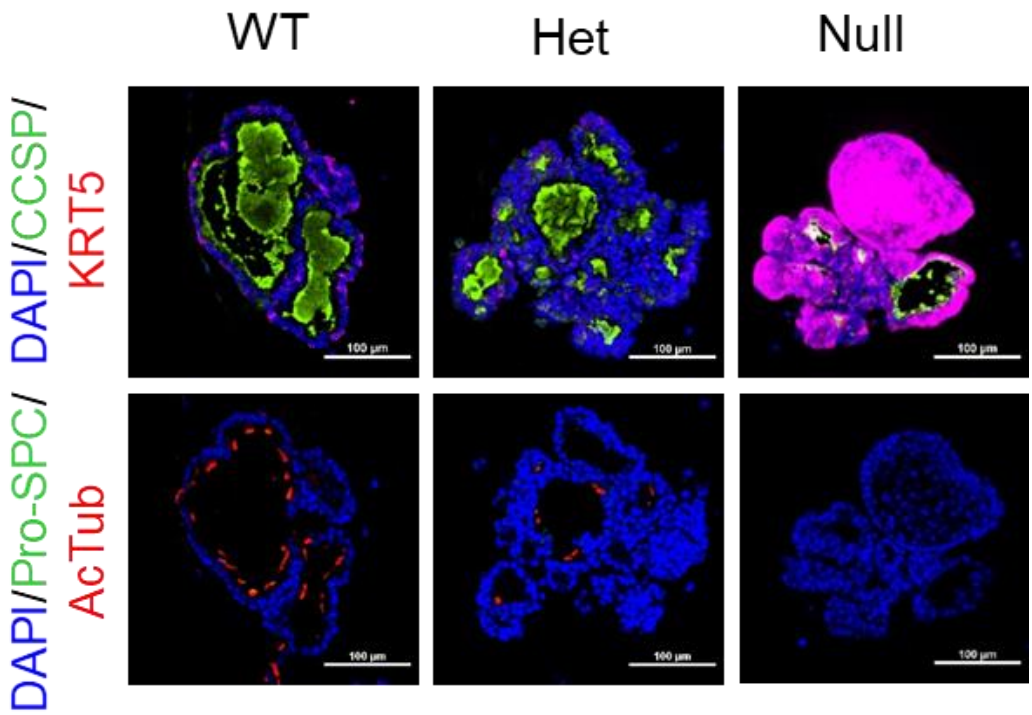

Figure 4.7 Mouse organoid immunofluourescence representative images, scale bar = 100µm.

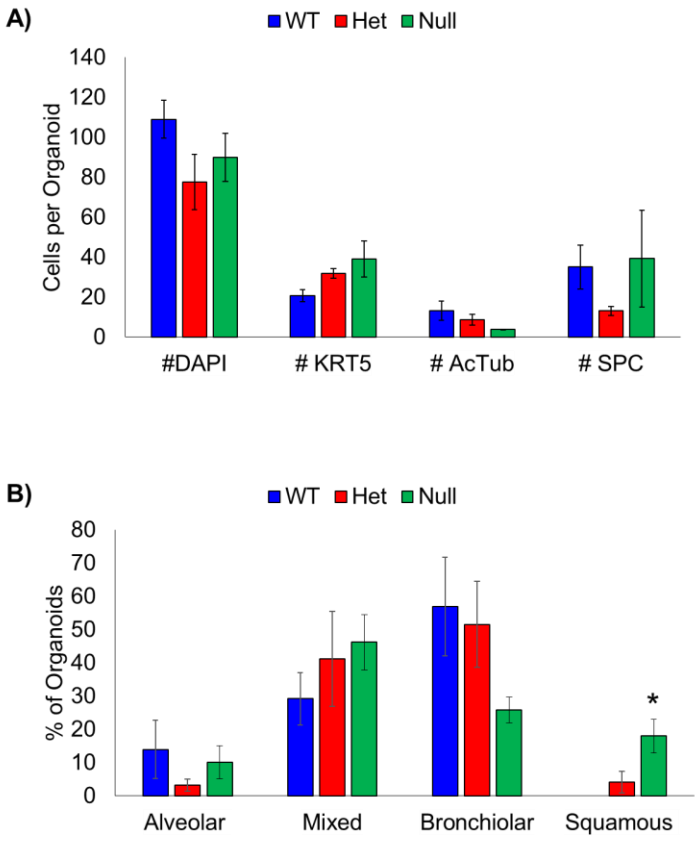

Figure 4.8 Mouse organoid immunofluorescence analysis

A) Average number of cells per organoid expressing basal cell marker, keratin 5 (KRT5), ciliated cell marker, acetylated tubulin (AcTub), and alveolar type 2 cell marker, surfactant protein C (SPC). Only organoids that had at least one positive cell for each marker were graphed. **B)** Average organoid type, based on IF and H&E stain evaluations of *Ezh2* wild type (n=4) and heterozygous (n=4) and null (n=3) mouse donors, * indicates p=0.0124 using ANOVA comparing *Ezh2* wild type and null.

CHAPTER 5. EZH2 DEPLETION RESULTS IN DISTINCT TRANSCRIPTIONALLY DEFINED CELL TYPES IN ORGANOID CULTURES

A cell's transcriptional profile indicates which genes are being expressed or not expressed at any given moment. In the laboratory, this expression pattern is determined through the isolation, quantification and sequencing of messenger ribonucleic acid (mRNA) through a process known as Single-Cell RNA sequencing (scRNA-seq). In short, a heterogeneous mixture of cells are separated in order to isolate their mRNA. The mRNA is then reverse transcribed and a complimentary DNA (cDNA) library is generated. Finally, the comparison of different cDNA libraries offer insight into unique cell subpopulations and ultimately into potential genetic variances among healthy and diseased tissues. Thanks to the innovation of scRNA-seq, great strides have recently been made in the field of pulmonary fibrosis (PF) [60, 62], chronic lung inflammation [61, 65], and chronic obstructive pulmonary disease *ex vivo* [64]. In the past, genome wide location analysis was employed to characterize the transcriptome of 2D cultured, human embryonic fibroblasts following Ezh2 siRNA transfection [94]. Given that 3D spheroid models have shown to be more physiologically relevant compared to 2D cultures [108], specifically regarding noticeable differences in differentiation and proliferation patterns, cell cross talk, and comparable gene expression patterns to *in vivo* experiments, we reasoned that transcriptional analysis of mouse-derived organoids would yield novel findings.

5.1 Single cell RNA sequencing reveals 15 unique cell types in murine lung organoids

To better characterize the heterogeneity of these organoid cultures, singe cell RNA-sequencing was conducted (**Figure 4.1**). Analysis of all cells captured from organoids of *Ezh2*

wild-type, heterozygous, and null cultures allowed for the identification of fifteen distinct lung cell populations that were characterized based on the expression of conserved hallmark genes (**Table 5.1-5.2; Figure 5.1**). Among the identified cells were basal cells, club cells, bronchioloalveolar stem cells, transitioning basal cells, ciliated cells, replicating and mitotic cells, and dead/dying cells. Interestingly, we identified a unique population of basal cells that express *Trp63* and *Itga6*, but had low expression of basal cell keratins *Krt5*, *Krt14* and, in particular, *Krt17*. We also identified the recently characterized *Krt17+/Krt8+* progenitor cell population that lacked expression of *Krt5*, but had strong expression of *Fn1* and *Ager* [60-62, 65].

5.2 Perturbation of Ezh2 expression in vitro drives changes in differentiation patterns and transcriptional programs

We next examined the proportions of each cell clusters based on *Ezh2* genotype (**Figure 5.4; 5.6**). We found that the *Ezh2* wild-type organoids were largely composed of *Trp63+*/*Krt17+* classical basal cells, cycling and transitioning basal cells, *Krt8+* progenitor cells, and club cells. In contrast, *Ezh2* null organoids were composed largely of *Trp63+/Krt17-* basal cells, cycling BASC, dead/dying cells, and cells transitioning into alveolar type 2 or bronchioalveolar stem cells. *Ezh2* heterozygous cultures contained all cell populations seen in the *Ezh2* wild-type and *Ezh2* null cultures. Relative gene expression analysis between genotypes showed a drastic loss in *Krt17* and *Sox9* when *Ezh2* expression was diminished ($p<0.0001$, **Figure 5.5**). Furthermore, loss of *Ezh2* expression was accompanied with an increased expression of the alveolar type 2 cell marker, *Lamp3* ($p<0.0001$), as well as *Foxp2* ($p<0.0001$), which is known to be involved in the alveolarization of developing mouse lung [126, 127]. *Ezh2* null BASC and club cells expressed higher levels of the goblet cell marker, *Muc5ac,* than *Ezh2* wild type cells ($p=0.001$). With the

exception of cells undergoing EMT, *Ezh2* wild-type and null cells exhibited significant differences in proportions of population (**Figure 5.6**). In particular, *Ezh2* null organoids contained significantly more dead/dying cells, suggesting a mechanism for the decreased organoid self-renewal.

In order to understand changes in transcriptional programs caused by *Ezh2* deletion in the predominant cell types, rank-ordered lists comparing *Ezh2* null to *Ezh2* wild type or *Ezh2* heterozygous to *Ezh2* wild type were constructed. Gene set enrichment analysis or these rank-ordered gene lists revealed that *Ezh2* null organoids had significant enrichment in gene programs associated with lung development, lung disease, epithelial to mesenchymal transition and lung cancers (**Figure 5.8; Table 5.3**). In addition to the same pathways enriched in *Ezh2* null cells, *Ezh2* heterozygous organoids also exhibited enrichment of inflammatory response pathways when compared to *Ezh2* wild type (**Figure 5.8**). To link these results to human samples, we next generated a list of significantly differentially expressed genes within the *Krt17*- basal cell populations by comparing *Ezh2* heterozygous to *Ezh2* wild type and *Ezh2* null to *Ezh2* wild type populations. We compared these gene signatures to a rank ordered gene list from smokers with severe emphysema compared to healthy smokers [128]. Interestingly, we found that genes highly enriched in *Krt17*- basal cells of *Ezh2* heterozygous and null organoids were also highly enriched in emphysemic lungs (**Figure 5.9)**. These data show the heterogeneous outcomes of depleting PRC2 activity while challenging lung stem and progenitor cells to proliferate and differentiate and suggest that *Ezh2* deficiency greatly decreases *Krt17*+ cell types including classical basal cells and *Krt8*+ progenitor cells. Furthermore, these changes in transcriptional states are enriched in human COPD patients [64]. Finally, in order to link our findings in the murine lung organoids to CBS over-expression in the human system, we generated rank ordered gene lists of *Ezh2* null vs wild

type, *Krt17*- and *Krt17*+ basal cell clusters and compared them to significantly differentially expressed genes of CBS overexpressing HBECs. Interestingly, gene set enrichment analysis revealed that genes highly expressed in CBS overexpressing HBECs were also highly enriched in *Ezh2* null, *Krt17*+ and *Krt17*- basal cells (**Figure 5.10**).

Table 5.1 Genes that define cell clusters from scRNA-seq analysis

Cell Type	Gene Name	Reference Number
Miochondrial (Dead/Dying)	*Mt-Co3*	6
	Mt-Atp6	6
	Mt-Cytb	6
	Mt-Nd4	6
Ciliated	*Ccdc153*	9,10
	Foxj1	3,5,8,9,10,15,17
	Tuba1a	5,17,18
EMT	*Col1a1*	3,4,14
	Col1a2	2,14
	Bgn	2,15
	Vim	2
Krt8 progenitor	*Fn1*	2,4,7
	Krt8	1,7,13
	Areg	7,13
AT2	*Lamp3*	7,9
	Sftpa1	1,8,13,14,16
	Sftpb	7,14,16
Proliferating/Cycling	*Top2a*	3,5,7,14,15,17,18
	Mki67	1,3,7,13,15,18
S Phase	*Mcm2*	11
	Mcm3	11
Club	*Scgb1a1*	3,4,5,9,10,13,15,17,18
	Scgb3a1	8,13,15
	Scgb3a2	4,8,13,18
	Cyp2f2	10,13,17
	Pigr	5,13,17
	Bpifa1	3
Goblet	*Muc5AC*	3,4,5,14,15,17
	Muc5B	3,4,10,15
	Tff2	10
	Agr2	2,3,5,10,17
Intermediate	*Aldh3a1*	This manuscript
	Il33	15,17
	Aqp3	3,17,18
Basal	*Krt17*	14,18
	Sox9	4,16
	Ngfr	12
	Krt5	3,14,15,16,17,18
	Krt14	3,16
	Itga6	5
	Trp63	3,10,15,16,17
	Dapl1	10

Table 5.2 Reference Numbers for Table 5.1

Table 5.1 Reference Number	
1	Choi et al. Inflammatory Signals Induce AT2 Cell-Derived Damage-Associated Transient Progenitors that Mediate Alveolar Regeneration. Cell Stem Cell 27, 366–382
2	Deprez et al. A Single-cell Atlas of the Human Healthy Airways. AJRCCM Articles in Press. Published July 29, 2020 as 10.1164/rccm.201911-2199OC
3	Garcia et al. Novel dynamics of human mucociliary differentiation revealed by single-cell RNA sequencing of nasal epithelial cultures. Development (2019) 146, dev177428. doi:10.1242/dev.177428
4	Habermann et al. Single-cell RNA sequencing reveals profibrotic roles of distinct epithelial and mesenchymal lineages in pulmonary fibrosis. Sci. Adv. 2020; 6 : eaba1972
5	Duclos G.E. et al. Characterizing smoking-induced transcriptional heterogeneity in the human bronchial epithelium at single-cell resolution. Sci.Adv. 5(12),eaaw3413. • DOI: 10.1126/sciadv.aaw3413
6	Ilicic et al. Classification of low quality cells from single-cell RNA-seq data. Genome Biology volume 17, Article number: 29 (2016)
7	Kobayashi Y et al., Persistence of a regeneration-associated, transitional alveolar epithelial cell state in pulmonary fibrosis. Nat Cell Biol. 2020 Aug;22(8):934-946. doi: 10.1038/s41556-020-0542-8. Epub 2020 Jul 13. PMID: 32661339; PMCID: PMC7461628.
8	Li X et al. Single cell RNA sequencing identifies IGFBP5 and QKI as ciliated epithelial cell genes associated with severe COPD. Respir Res. 2021 Apr 6;22(1):100. doi: 10.1186/s12931-021-01675-2. PMID: 33823868; PMCID: PMC8022543.
9	Liu Q et al. Lung regeneration by multipotent stem cells residing at the bronchioalveolar-duct junction. Nat Genet 2019 Apr;51(4):728-738. doi: 10.1038/s41588-019-0346-6. Epub 2019 Feb 18.
10	Montoro et al. A revised airway epithelial hierarchy includes CFTR-expressing ionocytes. Nature. Author manuscript; available in PMC 2019 Feb 1.
11	Riba, et al. Cell cycle gene regulation dynamics revealed by RNA velocity and deep-learning. bioRxiv 2021.03.17.435887; doi: https://doi.org/10.1101/2021.03.17.435887
12	Rock JR, Onaitis MW, Rawlins EL, Lu Y, Clark CP, Xue Y, Randell SH, Hogan BL. Basal cells as stem cells of the mouse trachea and human airway epithelium. Proc Natl Acad Sci U S A. 2009 Aug 4;106(31):12771-5. doi: 10.1073/pnas.0906850106. Epub 2009 Jul 22. PMID: 19625615; PMCID: PMC2714281.
13	Strunz M et al. Alveolar regeneration through a Krt8+ transitional stem cell state that persists in human lung fibrosis. Nat Commun. 2020 Jul 16;11(1):3559. doi: 10.1038/s41467-020-17358-3. PMID: 32678092; PMCID: PMC7366678.
14	Travaglini KJ, et al. A molecular cell atlas of the human lung from single-cell RNA sequencing. Nature. 2020 Nov;587(7835):619-625. doi: 10.1038/s41586-020-2922-4. Epub 2020 Nov 18. PMID: 33208946; PMCID: PMC7704697.
15	Vieira Braga et al. A cellular census of human lungs identifies novel cell states in health and in asthma Nature Medicine | VOL 25 | JULY 2019 | 1153–1163 | www.nature.com/naturemedicine
16	Xu et al. Single-cell RNA sequencing identifies diverse roles of epithelial cells in idiopathic pulmonary fibrosis. JCI Insight 2016 Dec 8;1(20):e90558. doi: 10.1172/jci.insight.90558.
17	Zuo WL et al. Cell-specific expression of lung disease risk-related genes in the human small airway epithelium. Respir Res. 2020 Jul 29;21(1):200. doi: 10.1186/s12931-020-01442-9. PMID: 32727470; PMCID: PMC7389881.
18	Hawkins FJ et al. Derivation of Airway Basal Stem Cells from Human Pluripotent Stem Cells. Cell Stem Cell 2021 Jan 7;28(1):79-95.e8. doi: 10.1016/j.stem.2020.09.017. Epub 2020 Oct 23.

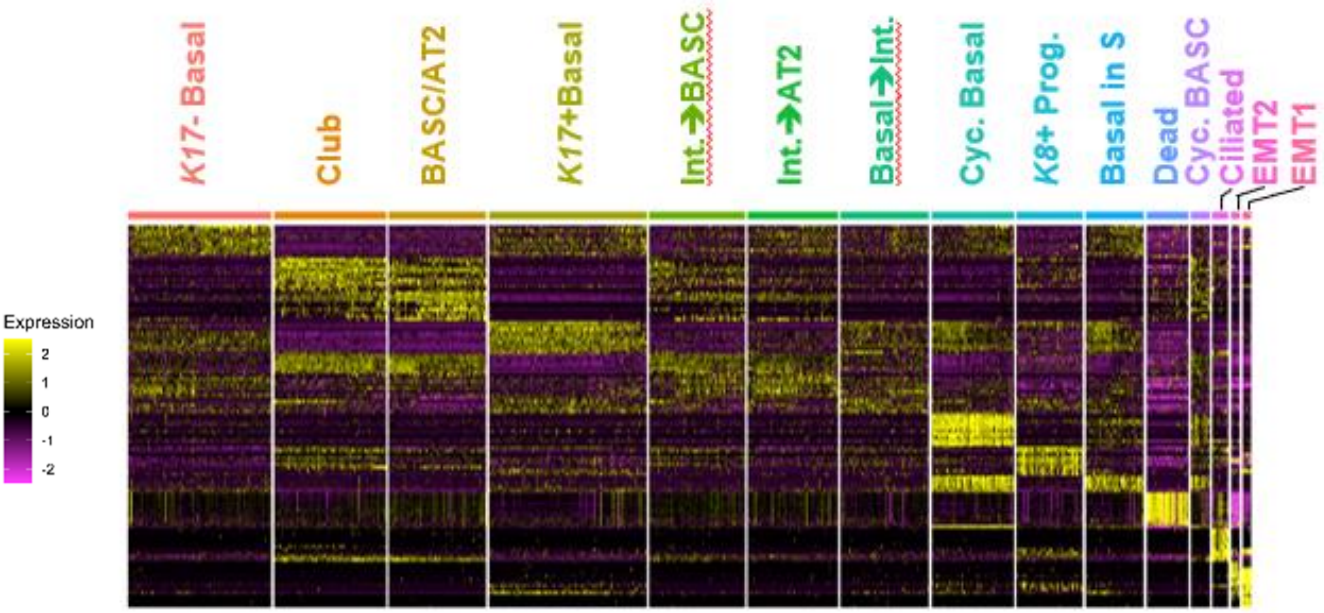

Figure 5.1 Subpopulations Heat Map

Heat map depicting differential gene expression among the 15 identified cell populations. Yellow indicates highly expressed. Heat map was generated by Xufeng Qu and Jinze Liu.

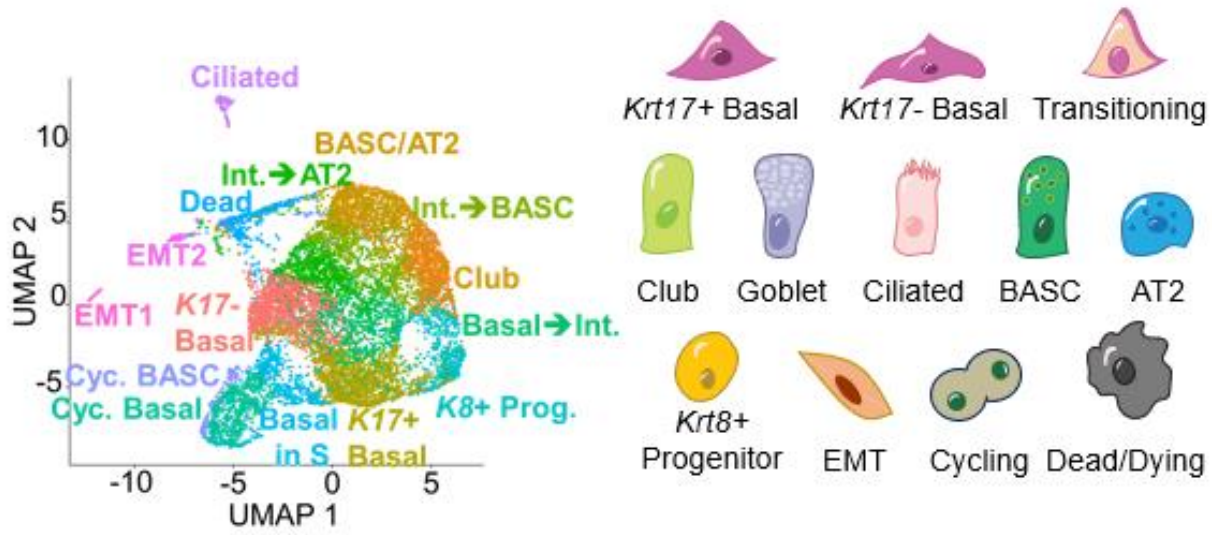

Figure 5.2 Subpopulations Umap

UMAP plot of *Ezh2* wild type, heterozygous, and null organoids annotated with their identified cell types and representative cartoon. Umap was generated by Xufeng Qu and Jinze Liu.

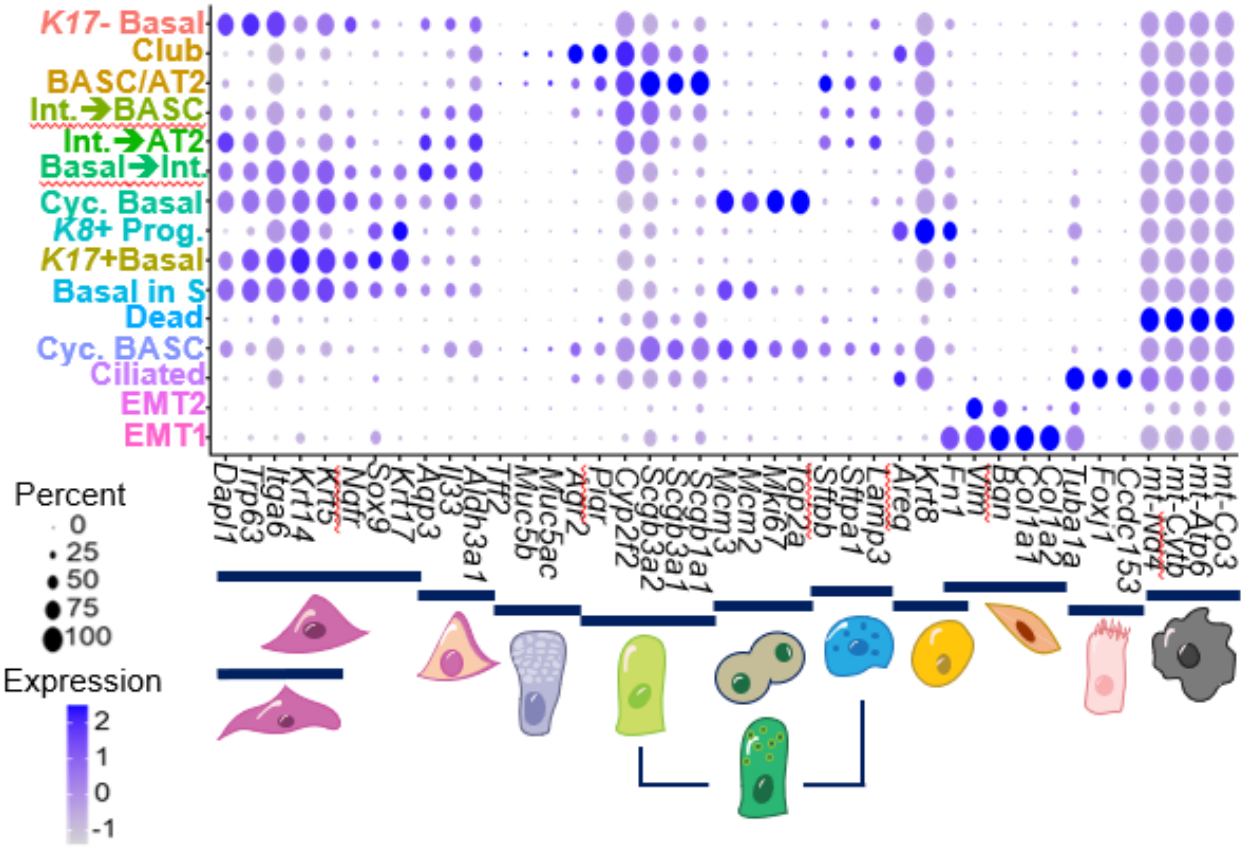

Figure 5.3 Subpopulations Dot Plot

Dot plot showing the relative expression of marker genes (x-axis) and their respective cell types (y-axis). Representative cell types are positioned below their respective gene hallmarks. Dot plot was generated by Xufeng Qu and Jinze Liu.

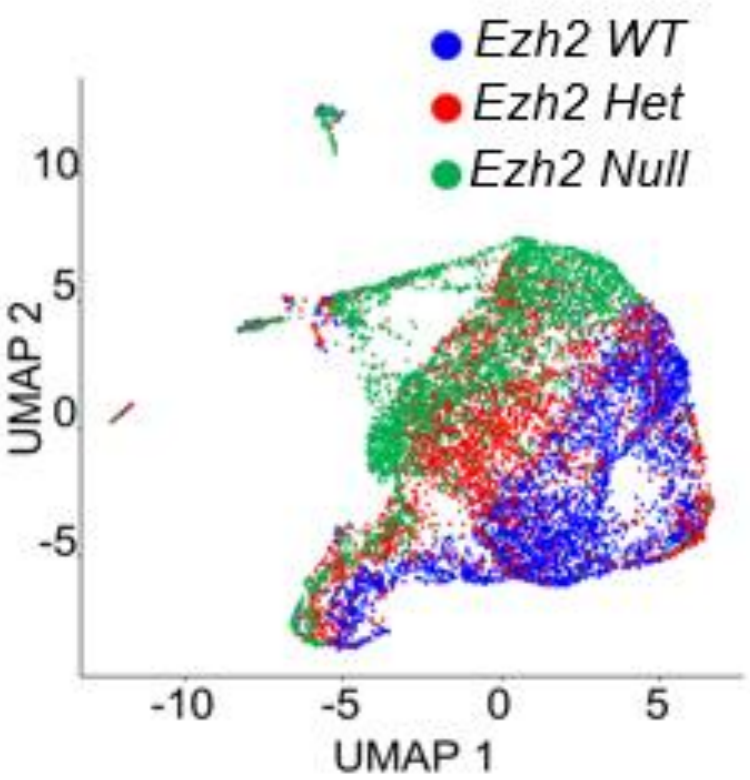

Figure 5.4 Subpopulations Distribution Umap

UMAP plot of *Ezh2* wild type, heterozygous, and null organoids showing a heterogeneous distribution of cell clusters across genotypes. UMap was generated by Xufeng Qu and Jinze Liu.

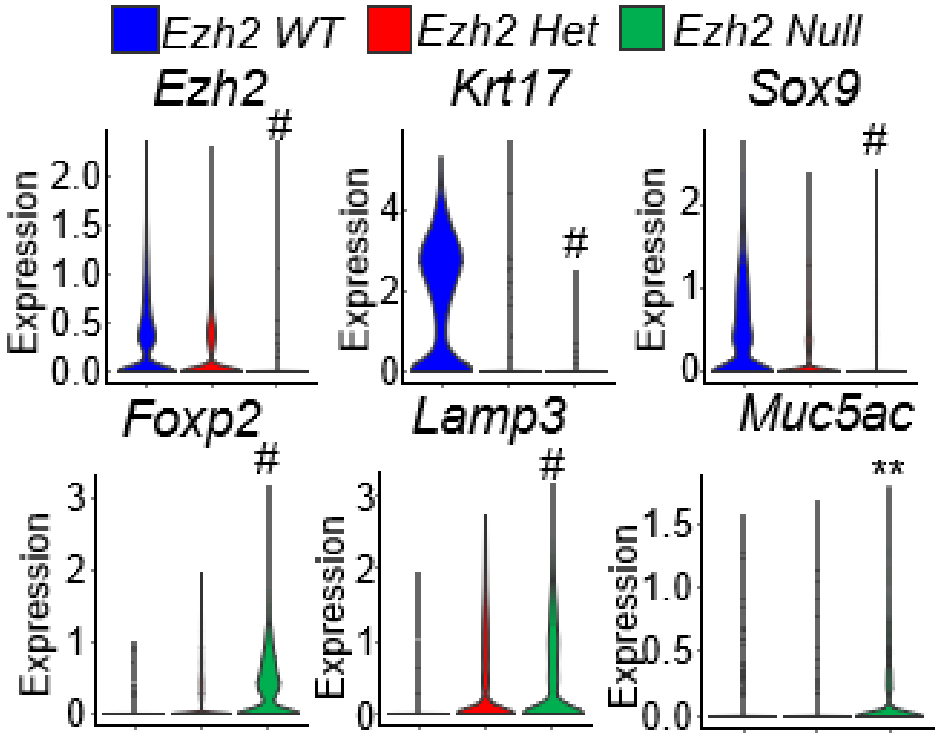

Figure 5.5 Gene Expression Violin Plots

Violin plots showing the relative abundance of gene expression across genotypes. # indicates adjusted p<0.0001 comparing wild type to null organoids. Relative *Muc5ac* expression was quantified in club and basal cells. ** indicates p=0.001 comparing *Ezh2* wild type to *Ezh2* null organoids. Expression plots were generated by Xufeng Qu and Jinze Liu.

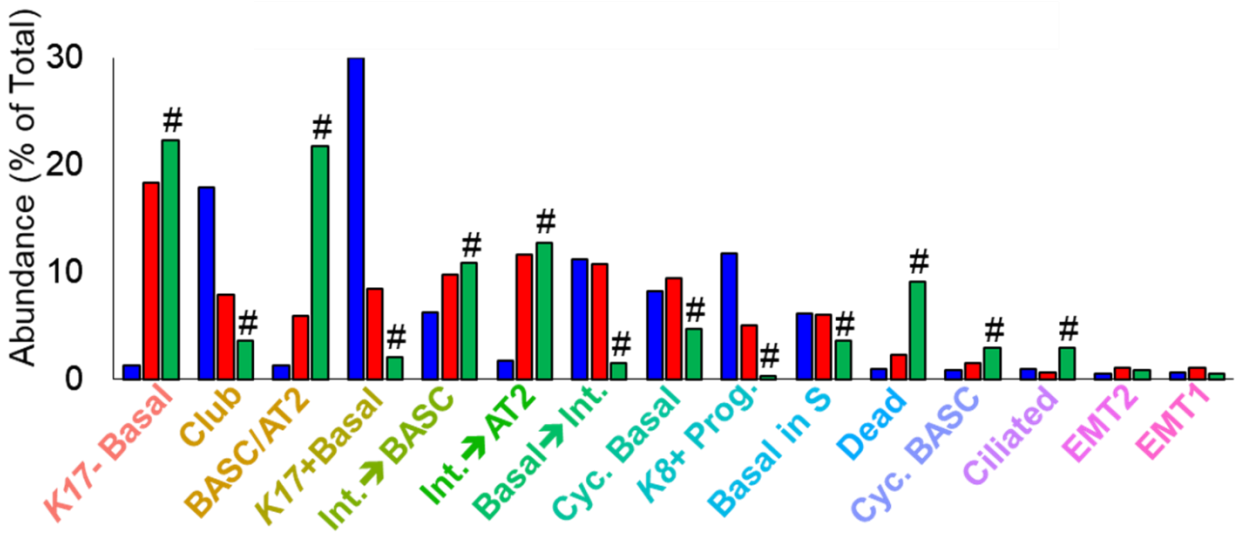

Figure 5.6 Subpopulations Distribution Bar Graph

Bar graph showing the distribution of cell clusters across genotypes. # indicates adjusted $p<0.0001$ for ratio differences based on z-test. Bar plot was generated by Xufeng Qu and Jinze Liu.

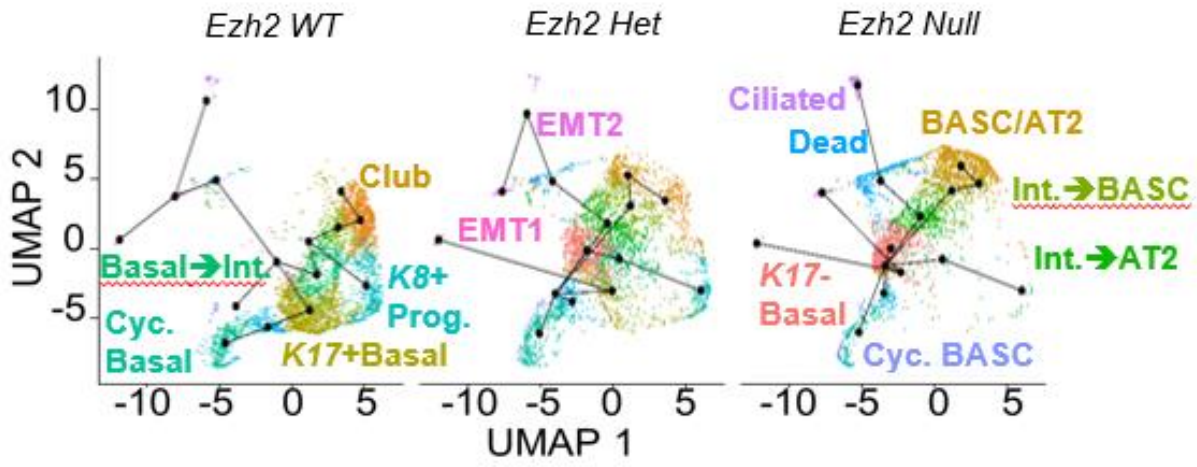

Figure 5.7 Subpopulations Distribution Umaps with Trajectories

Annotated Uniform Manifold Approximation and Projection (UMAP) plots showing distinct differences in cell clusters and trajectories across genotypes. Umaps were generated by Xufeng Qu and Jinze Liu.

Table 5.3 Selected MSigDB Gene Signatures	Designated Signature Associations
GOBP_GLAND_MORPHOGENESIS.grp	Lung Development
GOBP_LUNG_ALVEOLUS_DEVELOPMENT.grp	
GOBP_LUNG_EPITHELIUM_DEVELOPMENT.grp	
GOBP_OUTFLOW_TRACT_SEPTUM_MORPHOGENESIS.grp	
GOBP_REGULATION_OF_STEM_CELL_DIFFERENTIATION.grp	
GOBP_RESPIRATORY_GASEOUS_EXCHANGE_BY_RESPIRATORY_SYSTEM.grp	
HP_ABNORMAL_BREATH_SOUND.grp	Lung Disease
HP_ABNORMAL_PULMONARY_INTERSTITIAL_MORPHOLOGY.grp	
HP_ABNORMAL_PULMONARY_THORACIC_IMAGING_FINDING.grp	
HP_BRONCHITIS.grp	
HP_CHRONIC_LUNG_DISEASE.grp	
HP_COUGH.grp	
HP_NEONATAL_RESPIRATORY_DISTRESS.grp	
HP_PNEUMONIA.grp	
HP_PNEUMOTHORAX.grp	
HP_PULMONARY_INFILTRATES.grp	
HP_RESPIRATORY_FAILURE.grp	
WANG_BARRETTS_ESOPHAGUS_UP.grp	
WP_LUNG_FIBROSIS.grp	
GOBP_REGULATION_OF_RESPONSE_TO_WOUNDING.grp	Epithelial-Mesenchymal Transition (EMT)
GOBP_REGULATION_OF_WOUND_HEALING.grp	
GOBP_RESPONSE_TO_WOUNDING.grp	
GOBP_WOUND_HEALING.grp	
HALLMARK_EPITHELIAL_MESENCHYMAL_TRANSITION.grp	
HALLMARK_TGF_BETA_SIGNALING.grp	
JECHLINGER_EPITHELIAL_TO_MESENCHYMAL_TRANSITION_UP.grp	
CROMER_TUMORIGENESIS_UP.grp	Cancer
HUPER_BREAST_BASAL_VS_LUMINAL_UP.grp	
KEGG_BASAL_CELL_CARCINOMA.grp	
KEGG_BLADDER_CANCER.grp	
KEGG_NON_SMALL_CELL_LUNG_CANCER.grp	
KEGG_PATHWAYS_IN_CANCER.grp	
KEGG_SMALL_CELL_LUNG_CANCER.grp	
ZHONG_SECRETOME_OF_LUNG_CANCER_AND_FIBROBLAST.grp	
GOBP_ADAPTIVE_IMMUNE_RESPONSE_BASED_ON_SOMATIC_RECOMBINATION_OF_IMMUNE_RECEPTORS_BUILT_FROM_IMMUNOGLOBULIN_SUPERFAMILY_DOMAINS.grp	Inflammatory Response
GOBP_ANTIGEN_PROCESSING_AND_PRESENTATION_OF_EXOGENOUS_PEPTIDE_ANTIGEN_VIA_MHC_CLASS_I.grp	
GOBP_ANTIGEN_PROCESSING_AND_PRESENTATION_OF_PEPTIDE_ANTIGEN_VIA_MHC_CLASS_I.grp	
GOBP_CYTOKINE_PRODUCTION_INVOLVED_IN_IMMUNE_RESPONSE.grp	
GOBP_INTERFERON_GAMMA_PRODUCTION.grp	
GOBP_TUMOR_NECROSIS_FACTOR_MEDIATED_SIGNALING_PATHWAY.grp	
HALLMARK_IL6_JAK_STAT3_SIGNALING.grp	
HALLMARK_INFLAMMATORY_RESPONSE.grp	
HALLMARK_INTERFERON_ALPHA_RESPONSE.grp	
HALLMARK_INTERFERON_GAMMA_RESPONSE.grp	
HALLMARK_TNFA_SIGNALING_VIA_NFKB.grp	
REACTOME_CROSS_PRESENTATION_OF_SOLUBLE_EXOGENOUS_ANTIGENS_ENDOSOMES.grp	
REACTOME_INTERLEUKIN_4_AND_INTERLEUKIN_13_SIGNALING.grp	
SANA_RESPONSE_TO_IFNG_UP.grp	
WUNDER_INFLAMMATORY_RESPONSE_AND_CHOLESTEROL_UP.grp	

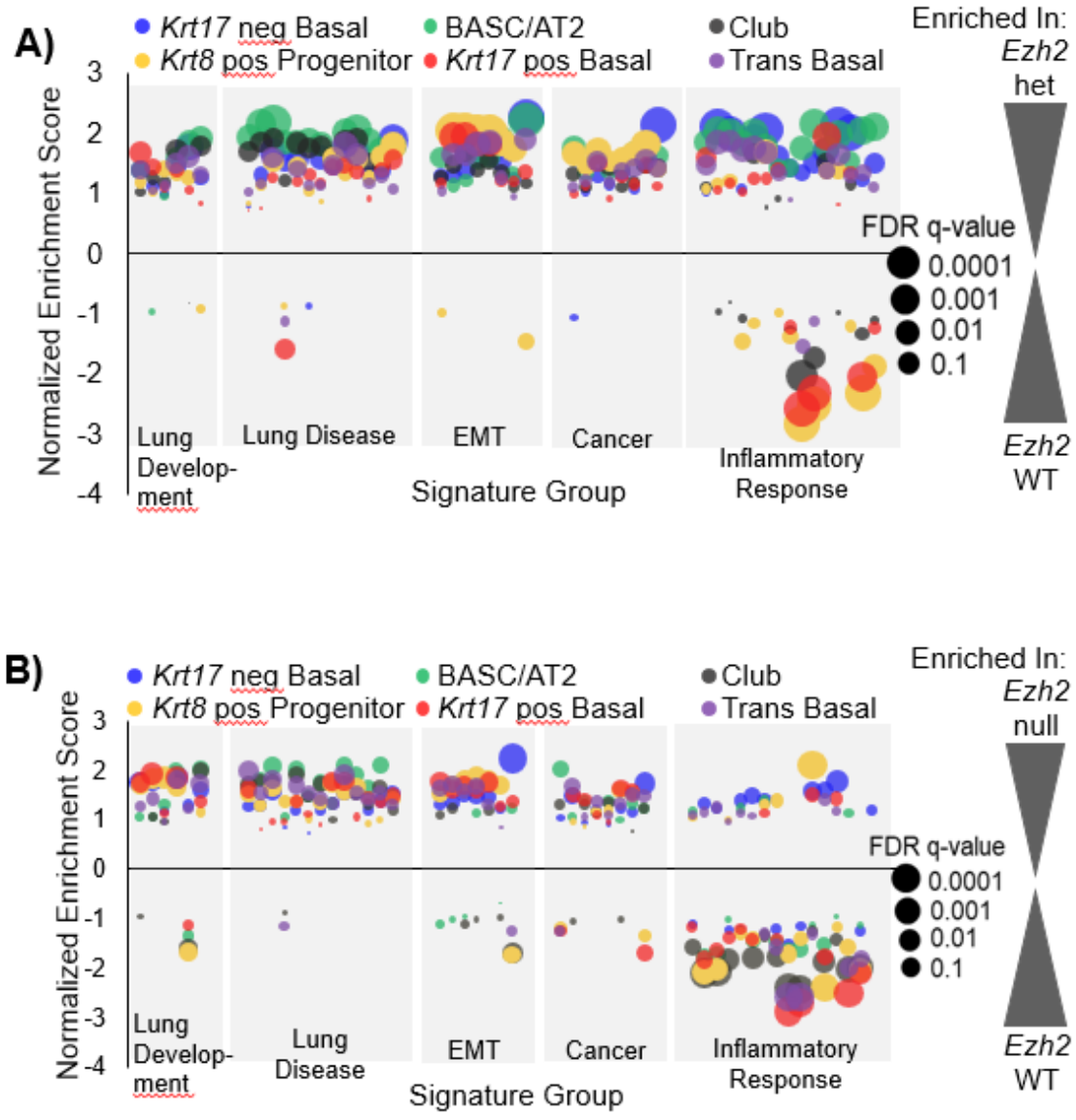

Figure 5.8 Select Subpopulations Enrichment Score Maps

A) Dot plot showing gene normalized enrichment scores (y-axis) and false discovery rates (bubble size) between Ezh2 heterozygous and wild type clusters. B) Dot plot showing gene normalized enrichment scores (y-axis) and false discovery rates (bubble size) between *Ezh2* null and wild type clusters.

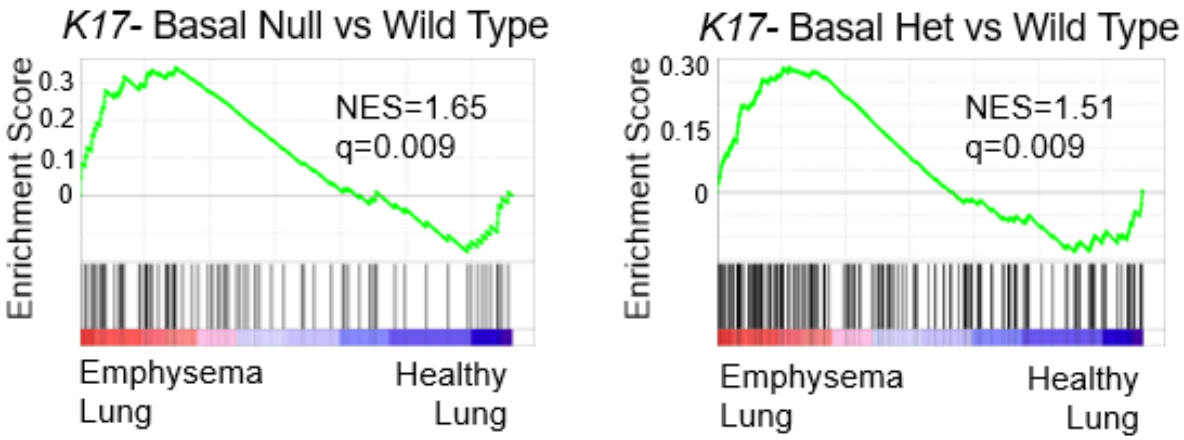

Figure 5.9 Organoids and Human Lung Tissue V. Organoids Gene Set Enrichment Analysis

Gene set enrichment analysis showing similarities in transcription profiles of Krt17- basal cells in mouse organoids and emphysema human lung.

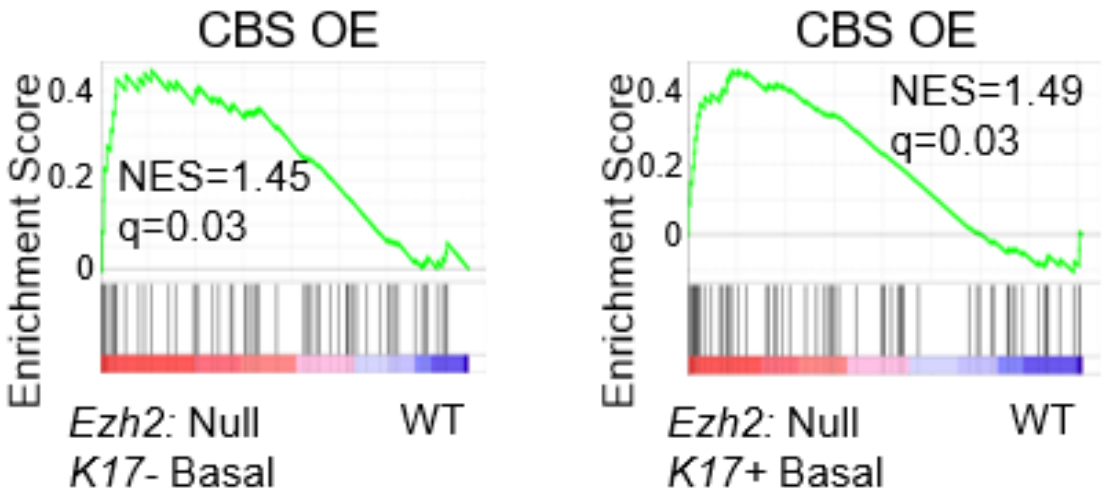

Figure 5.10 Human Bronchiolar Epithelial Cells V. Organoids Gene Set Enrichment Analysis

GSEA showing similarities in transcription profiles of *Krt17*+ and *Krt17*- null mouse organoids and HBECs overexpressing CBS (CBS OE). RNA sequence analysis on CBS overexpressing organoids was conducted by Jinpeng Liu.

CHAPTER 6. *EZH2* HETEROZYGOUS MICE EXPOSED TO OVALBUMIN EXHIBIT INCREASED BRONCHIOLAR RESPONSE

Inflammation is a major pathological entity of COPD, and ovalbumin inhalation by mice elicits a phenotype similar to COPD, noted with temporary epithelium wall thickening and goblet cell secretion [129]. Given that epigenetic modifications is a plastic phenomenon that occurs over time, we decided to employ murine models to evaluate the role of EZH2 in epithelial cell resolution following allergic inflammation.

6.1 Mouse lung analysis elucidates the effects of dose dependent gene expression in vivo

In order to elucidate how *Ezh2* expression alters bronchiolar lung cell fate decisions *in vivo*, we established cohorts of adult mice that were administered doxycycline through *ad libitum* water for a period of 4 months (**Figure 6.1**). We reasoned this was sufficient time for lung epithelial cell turnover that could be altered in the absence of proper PRC2 function. Tail DNA from these mice showed nearly complete recombination of *Ezh2* (**Figure 6.2**).

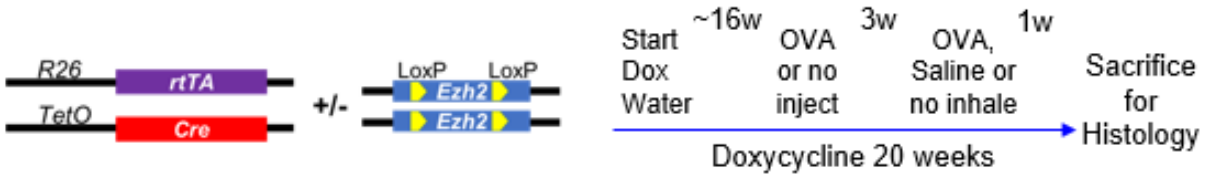

Figure 6.1 Mouse treatment schematic

Schematic: *Ezh2* conditional knockout mice were generated using a Tet-on system. Mice ingested doxycycline water (Dox Water) ad libitum throughout the experiment, underwent two separate ovalbumin (OVA) intraperitoneal injections or no OVA injection, then received a single inhalation treatment of OVA, saline or no inhalation, and were sacrificed the following week.

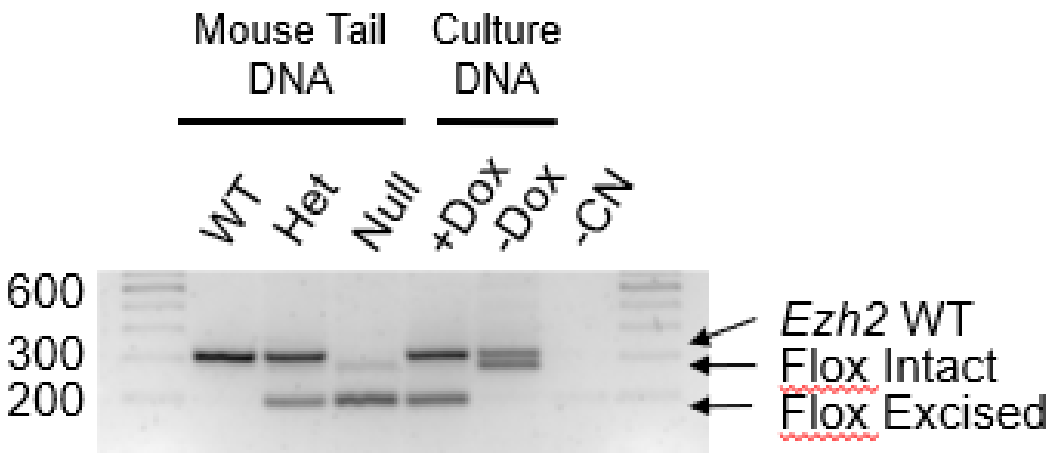

Figure 6.2 Mouse Genotype Verification

Gel electrophoresis of *Ezh2* wild-type, heterozygous, and null mouse tail DNA showing recombination of *Ezh2* floxed alleles. Culture DNA is from 3D Matrigel, co-cultured *Ezh2* null bronchioalviolar stem cells and neonatal mouse lung endothelial cells treated with doxycycline (+Dox) and without (-Dox).

6.2 Ovalbumin significantly up regulates mucus secretion and lung epithelium width in Ezh2 heterozygous mice

To investigate the role of PRC2 in how bronchiolar lung epithelium responds to inflammatory signals and how the epithelium resolves after this response, we sensitized mice by injecting ovalbumin (OVA), challenged mice with aerosolized OVA, and conducted immunostaining on the whole lung (**Figure 6.3;6.4;6.7**). In non-challenged mice, there were no obvious differences in bronchiolar lung epithelial morphology among the three *Ezh2* genotypes. When examining the OVA-challenged mice, we first noticed that the bronchiolar epithelium of *Ezh2* wild type and heterozygous mice showed signs of an allergic response to OVA, while the epithelia of *Ezh2* null mice did not. Given that our approach was not tissue or cell specific, this result is consistent with a loss of OVA response in mice where *Ezh2* has been depleted in T cells [130]. Despite the lack of OVA response in *Ezh2* null mice, Alcian Blue staining revealed that OVA challenged *Ezh2* heterozygous mice were the only genotype to exhibit a very significant increase in mucin production in the bronchiolar epithelium when compared to OVA challenged *Ezh2* null mice ($p=0.0009$, **Figure 6.5**). Furthermore, bronchiolar lung epithelium was significantly wider in OVA challenged *Ezh2* heterozygous mice when compared to OVA challenged *Ezh2* null ($p=0.0012$) mice (**Figure 6.6**).

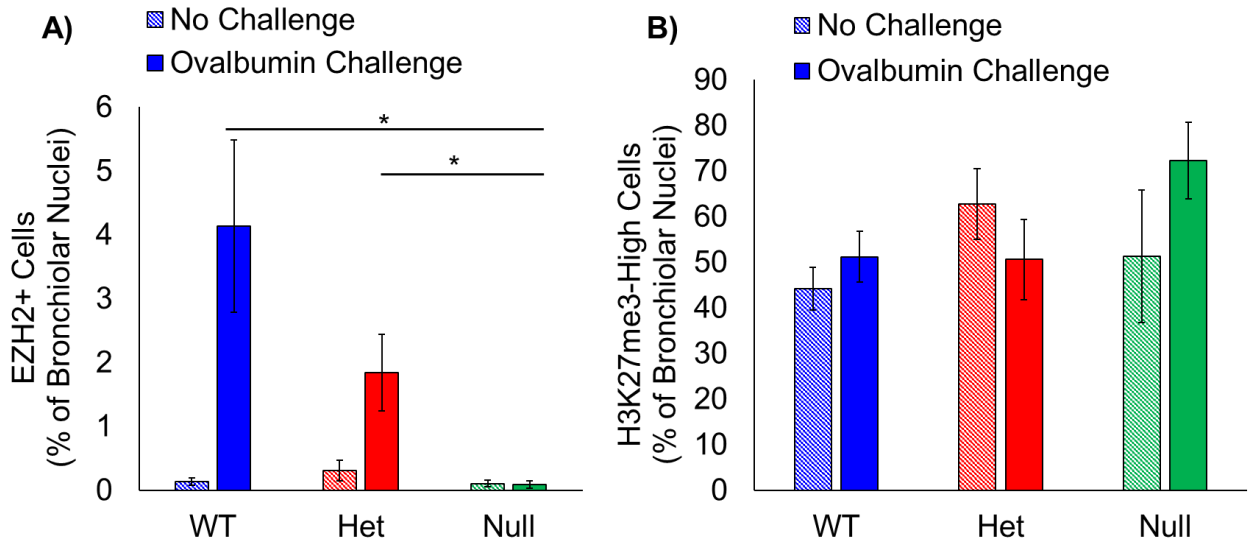

Figure 6.3 Mouse lung H3K27me3 and EZH2 immunohistochemistry analysis

A) Average percentage of epithelial cells expressing moderate to high levels of EZH2, * indicates $p<0.041$ using ANOVA comparing ovalbumin challenged *Ezh2* wild type to *Ezh2* null and *Ezh2* heterozygous to *Ezh2* null. **B)** Average percentage of cells expressing moderate to high levels of H3K27me3. Analysis is based on *Ezh2* wild type (n=6), heterozygous (n=11), and null (n=5) that received saline or were no challenge, and *Ezh2* wild type (n=9), heterozygous (n=10), and null (n=6) mice that received OVA challenge. Throughout, WT indicates *Ezh2* wild-type, Het indicates *Ezh2* heterozygous and Null indicates *Ezh2* null.

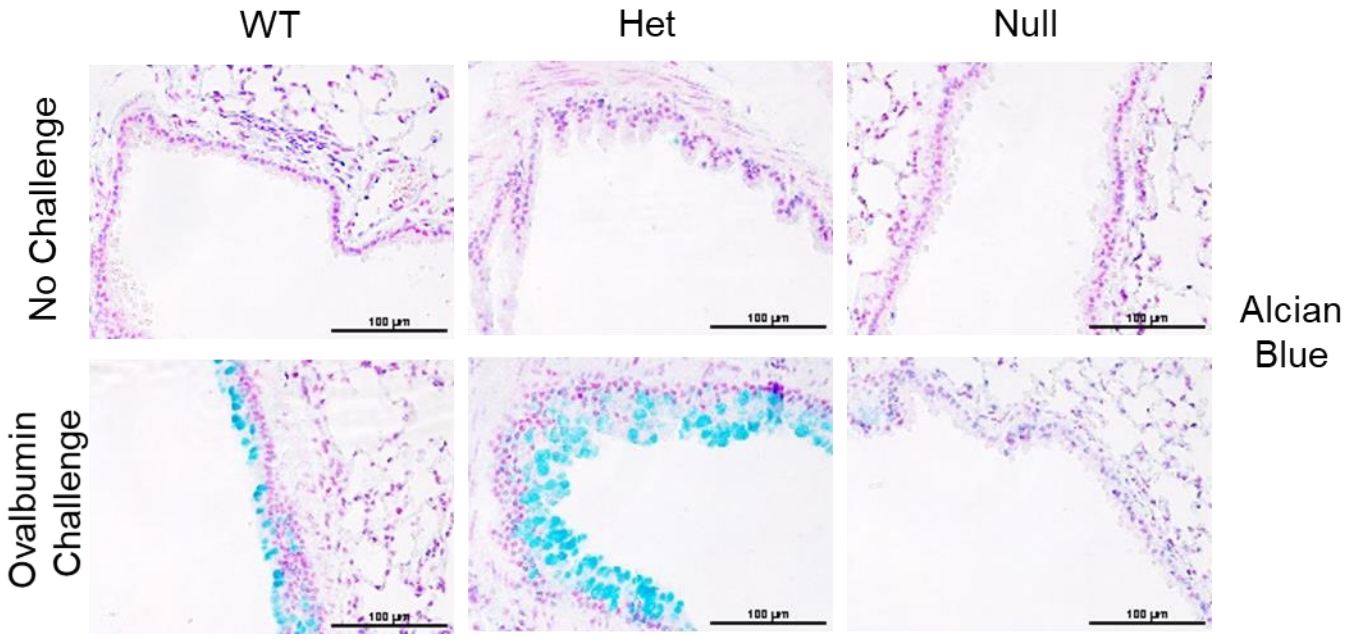

Figure 6.4 Mouse lung Alcian Blue stain representative images

Representative images of whole mouse lung Alcian Blue stains, scale bar = 100µm.

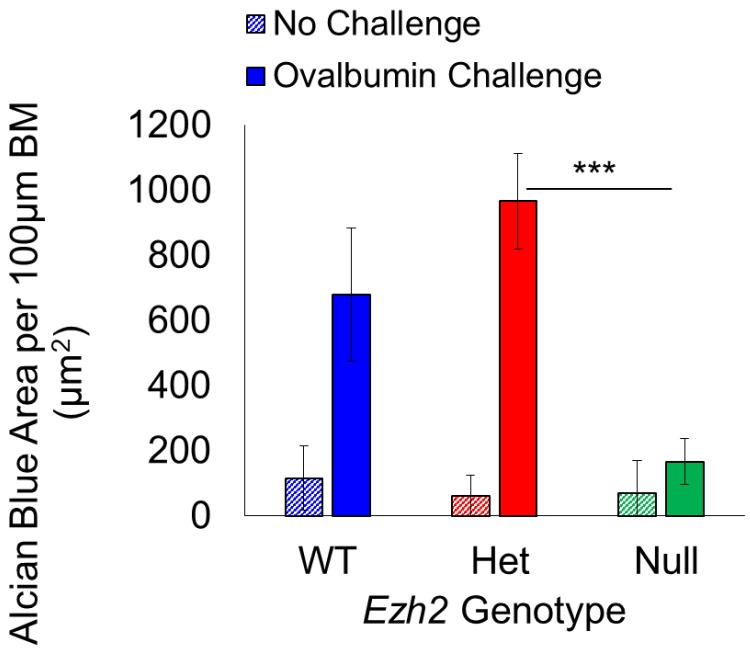

Figure 6.5 Mouse lung Alcian Blue stain analysis

Average area of Alcian Blue stain within mouse lung epithelium, *** indicates p=0.0009 using ANOVA comparing ovalbumin challenged *Ezh2* heterozygous to ovalbumin challenged *Ezh2* null.

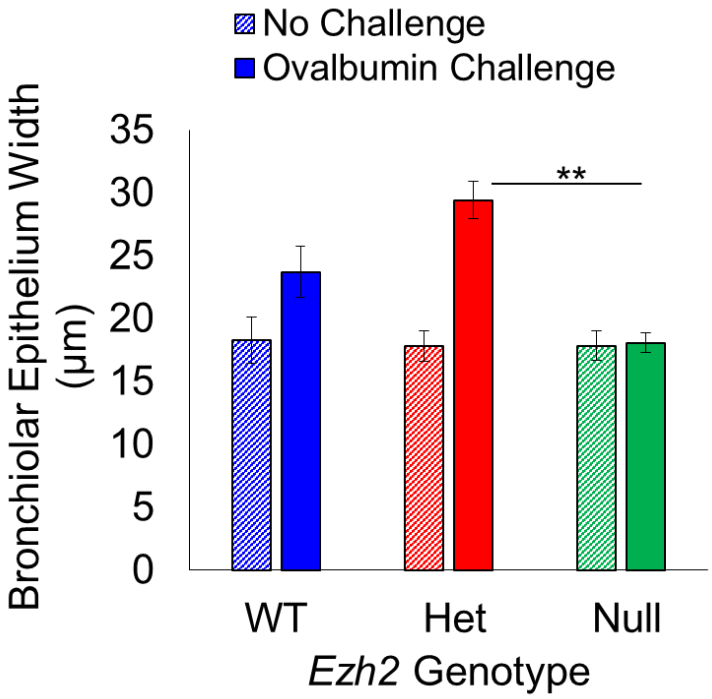

Figure 6.6 Mouse lung bronchiolar epithelium width analysis

Average width of bronchial epithelium, *** indicates $p<0.0001$ using ANOVA comparing ovalbumin challenged *Ezh2* heterozygous to ovalbumin challenged *Ezh2* null.

6.3 Partial loss of Ezh2 expression is associated with aberrant club and goblet cell differentiation

Compared to *Ezh2* wild type and *Ezh2* null mice, OVA challenged *Ezh2* heterozygous mice possessed a significantly higher number of MUC5AC+ cells ($p=0.0494$, $p<0.0001$) and CCSP+ cells ($p=0.0069$, $p<0.0001$) in the bronchiolar epithelium (**Figure 6.8**). Consistent with a transdifferentiation of club cells to mucus producing cells, OVA challenged *Ezh2* heterozygous mice also had significantly higher percentages of MUC5AC+/CCSP+ cells compared to *Ezh2* null mice ($p=0.0019$, **Figure 6.8**).

6.4 Ovalbumin significantly up regulates EZH2 expression

Quantitative immunohistochemistry showed that EZH2 expression was increased by OVA challenge, and that as expected, EZH2 expression was significantly lower in OVA challenged *Ezh2* null mouse lung epithelium compared to *Ezh2* wild type and *Ezh2* heterozygous ($p=0.04$). However, H3K27me3 levels did not change as dramatically, which could be due to a lack of proliferation in the *Ezh2* null lungs leading to build up of the epigenetic mark (**Figure 6.3**). Together, these data indicate that *Ezh2* heterozygous mice have an exacerbated response to OVA-challenge and this may mimic the PRC2-low state observed in bronchiolar epithelial cells of COPD patients.

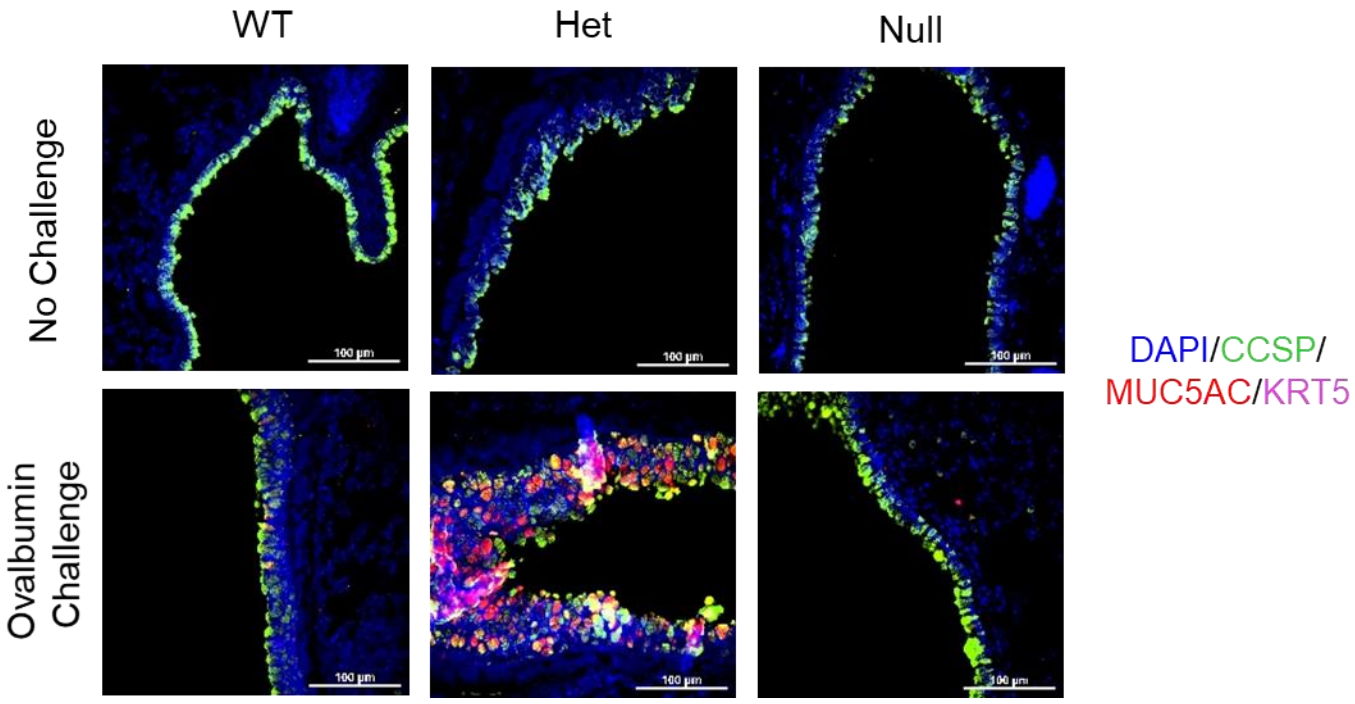

Figure 6.7 Mouse lung immunofluorescence representative images

Representative images of immunofluorescence stain of Keratin 5 (KRT5), club cell secretory protein (CCSP), and Mucin 5AC (MUC5AC), scale bar = 100µm. Immunofluorescence analysis was conducted by Tanner Ducote

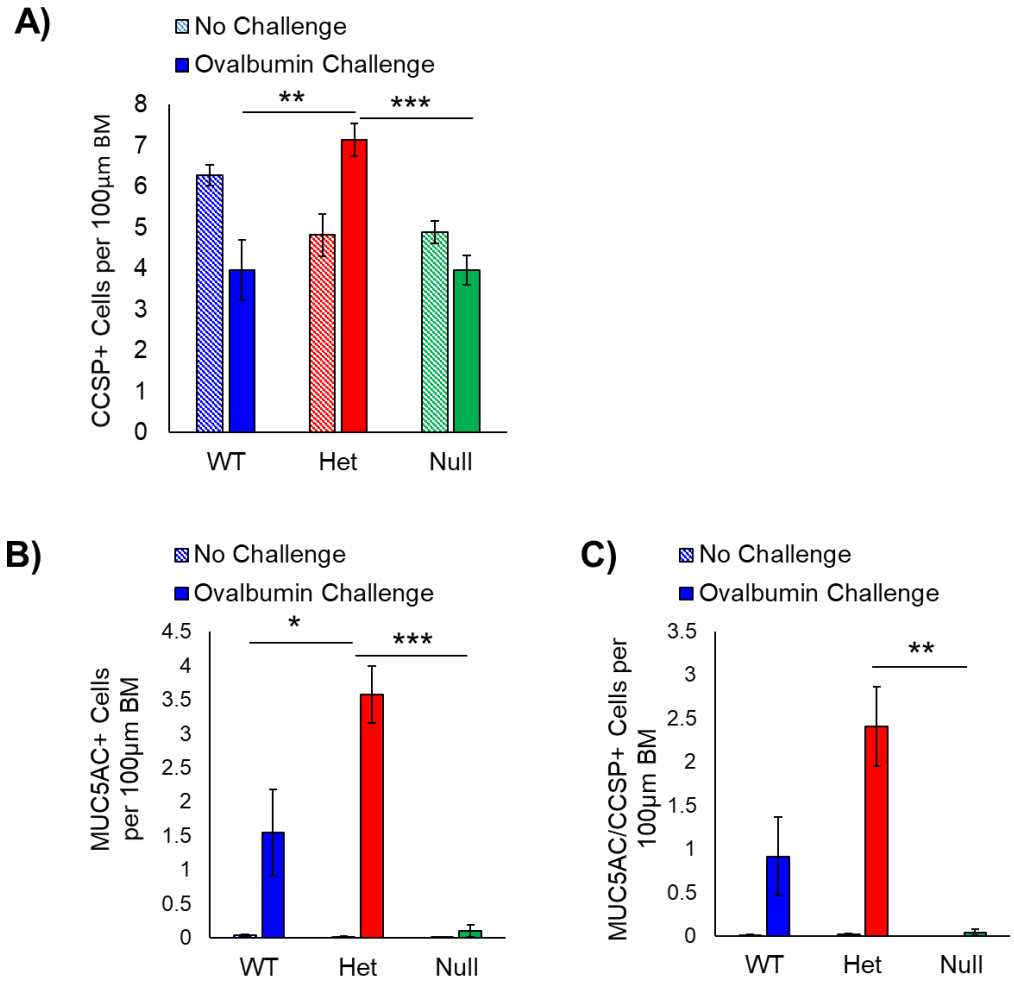

Figure 6.8 Mouse lung immunofluorescence analysis

A) Average number of CCSP+ cells, ** indicates p=0.0069 using ANOVA comparing ovalbumin challenged *Ezh2* wild type to ovalbumin challenged *Ezh2* heterozygous, *** indicates p=0.0002 using ANOVA comparing ovalbumin challenged *Ezh2* heterozygous to ovalbumin challenged *Ezh2* null. **B)** Average number of MUC5AC+ cells, * indicates p=0.0494 using ANOVA test with equal variance comparing ovalbumin challenged *Ezh2* wild type to ovalbumin challenged *Ezh2* heterozygous, *** indicates p<0.0001 using ANOVA test with equal variance comparing ovalbumin challenged *Ezh2* heterozygous to ovalbumin challenged *Ezh2* null. **C)** Average number of MUC5AC+/CCSP+ cells, ** indicates p=0.0019 ANOVA test with equal variance comparing ovalbumin challenge *Ezh2* heterozygous to ovalbumin challenge *Ezh2* null. Analysis is based on

Ezh2 wild type (n=6), heterozygous (n=10), and null (n=6) that received saline or were no challenge, and *Ezh2* wild type (n=9), heterozygous (n=10), and null (n=6) mice that received OVA challenge. Throughout, WT indicates *Ezh2* wild-type, Het indicates *Ezh2* heterozygous and Null indicates *Ezh2* null.

CHAPTER 7. SUMMARY AND FUTURE DIRECTIONS

In this study, we sought to elucidate the role of Polycomb Repressive Complex 2 (PRC2) in adult lung stem cell fate. We show that loss of PRC2 activity was strongly associated with COPD lung pathophysiology such as basal and goblet cell hyperplasia. Complete knockout of *Ezh2* in adult mouse lung organoid cultures led to a loss in stem cell self-renewal capabilities and gain of squamous morphology. scRNA-seq analysis revealed that full loss of *Ezh2* resulted in the accumulation of a newly identified *Krt17*- basal-like cell, and a decrease in classical basal stem cells, club cell progenitors, and alveolar transition cells. On the other hand, partial loss of *Ezh2* results in increased expression of inflammatory genes while complete loss of *Ezh2* does not. Furthermore, partial *Ezh2* expression in ovalbumin challenged mice resulted in mimicry of COPD traits in the lung such as increased club to mucus cell transdifferentiation, increased MUC5AC expression, and thickened epithelium. Finally, we established a strong association between CBS expression and aberrant secretory cell differentiation in COPD lung, and showed that its overexpression may interfere with PRC2 activity. Taken together, our data suggests that PRC2 is integral to facilitating proper lung stem cell differentiation in adult humans and mice.

It is notable that the organoid cultures that we established from murine lung epithelial cells shared numerous cell populations with those recently identified by scRNA sequencing in patient lung samples. Analysis of pulmonary fibrotic (PF) lung unveiled the presence of an aberrant basaloid cell population that were *KRT17+/KRT5-*, likely derived from club and AT2 cells, that is involved along the alveolar type 1 (AT1) terminal differentiation pathway [60, 62]. Similarly, evaluation of bleomycin-induced PF mouse lung led to the identification of a *Krt8+* population that were also derived from club and AT2 cells and involved in AT1 terminal differentiation. Notably, mimicry of chronic inflammation, through sustained Il-1β treatment, halted AT1

differentiation and led to the accumulation of these intermediate cells [61, 65, 131]. These populations are likely overlapping with a consensus phenotype of KRT5-/KRT17+/KRT8+/FN1+ and increased cellular senescence. Our finding that *Ezh2* null organoids have a significant loss in a *Krt5-/Krt8+/Krt17+/Fn1+* cell population suggests that *Ezh2* expression may be a key contributor toward the pathology of pulmonary fibrosis. A recent paper showed that inhibition of EZH2 through the inhibitor GSK126 was able to abrogate TGFβ-induced lung fibrosis phenotypes, and our organoid model presents additional cellular mechanistic insight into this phenomenon [132]. Furthermore, the increased expression of AT2 marker *Lamp3*, and the alveolar developmental marker *Foxp2* suggests that loss of *Ezh2* expression could serve as a potential therapeutic avenue to restore proper alveolar regeneration. However, the drastic loss in a key distal airway repair transcription factor, *Sox9*, infers that additional evaluation is needed to fully elucidate the role of *Ezh2* expression on alveolarization.

One of our most interesting findings is the stark contrast in *Krt17* expression between *Ezh2* wild-type and null organoids, where *Krt17+/Trp63+/Krt5+* classical basal cells were predominate in *Ezh2* wild-type and *Krt17-/Trp63+/Krt5-* basal-like cells were predominate in *Ezh2* null organoids. Previous studies have identified an intrapulmonary *Trp63+/Krt5-* progenitor population that initially resides in mouse airway, but upon exposure to H1N1 influenza virus, migrates to the alveolar region and forms ectopic *Trp63+/Krt5+* bronchiolar-like epithelia "pods" [133, 134]. The phenomenon of bronchiolization has been previously observed in idiopathic PF lung [135, 136], and the expansion of KRT5+ cells is believed to occur in response to severe lung injury, after AT2 and AT1 populations have been extensively destroyed [137]. TP63+/KRT5+ pods have also been identified in the lungs of Acute Respiratory Distress Syndrome patients diagnosed with Diffuse Alveolar Damage [138], which are two diseases commonly observed in SARS-CoV-2 (COVID-

19) infected patients [139-141]. Again, our data suggest a lack of differentiation of this cell type and rather an accumulation of the precursor *Krt17-/Trp63+/Krt5-* cells, suggesting that *Ezh2* may be integral to allowing proper differentiation of these cells.

Inflammation is a major pathological entity of COPD, and ovalbumin inhalation by mice elicits a phenotype similar to COPD, with noted temporary epithelium thickening and increases in goblet cells [129]. OVA-challenged *Ezh2* heterozygous mice exhibited a more robust bronchiolar phenotypes than *Ezh2* wild-type mice. Similarly, gene enrichment pattern analysis revealed that *Ezh2* heterozygous organoids expressed more inflammatory-associated genes than *Ezh2* wild-type organoids. These data suggests that epithelial cells with diminished *Ezh2* expression could amplify and exacerbate the immune response observed in COPD lung. Previous literature has demonstrated that genetic deletion of *Ezh2* in CD4+ T cells prevented their clonal expansion *in vivo* and prevented ovalbumin response [130], and given the model we chose, we believe deletion of *Ezh2* in immune cells may account for the diminished immune response observed in the *Ezh2* null mice. In order to determine the role of *Ezh2* specifically in epithelial cell resolution following allergic inflammation, we are in the process of generating a CC10-CreER, *Ezh2* floxed mouse strain [142]. Lastly, we observed a strong decrease in H3K27me3 in COPD bronchiolar epithelium, and importantly, the percentages of H3K27me3-high cells significantly correlated with fewer KRT5+, MUC5AC+ and MUC5AC+/CCSP+ cells. This is in contrast to a study that revealed a significantly higher number of H3K27me3 cells in COPD lung. These data could represent differences in patient populations, or also be due to the differences in analysis as we measured stain per nucleus and the former study measured positive cells per basement membrane length. Our data are supported by findings in other mouse models of PRC2 deficiency where aberrant expression of KRT5+ and mucins cells were observed [103, 104, 143, 144]. Similarly, our previous

work has found that lung squamous cell carcinomas, which can typically be characterized as KRT5+, have a marked loss of H3K27me3 levels when compared to adenocarcinomas [145]. Given that squamous lung cancer is more common in COPD patients [146], this finding could help us to better understand and address the increased prevalence of squamous lung cancers in our home state of Kentucky [147] Finally, although high CBS expression has already been observed in COPD lung [105], we report a strong positive correlation between its expression and aberrant epithelial cell differentiation. Additionally, we show that a substantial increase in CBS expression yields significantly lower EZH2 and *KRT17* expression *in vitro*. These findings, coupled with the strong negative correlations observed between H3K27me3 and aberrant cell differentiation, imply a close relationship between methionine cycling and gene expression patterns in human tissue. The transcriptional profile similarities shared between the *Ezh2* knockout organoids and CBS overexpressing HBECs offers a promising avenue for understanding how reactive oxygen stress could influence epigenetic programming in lung epithelium.

Based on a comprehensive evaluation of our findings, we offer a working hypothesis which demonstrates a relationship between PRC2 activity, CBS expression, and aberrant bronchiolar cell differentiation (**Figure 7.1**). Patient derived tissue analysis reveals that a loss in PRC2 activity and gain in CBS expression leads to increased instances of bronchiolar cell transdifferentiation and basal cell metaplasia. Furthermore, mouse lung organoid analysis reveals that ample loss of EZH2 expression leads to the appearance of squamous organoids and the enrichment of Krt17- basal-like cells whose transcriptional programs match that of CBS-overexpressing human bronchiolar epithelial cells.

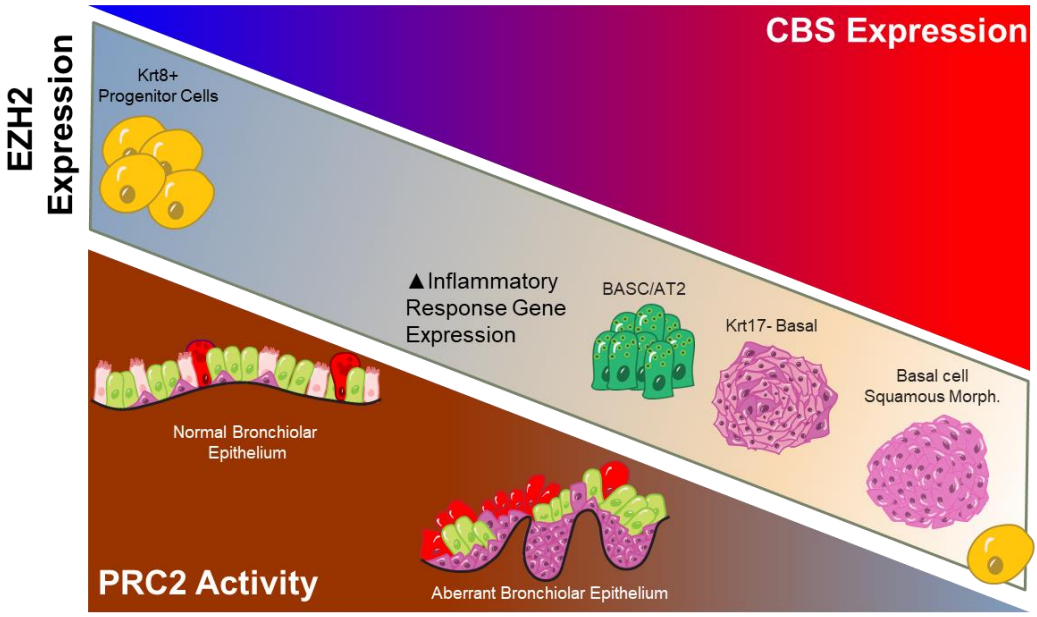

Figure 7.1 Working Hypothesis Schematic

The high expression of CBS and low abundance of H3K27me3 are both correlated with aberrant bronchiolar epithelium phenotypes. Loss of PRC2 activity and gain in CBS expression correlates with club-goblet cell transdifferentiation and metaplasia of goblet and basal cells in human lung. Reduction of H3K27me3 through deletion of EZH2 in mouse-derived organoids leads to the morphological development of squamous organoids, accumulation of BASC/AT2 cells, and emergence of *Krt17*- basal cells. Similarly, overexpression of CBS in human bronchiolar epithelial cell lines reduced EZH2 expression and H3K27me3 levels, and engendered cells that were transcriptionally similar to *Ezh2* null basal cells. Additionally, partial knockout of *Ezh2* led to a drastic increase in inflammatory response gene expression while complete knockout led to a drastic decrease in a Krt8+ progenitor cell population that is believed to persist in the parenchyma of pulmonary fibrotic lung.

Restoring PRC2's ability to repress lineage specific genes serves as a promising therapeutic target to induce proper stem cell differentiation in COPD lung. Additionally, further characterization of the role of PRC2 in lung stem and progenitor cells will have a vertical impact on potential therapeutic interventions for diseases rooted in cell reprogramming; i.e. lung cancer and pulmonary fibrosis.

Two of the most intriguing discoveries from this study was the emergence of the *Krt17*- basal cell variant in *Ezh2* heterozygous and null organoids, and the diminished expression of inflammatory response genes observed in *Ezh2* null organoids compared to heterozygous. Because basal cells were the most prominent cell population in all genotypes, it prompts the questions: 1. What is the critical mass of EZH2 expression that allows for maintenance of normal basal cell identity? 2. What concentration of EZH2 expression promotes diminished expression of inflammatory response genes? 3. Is there an ideal concentration of EZH2 expression that could allow for the expansion of a less immunogenic basal cell population and could *Krt17* be a biomarker for this unique cell type? To address these questions, future work could utilize the FDA approved global EZH2 inhibitor, EPZ-6438, in cell differentiation assays. One possible experiment would be to grow human bronchial epithelial cells as air liquid interphase cultures, treat with gradually increasing doses of EPZ-6438, induce differentiation, and then quantify cell fate, KRT17 expression levels, and H3K27me3. Additionally, one could treat these differentiated cells with allergens then examine their ability to produce various chemokines, cytokines and endogenous danger signals. Ideally, further characterization of KRT17- basal cells could provide a potential therapeutic avenue for combating chronic inflammation in COPD lung and offer insight into the effects of the global EZH2 inhibition on lung cell differentiation.

Given that we have demonstrated a relationship between CBS overexpression, PRC2 dysfunction, and aberrant lung epithelial cell differentiation, interrogation of potential therapeutic interventions is appropriate. One potential intervention could be diminishing methionine intake, as previous literature has shown that a low methionine diet can decrease CBS protein levels, which may lead to an increase in SAM availability, by way of homocysteine metabolism modulations [148-150]. CBS can be inhibited by aminooxyacetic acid (AOAA). This small molecule is a nonselective inhibitor of Pyridoxal 5′-phosphate (PLP)-dependent aminotransferases and is primarily utilized as a tool compound for the suppression of tumor cell proliferation in basic science experiments [151, 152]. However, because PLP enzymes are critical for stabilizing numerous amino acid biosynthetic and degradation pathways in humans, the therapeutic window for treating COPD would likely be too small for commercial use [153]. Alternatively, utilization of GSK-J4[154], a selective inhibitor for the H3K27 demethylases JMJD3/UTX, would be useful to maintain PRC2 activity and ultimately allow for re-normalization of the lung epithelium overtime.

One popular theory of aging states that the gradual decline in organ function is due to a natural decrease in stem cell self-renewal and division rates overtime [155]. COPD is largely considered a disease of an aging lung, with prevalence significantly increasing after the age of 60 and the mean patient age being 71 [156, 157]. Notably, histone methylation is a process largely employed during S phase with H3K27me3 being fully complete following the G1 phase, after cells have divided [158]. Thus, if we adopt the notion that lung stem cell activity decreases overtime, it will also be beneficial to understand how PRC2 activity changes. To this end, I propose a mouse study that seeks to characterize PRC2 activity and function in mature, middle aged, and old mice.

Additionally, episodically or chronically exposing these mice to noxious agents will help to elucidate how, and to what degree, environmental agents influence PRC2-mediated stem cell fate.

REFERENCES

1. Hsia, C.C., D.M. Hyde, and E.R. Weibel, *Lung Structure and the Intrinsic Challenges of Gas Exchange.* Compr Physiol, 2016. **6**(2): p. 827-95.
2. Furlow, P.W. and D.J. Mathisen, *Surgical anatomy of the trachea.* Ann Cardiothorac Surg, 2018. **7**(2): p. 255-260.
3. Nikolic, M.Z., D. Sun, and E.L. Rawlins, *Human lung development: recent progress and new challenges.* Development, 2018. **145**(16).
4. Patwa, A. and A. Shah, *Anatomy and physiology of respiratory system relevant to anaesthesia.* Indian J Anaesth, 2015. **59**(9): p. 533-41.
5. Young, R.E., et al., *Smooth Muscle Differentiation Is Essential for Airway Size, Tracheal Cartilage Segmentation, but Dispensable for Epithelial Branching.* Dev Cell, 2020. **53**(1): p. 73-85 e5.
6. Davis, J.D. and T.P. Wypych, *Correction: Cellular and functional heterogeneity of the airway epithelium.* Mucosal Immunol, 2022.
7. Knight, D.A. and S.T. Holgate, *The airway epithelium: structural and functional properties in health and disease.* Respirology, 2003. **8**(4): p. 432-46.
8. Gohy, S., et al., *Altered generation of ciliated cells in chronic obstructive pulmonary disease.* Sci Rep, 2019. **9**(1): p. 17963.
9. Crandall, E.D. and M.A. Matthay, *Alveolar epithelial transport. Basic science to clinical medicine.* Am J Respir Crit Care Med, 2001. **163**(4): p. 1021-9.
10. Hiemstra, P.S. and A. Bourdin, *Club cells, CC10 and self-control at the epithelial surface.* Eur Respir J, 2014. **44**(4): p. 831-2.
11. Rokicki, W., et al., *The role and importance of club cells (Clara cells) in the pathogenesis of some respiratory diseases.* Kardiochir Torakochirurgia Pol, 2016. **13**(1): p. 26-30.
12. Mason, R.J., *Biology of alveolar type II cells.* Respirology, 2006. **11 Suppl**: p. S12-5.
13. Jiao, L. and X. Liu, *Structural basis of histone H3K27 trimethylation by an active polycomb repressive complex 2.* Science, 2015. **350**(6258): p. aac4383.
14. World Health Organization, *Cancer; The Problem*. 2022: https://www.who.int/news-room/fact-sheets/detail/cancer.
15. in *How Tobacco Smoke Causes Disease: The Biology and Behavioral Basis for Smoking-Attributable Disease: A Report of the Surgeon General*. 2010: Atlanta (GA).
16. Miyauchi, E., et al., *Distinct Characteristics of Small Cell Lung Cancer Correlate With Central or Peripheral Origin: Subtyping Based on Location and Expression of Transcription Factor TTF-1.* Medicine (Baltimore), 2015. **94**(51): p. e2324.
17. Rudin, C.M., et al., *Small-cell lung cancer.* Nat Rev Dis Primers, 2021. **7**(1): p. 3.
18. Clark, S.B. and S. Alsubait, *Non Small Cell Lung Cancer*, in *StatPearls*. 2022: Treasure Island (FL).
19. Myers, D.J. and J.M. Wallen, *Lung Adenocarcinoma*, in *StatPearls*. 2022: Treasure Island (FL).
20. Pelosi, G., et al., *Large cell carcinoma of the lung: a tumor in search of an author. A clinically oriented critical reappraisal.* Lung Cancer, 2015. **87**(3): p. 226-31.
21. *American Thoracic Society. Idiopathic pulmonary fibrosis: diagnosis and treatment. International consensus statement. American Thoracic Society (ATS), and the European Respiratory Society (ERS).* Am J Respir Crit Care Med, 2000. **161**(2 Pt 1): p. 646-64.
22. Raghu, G., et al., *Incidence and prevalence of idiopathic pulmonary fibrosis in US adults 18-64 years old.* Eur Respir J, 2016. **48**(1): p. 179-86.
23. Dasaraju, P.V. and C. Liu, *Infections of the Respiratory System*, in *Medical Microbiology*, th and S. Baron, Editors. 1996: Galveston (TX).

24. Wilson, M.S. and T.A. Wynn, *Pulmonary fibrosis: pathogenesis, etiology and regulation.* Mucosal Immunol, 2009. **2**(2): p. 103-21.
25. Maher, T.M., A.U. Wells, and G.J. Laurent, *Idiopathic pulmonary fibrosis: multiple causes and multiple mechanisms?* Eur Respir J, 2007. **30**(5): p. 835-9.
26. Schafer, S.C., M. Funke-Chambour, and S. Berezowska, *[Idiopathic pulmonary fibrosis-epidemiology, causes, and clinical course].* Pathologe, 2020. **41**(1): p. 46-51.
27. Oggionni, T., et al., *Time course of matrix metalloproteases and tissue inhibitors in bleomycin-induced pulmonary fibrosis.* Eur J Histochem, 2006. **50**(4): p. 317-25.
28. Selman, M., et al., *TIMP-1, -2, -3, and -4 in idiopathic pulmonary fibrosis. A prevailing nondegradative lung microenvironment?* Am J Physiol Lung Cell Mol Physiol, 2000. **279**(3): p. L562-74.
29. Ramirez, G., et al., *Absence of Thy-1 results in TGF-beta induced MMP-9 expression and confers a profibrotic phenotype to human lung fibroblasts.* Lab Invest, 2011. **91**(8): p. 1206-18.
30. Hoshino, M., et al., *Bronchial subepithelial fibrosis and expression of matrix metalloproteinase-9 in asthmatic airway inflammation.* J Allergy Clin Immunol, 1998. **102**(5): p. 783-8.
31. Murphy, G. and A.J. Docherty, *The matrix metalloproteinases and their inhibitors.* Am J Respir Cell Mol Biol, 1992. **7**(2): p. 120-5.
32. Corbel, M., et al., *Involvement of gelatinases (MMP-2 and MMP-9) in the development of airway inflammation and pulmonary fibrosis.* Cell Biol Toxicol, 2002. **18**(1): p. 51-61.
33. Desmouliere, A., et al., *Transforming growth factor-beta 1 induces alpha-smooth muscle actin expression in granulation tissue myofibroblasts and in quiescent and growing cultured fibroblasts.* J Cell Biol, 1993. **122**(1): p. 103-11.
34. Hu, B., Z. Wu, and S.H. Phan, *Smad3 mediates transforming growth factor-beta-induced alpha-smooth muscle actin expression.* Am J Respir Cell Mol Biol, 2003. **29**(3 Pt 1): p. 397-404.
35. Ronnov-Jessen, L. and O.W. Petersen, *Induction of alpha-smooth muscle actin by transforming growth factor-beta 1 in quiescent human breast gland fibroblasts. Implications for myofibroblast generation in breast neoplasia.* Lab Invest, 1993. **68**(6): p. 696-707.
36. Sempowski, G.D., et al., *Subsets of murine lung fibroblasts express membrane-bound and soluble IL-4 receptors. Role of IL-4 in enhancing fibroblast proliferation and collagen synthesis.* J Immunol, 1994. **152**(7): p. 3606-14.
37. Fertin, C., et al., *Interleukin-4 stimulates collagen synthesis by normal and scleroderma fibroblasts in dermal equivalents.* Cell Mol Biol, 1991. **37**(8): p. 823-9.
38. Pauleau, A.L., et al., *Enhancer-mediated control of macrophage-specific arginase I expression.* J Immunol, 2004. **172**(12): p. 7565-73.
39. Liu, T., et al., *Regulation of found in inflammatory zone 1 expression in bleomycin-induced lung fibrosis: role of IL-4/IL-13 and mediation via STAT-6.* J Immunol, 2004. **173**(5): p. 3425-31.
40. Lee, E., et al., *Induction of Ym1/2 in mouse bone marrow-derived mast cells by IL-4 and identification of Ym1/2 in connective tissue type-like mast cells derived from bone marrow cells cultured with IL-4 and stem cell factor.* Immunol Cell Biol, 2005. **83**(5): p. 468-74.
41. Takatsu, K. and H. Nakajima, *IL-5 and eosinophilia.* Curr Opin Immunol, 2008. **20**(3): p. 288-94.
42. Global Initiative for Chronic Obstructive Lung Disease, *Global Strategy for the Diagnosis, Management, and Prevention of Chronic Obstructive Pulmonary Disease*, R. Hadfield, Editor. 2021. p. 164.
43. Brody, J.S. and A. Spira, *State of the art. Chronic obstructive pulmonary disease, inflammation, and lung cancer.* Proc Am Thorac Soc, 2006. **3**(6): p. 535-7.
44. Brusselle, G.G., G.F. Joos, and K.R. Bracke, *New insights into the immunology of chronic obstructive pulmonary disease.* Lancet, 2011. **378**(9795): p. 1015-26.

45. Saetta, M., *Airway inflammation in chronic obstructive pulmonary disease.* Am J Respir Crit Care Med, 1999. **160**(5 Pt 2): p. S17-20.
46. Wedzicha, J.A., *Role of viruses in exacerbations of chronic obstructive pulmonary disease.* Proc Am Thorac Soc, 2004. **1**(2): p. 115-20.
47. Balmes, J.R., *Occupational contribution to the burden of chronic obstructive pulmonary disease.* J Occup Environ Med, 2005. **47**(2): p. 154-60.
48. Faustini, A., et al., *Air pollution and multiple acute respiratory outcomes.* Eur Respir J, 2013. **42**(2): p. 304-13.
49. Gan, W.Q., et al., *Associations of ambient air pollution with chronic obstructive pulmonary disease hospitalization and mortality.* Am J Respir Crit Care Med, 2013. **187**(7): p. 721-7.
50. Zhao, J., et al., *Role of PM2.5 in the development and progression of COPD and its mechanisms.* Respir Res, 2019. **20**(1): p. 120.
51. Cavailles, A., et al., *Comorbidities of COPD.* Eur Respir Rev, 2013. **22**(130): p. 454-75.
52. Calverley, P.M., *Respiratory failure in chronic obstructive pulmonary disease.* Eur Respir J Suppl, 2003. **47**: p. 26s-30s.
53. Morgan, A.D., R. Zakeri, and J.K. Quint, *Defining the relationship between COPD and CVD: what are the implications for clinical practice?* Ther Adv Respir Dis, 2018. **12**: p. 1753465817750524.
54. Koshiol, J., et al., *Chronic obstructive pulmonary disease and altered risk of lung cancer in a population-based case-control study.* PLoS One, 2009. **4**(10): p. e7380.
55. Durham, A.L. and I.M. Adcock, *The relationship between COPD and lung cancer.* Lung Cancer, 2015. **90**(2): p. 121-7.
56. Papi, A., et al., *COPD increases the risk of squamous histological subtype in smokers who develop non-small cell lung carcinoma.* Thorax, 2004. **59**(8): p. 679-81.
57. Hogg, J.C., et al., *The nature of small-airway obstruction in chronic obstructive pulmonary disease.* N Engl J Med, 2004. **350**(26): p. 2645-53.
58. Crystal, R.G., *Airway basal cells. The "smoking gun" of chronic obstructive pulmonary disease.* Am J Respir Crit Care Med, 2014. **190**(12): p. 1355-62.
59. Randell, S.H., *Airway epithelial stem cells and the pathophysiology of chronic obstructive pulmonary disease.* Proc Am Thorac Soc, 2006. **3**(8): p. 718-25.
60. Adams, T.S., et al., *Single-cell RNA-seq reveals ectopic and aberrant lung-resident cell populations in idiopathic pulmonary fibrosis.* Sci Adv, 2020. **6**(28): p. eaba1983.
61. Choi, J., et al., *Inflammatory Signals Induce AT2 Cell-Derived Damage-Associated Transient Progenitors that Mediate Alveolar Regeneration.* Cell Stem Cell, 2020. **27**(3): p. 366-382 e7.
62. Habermann, A.C., et al., *Single-cell RNA sequencing reveals profibrotic roles of distinct epithelial and mesenchymal lineages in pulmonary fibrosis.* Sci Adv, 2020. **6**(28): p. eaba1972.
63. Kobayashi, Y., et al., *Persistence of a regeneration-associated, transitional alveolar epithelial cell state in pulmonary fibrosis.* Nat Cell Biol, 2020. **22**(8): p. 934-946.
64. Li, X., et al., *Single cell RNA sequencing identifies IGFBP5 and QKI as ciliated epithelial cell genes associated with severe COPD.* Respir Res, 2021. **22**(1): p. 100.
65. Strunz, M., et al., *Alveolar regeneration through a Krt8+ transitional stem cell state that persists in human lung fibrosis.* Nat Commun, 2020. **11**(1): p. 3559.
66. Holoch, D. and D. Moazed, *RNA-mediated epigenetic regulation of gene expression.* Nat Rev Genet, 2015. **16**(2): p. 71-84.
67. Chuang, J.C. and P.A. Jones, *Epigenetics and microRNAs.* Pediatr Res, 2007. **61**(5 Pt 2): p. 24r-29r.
68. Angrand, P.O., et al., *The role of long non-coding RNAs in genome formatting and expression.* Front Genet, 2015. **6**: p. 165.

69. Roberts, C.W. and S.H. Orkin, *The SWI/SNF complex--chromatin and cancer.* Nat Rev Cancer, 2004. **4**(2): p. 133-42.
70. Cheng, X., *Structure and function of DNA methyltransferases.* Annu Rev Biophys Biomol Struct, 1995. **24**: p. 293-318.
71. Kohli, R.M. and Y. Zhang, *TET enzymes, TDG and the dynamics of DNA demethylation.* Nature, 2013. **502**(7472): p. 472-9.
72. Bannister, A.J. and T. Kouzarides, *Regulation of chromatin by histone modifications.* Cell Res, 2011. **21**(3): p. 381-95.
73. Greer, E.L. and Y. Shi, *Histone methylation: a dynamic mark in health, disease and inheritance.* Nat Rev Genet, 2012. **13**(5): p. 343-57.
74. Ancelin, K., et al., *Blimp1 associates with Prmt5 and directs histone arginine methylation in mouse germ cells.* Nat Cell Biol, 2006. **8**(6): p. 623-30.
75. Gardner, K.E., et al., *Identification of lysine 37 of histone H2B as a novel site of methylation.* PLoS One, 2011. **6**(1): p. e16244.
76. Xiao, B., et al., *Structure and catalytic mechanism of the human histone methyltransferase SET7/9.* Nature, 2003. **421**(6923): p. 652-6.
77. Huang, S., M. Litt, and G. Felsenfeld, *Methylation of histone H4 by arginine methyltransferase PRMT1 is essential in vivo for many subsequent histone modifications.* Genes Dev, 2005. **19**(16): p. 1885-93.
78. Byvoet, P., et al., *The distribution and turnover of labeled methyl groups in histone fractions of cultured mammalian cells.* Arch Biochem Biophys, 1972. **148**(2): p. 558-67.
79. Murray, K., *THE OCCURRENCE OF EPSILON-N-METHYL LYSINE IN HISTONES.* Biochemistry, 1964. **3**: p. 10-5.
80. Fischle, W., et al., *Specificity of the chromodomain Y chromosome family of chromodomains for lysine-methylated ARK(S/T) motifs.* J Biol Chem, 2008. **283**(28): p. 19626-35.
81. Calo, E. and J. Wysocka, *Modification of enhancer chromatin: what, how, and why?* Mol Cell, 2013. **49**(5): p. 825-37.
82. Rice, J.C., et al., *Histone methyltransferases direct different degrees of methylation to define distinct chromatin domains.* Mol Cell, 2003. **12**(6): p. 1591-8.
83. Boyer, L.A., et al., *Polycomb complexes repress developmental regulators in murine embryonic stem cells.* Nature, 2006. **441**(7091): p. 349-53.
84. Barski, A., et al., *High-resolution profiling of histone methylations in the human genome.* Cell, 2007. **129**(4): p. 823-37.
85. Kuzmichev, A., et al., *Histone methyltransferase activity associated with a human multiprotein complex containing the Enhancer of Zeste protein.* Genes Dev, 2002. **16**(22): p. 2893-905.
86. Shi, B., et al., *Integration of estrogen and Wnt signaling circuits by the polycomb group protein EZH2 in breast cancer cells.* Mol Cell Biol, 2007. **27**(14): p. 5105-19.
87. Lee, S.T., et al., *Context-specific regulation of NF-kappaB target gene expression by EZH2 in breast cancers.* Mol Cell, 2011. **43**(5): p. 798-810.
88. Justin, N., et al., *Structural basis of oncogenic histone H3K27M inhibition of human polycomb repressive complex 2.* Nat Commun, 2016. **7**: p. 11316.
89. Brooun, A., et al., *Polycomb repressive complex 2 structure with inhibitor reveals a mechanism of activation and drug resistance.* Nat Commun, 2016. **7**: p. 11384.
90. Pasini, D., et al., *Suz12 is essential for mouse development and for EZH2 histone methyltransferase activity.* EMBO J, 2004. **23**(20): p. 4061-71.
91. Cao, R. and Y. Zhang, *SUZ12 is required for both the histone methyltransferase activity and the silencing function of the EED-EZH2 complex.* Mol Cell, 2004. **15**(1): p. 57-67.

92. Squazzo, S.L., et al., *Suz12 binds to silenced regions of the genome in a cell-type-specific manner.* Genome Res, 2006. **16**(7): p. 890-900.
93. Kirmizis, A., et al., *Silencing of human polycomb target genes is associated with methylation of histone H3 Lys 27.* Genes Dev, 2004. **18**(13): p. 1592-605.
94. Bracken, A.P., et al., *Genome-wide mapping of Polycomb target genes unravels their roles in cell fate transitions.* Genes Dev, 2006. **20**(9): p. 1123-36.
95. Ezhkova, E., et al., *Ezh2 orchestrates gene expression for the stepwise differentiation of tissue-specific stem cells.* Cell, 2009. **136**(6): p. 1122-35.
96. Yamaguchi, H. and M.C. Hung, *Regulation and Role of EZH2 in Cancer.* Cancer Res Treat, 2014. **46**(3): p. 209-22.
97. Chen, X., et al., *High expression of trimethylated histone H3 at lysine 27 predicts better prognosis in non-small cell lung cancer.* Int J Oncol, 2013. **43**(5): p. 1467-80.
98. Chang, C.J., et al., *EZH2 promotes expansion of breast tumor initiating cells through activation of RAF1-beta-catenin signaling.* Cancer Cell, 2011. **19**(1): p. 86-100.
99. Du, J., et al., *FOXC1, a target of polycomb, inhibits metastasis of breast cancer cells.* Breast Cancer Res Treat, 2012. **131**(1): p. 65-73.
100. Wei, Y., et al., *Loss of trimethylation at lysine 27 of histone H3 is a predictor of poor outcome in breast, ovarian, and pancreatic cancers.* Mol Carcinog, 2008. **47**(9): p. 701-6.
101. Cao, Q., et al., *Repression of E-cadherin by the polycomb group protein EZH2 in cancer.* Oncogene, 2008. **27**(58): p. 7274-84.
102. Bruggeman, S.W., et al., *Ink4a and Arf differentially affect cell proliferation and neural stem cell self-renewal in Bmi1-deficient mice.* Genes Dev, 2005. **19**(12): p. 1438-43.
103. Galvis, L.A., et al., *Repression of Igf1 expression by Ezh2 prevents basal cell differentiation in the developing lung.* Development, 2015. **142**(8): p. 1458-69.
104. Snitow, M.E., et al., *Ezh2 represses the basal cell lineage during lung endoderm development.* Development, 2015. **142**(1): p. 108-17.
105. Numakura, T., et al., *Production of reactive persulfide species in chronic obstructive pulmonary disease.* Thorax, 2017. **72**(12): p. 1074-1083.
106. Sundar, I.K., et al., *Cigarette smoke induces distinct histone modifications in lung cells: implications for the pathogenesis of COPD and lung cancer.* J Proteome Res, 2014. **13**(2): p. 982-96.
107. Anzalone, G., et al., *Cigarette smoke affects the onco-suppressor DAB2IP expression in bronchial epithelial cells of COPD patients.* Sci Rep, 2019. **9**(1): p. 15682.
108. Jensen, C. and Y. Teng, *Is It Time to Start Transitioning From 2D to 3D Cell Culture?* Front Mol Biosci, 2020. **7**: p. 33.
109. Shen, X., et al., *EZH1 mediates methylation on histone H3 lysine 27 and complements EZH2 in maintaining stem cell identity and executing pluripotency.* Mol Cell, 2008. **32**(4): p. 491-502.
110. Neff, T., et al., *Polycomb repressive complex 2 is required for MLL-AF9 leukemia.* Proc Natl Acad Sci U S A, 2012. **109**(13): p. 5028-33.
111. Tumbar, T., et al., *Defining the epithelial stem cell niche in skin.* Science, 2004. **303**(5656): p. 359-63.
112. Perl, A.K., et al., *Early restriction of peripheral and proximal cell lineages during formation of the lung.* Proc Natl Acad Sci U S A, 2002. **99**(16): p. 10482-7.
113. Hochedlinger, K., et al., *Ectopic expression of Oct-4 blocks progenitor-cell differentiation and causes dysplasia in epithelial tissues.* Cell, 2005. **121**(3): p. 465-77.
114. Lee, J.-H., et al., *Lung Stem Cell Differentiation in Mice Directed by Endothelial Cells via a BMP4-NFATc1-Thrombospondin-1 Axis.* Cell, 2014. **156**(3): p. 440-455.

115. Stuart, T., et al., *Comprehensive Integration of Single-Cell Data.* Cell, 2019. **177**(7): p. 1888-1902 e21.
116. McInnes, L., et al., *UMAP: Uniform Manifold Approximation and Projection.* Journal of Open Source Software, 2018. **3**(29): p. 1.
117. Finak, G., et al., *MAST: a flexible statistical framework for assessing transcriptional changes and characterizing heterogeneity in single-cell RNA sequencing data.* Genome Biol, 2015. **16**: p. 278.
118. Street, K., et al., *Slingshot: cell lineage and pseudotime inference for single-cell transcriptomics.* BMC Genomics, 2018. **19**(1): p. 477.
119. Bolger, A.M., M. Lohse, and B. Usadel, *Trimmomatic: a flexible trimmer for Illumina sequence data.* Bioinformatics, 2014. **30**(15): p. 2114-20.
120. Li, B. and C.N. Dewey, *RSEM: accurate transcript quantification from RNA-Seq data with or without a reference genome.* BMC Bioinformatics, 2011. **12**: p. 323.
121. Robinson, M.D., D.J. McCarthy, and G.K. Smyth, *edgeR: a Bioconductor package for differential expression analysis of digital gene expression data.* Bioinformatics, 2010. **26**(1): p. 139-40.
122. Fillmore, C.M., et al., *Estrogen expands breast cancer stem-like cells through paracrine FGF/Tbx3 signaling.* Proceedings of the National Academy of Sciences, 2010. **107**(50): p. 21737-21742.
123. Crystal, R.G., *Airway basal cells. The "smoking gun" of chronic obstructive pulmonary disease.* American journal of respiratory and critical care medicine, 2014. **190**(12): p. 1355-1362.
124. Bracken, A.P. and K. Helin, *Polycomb group proteins: navigators of lineage pathways led astray in cancer.* Nat Rev Cancer, 2009. **9**(11): p. 773-784.
125. Sundar, I.K., et al., *Cigarette Smoke Induces Distinct Histone Modifications in Lung Cells: Implications for the Pathogenesis of COPD and Lung Cancer.* Journal of Proteome Research, 2014. **13**(2): p. 982-996.
126. Yang, Z., et al., *The mouse forkhead gene Foxp2 modulates expression of the lung genes.* Life Sci, 2010. **87**(1-2): p. 17-25.
127. Shu, W., et al., *Foxp2 and Foxp1 cooperatively regulate lung and esophagus development.* Development, 2007. **134**(10): p. 1991-2000.
128. Spira, A., et al., *Gene Expression Profiling of Human Lung Tissue from Smokers with Severe Emphysema.* American Journal of Respiratory Cell and Molecular Biology, 2004. **31**(6): p. 601-610.
129. Donovan, C., et al., *Differential effects of allergen challenge on large and small airway reactivity in mice.* PLoS One, 2013. **8**(9): p. e74101.
130. Keenan, C.R., et al., *Polycomb repressive complex 2 is a critical mediator of allergic inflammation.* JCI Insight, 2019. **4**(10).
131. Kobayashi, Y., et al., *Persistence of a regeneration-associated, transitional alveolar epithelial cell state in pulmonary fibrosis.* Nature Cell Biology, 2020. **22**(8): p. 934-946.
132. Le, H.Q., et al., *An EZH2-dependent transcriptional complex promotes aberrant epithelial remodelling after injury.* 2021. **22**(8): p. e52785.
133. Kumar, P.A., et al., *Distal Airway Stem Cells Yield Alveoli In Vitro and during Lung Regeneration following H1N1 Influenza Infection.* Cell, 2011. **147**(3): p. 525-38.
134. Vaughan, A.E., et al., *Lineage-negative progenitors mobilize to regenerate lung epithelium after major injury.* Nature, 2015. **517**(7536): p. 621-625.
135. Plantier, L., et al., *Ectopic respiratory epithelial cell differentiation in bronchiolised distal airspaces in idiopathic pulmonary fibrosis.* Thorax, 2011. **66**(8): p. 651-7.
136. Seibold, M.A., et al., *The idiopathic pulmonary fibrosis honeycomb cyst contains a mucocilary pseudostratified epithelium.* PLoS One, 2013. **8**(3): p. e58658.
137. Yee, M., et al., *Alternative Progenitor Lineages Regenerate the Adult Lung Depleted of Alveolar Epithelial Type 2 Cells.* Am J Respir Cell Mol Biol, 2017. **56**(4): p. 453-464.

138. Taylor, M.S., et al., *A Conserved Distal Lung Regenerative Pathway in Acute Lung Injury.* Am J Pathol, 2018. **188**(5): p. 1149-1160.
139. Huang, C., et al., *Clinical features of patients infected with 2019 novel coronavirus in Wuhan, China.* Lancet, 2020. **395**(10223): p. 497-506.
140. Borczuk, A.C., et al., *COVID-19 pulmonary pathology: a multi-institutional autopsy cohort from Italy and New York City.* Mod Pathol, 2020. **33**(11): p. 2156-2168.
141. Xu, Z., et al., *Pathological findings of COVID-19 associated with acute respiratory distress syndrome.* Lancet Respir Med, 2020. **8**(4): p. 420-422.
142. Rawlins, E.L., et al., *The role of Scgb1a1+ Clara cells in the long-term maintenance and repair of lung airway, but not alveolar, epithelium.* Cell Stem Cell, 2009. **4**(6): p. 525-34.
143. Chiacchiera, F., et al., *PRC2 preserves intestinal progenitors and restricts secretory lineage commitment.* EMBO J, 2016. **35**(21): p. 2301-2314.
144. Serresi, M., et al., *Polycomb Repressive Complex 2 Is a Barrier to KRAS-Driven Inflammation and Epithelial-Mesenchymal Transition in Non-Small-Cell Lung Cancer.* Cancer Cell, 2016. **29**(1): p. 17-31.
145. Zhang, H., et al., *Lkb1 inactivation drives lung cancer lineage switching governed by Polycomb Repressive Complex 2.* Nat Commun, 2017. **8**: p. 14922.
146. Papi, A., et al., *COPD increases the risk of squamous histological subtype in smokers who develop non-small cell lung carcinoma.* Thorax, 2004. **59**(8): p. 679.
147. Brainson, C.F., et al., *Description of a Lung Cancer Hotspot: Disparities in Lung Cancer Histology, Incidence, and Survival in Kentucky and Appalachian Kentucky.* Clin Lung Cancer, 2021.
148. Choumenkovitch, S.F., et al., *In the Cystathionine β-Synthase Knockout Mouse, Elevations in Total Plasma Homocysteine Increase Tissue S-Adenosylhomocysteine, but Responses of S-Adenosylmethionine and DNA Methylation Are Tissue Specific.* The Journal of Nutrition, 2002. **132**(8): p. 2157-2160.
149. Prudova, A., et al., *S-adenosylmethionine stabilizes cystathionine beta-synthase and modulates redox capacity.* Proc Natl Acad Sci U S A, 2006. **103**(17): p. 6489-94.
150. Tang, B., et al., *Methionine-deficient diet induces post-transcriptional downregulation of cystathionine β-synthase.* Nutrition, 2010. **26**(11): p. 1170-1175.
151. Szabo, C., et al., *Tumor-derived hydrogen sulfide, produced by cystathionine-beta-synthase, stimulates bioenergetics, cell proliferation, and angiogenesis in colon cancer.* Proc Natl Acad Sci U S A, 2013. **110**(30): p. 12474-9.
152. Wang, D., et al., *Inhibition of cystathionine beta-synthase promotes apoptosis and reduces cell proliferation in chronic myeloid leukemia.* Signal Transduct Target Ther, 2021. **6**(1): p. 52.
153. Percudani, R. and A. Peracchi, *A genomic overview of pyridoxal-phosphate-dependent enzymes.* EMBO Rep, 2003. **4**(9): p. 850-4.
154. Heinemann, B., et al., *Inhibition of demethylases by GSK-J1/J4.* Nature, 2014. **514**(7520): p. E1-2.
155. Schultz, M.B. and D.A. Sinclair, *When stem cells grow old: phenotypes and mechanisms of stem cell aging.* Development, 2016. **143**(1): p. 3-14.
156. James, G.D., et al., *Trends in management and outcomes of COPD patients in primary care, 2000-2009: a retrospective cohort study.* NPJ Prim Care Respir Med, 2014. **24**: p. 14015.
157. MacNee, W., *Is Chronic Obstructive Pulmonary Disease an Accelerated Aging Disease?* Ann Am Thorac Soc, 2016. **13 Suppl 5**: p. S429-S437.
158. Zee, B.M., et al., *Origins and formation of histone methylation across the human cell cycle.* Mol Cell Biol, 2012. **32**(13): p. 2503-14.

VITA

Education

- University of Kentucky, Lexington, KY
  [2016-Present]
  Doctor of Philosophy- Toxicology and Cancer Biology (GPA: 3.8)
- North Carolina Agricultural and Technical State University, Greensboro, NC
  [2013-2015]
  Master of Science Degree- Biology (GPA: 4.0)
- Albany State University, Albany, GA
  [2007-2011]
  Bachelors of Science Degree-Biology
  Biotechnology concentration

Research Experience

- Graduate Student
  [August 2016-Present]
  Location: University of Kentucky
  Principle Investigator: Christine Fillmore Brainson
  Project: Elucidate the epigenetic mechanisms that lead to chronic obstructive pulmonary disease (COPD) and other lung diseases such as squamous cell carcinoma. I am using a mouse model of deletion of the histone methyltransferase EZH2, sorting mouse lung stem and progenitor cells and deleting EZH2 in vitro, staining human COPD and normal lung sections, and using human air-liquid-interface cultures to knock-down EZH2.
- Laboratory Assistant
  [July 2015-August 2016]
  Location: Emory University
  Principle Investigator: Dr. Edward Morgan
  Project: Understand how nitric oxide affects cytochrome P450, CYP51A1 degradation. I executed cell culture techniques, dose and time dependent experiments, western blot analyses, and cell transduction.
- Research Scientist
  [May 2013-June 2015]
  Location: North Carolina Agricultural and Technical State University, Greensboro, NC
  Principle Investigator: Dr. Jessica Han
  Project 1: Investigate brain iron mishandling as a potential contributor to neurodegeneration in obesity models by determining the effects of high fat diet on regional brain iron and ferritin (a good indicator of iron biology) and alpha synuclein (a protein linked with neurodegenerative processes) protein expression. I worked with C57BL/6J mice for ~17 weeks. After which, collect blood and organs and conduct western blot of iron response proteins, triglyceride concentration assay, hemoglobin concentration assay, hematocrit, Insulin tolerance test, ELISA and immunohistochemistry. Additionally, gain literary knowledge in obesity, iron content and neurodegenerative diseases.
  Project 2: Investigate brain iron content and behavior in dietary-induced obesity developing mice. I conducted atomic absorption spectrometry and home-cage scan behavior analysis.

- Graduate Research Assistant; Accountability for Cancer Care through Undoing Racism and Equity (ACCURE) Study
  [July 2013-September 2013]
  Location: Moses Cone Memorial Hospital, Greensboro, NC/University of North Carolina at Chapel Hill, Chapel Hill, NC
  Co-Principle Investigators: Dr. Sam Cykert and Dr. Geni Eng
  Project: Clinical trial that aimed to increase transparency and accountability in the health care system in an effort to reduce racial inequities in cancer treatment outcomes. I successfully recruited and consented patients to the study, refined intervention components, conducted database maintenance, successfully navigated through the electronic medical record review, gained literary knowledge on breast and lung cancer, successfully completed racial equity training, interpreted magnetic resonance imaging (MRI) and positron emission tomography (PET) scans, Attended multidisciplinary breast and lung cancer clinic, successfully determined breast and lung cancer stages.
- Research Assistant; GEMM Study: A Risky Sex Prevention for African American Adolescent Girls
  [May 2013-June 2013]
  Location: University of North Carolina at Greensboro, Greensboro, NC
  Principle Investigator: Dr. Robin Bartlett
  Project: Investigated the feasibility and efficacy of HIV prevention intervention for black adolescent girls. Specifically examining the role that racial pride plays in this intervention process and how it affects risky sexual behavior. Successfully completed CITI training. Conducting data collection, data coding and input, assist PI in delivering interventions and control conditions. Gain knowledge in cultural competence, participation consent and assent contracts, HIV knowledge, health literacy and public health research protocols.
- Student Research Assistant; Biomass to Energy Project
  [September 2011-June 2012]
  Location: Albany State University, Albany, GA
  Principle Investigator: Dr. Kwaichow Chan
  Project: Identified gasification systems around the world to potentially collaborate with and provide an alternative fuel for the city of Albany, Georgia. Researched various gasification systems around the world, crafting surveys, conducting phone interviews, creating power point presentations.
- Summer Intern; Health Education Research Opportunities (HERO) Program
  [June 2011-August 2011]
  Location: Virginia Commonwealth University, Richmond, VA
  Principle Investigator: Dr. Daniel Conrad (Doctoral candidates: Sarah Norton, Sheinei Saleem)
  Project: Identified the role of myeloid-derived suppressor cells (MDSC) in asthma. Worked with C57BL/6J mice for ~9 weeks. Induced allergenic response through intraperitoneal and intranasal injections. After which, measured bronchoconstriction using the flexivent system collected blood bronchoalveolar lavage (BAL) fluid, cardiac blood, fixed and extracted lungs and heart from mice. Additionally, counted cells with hemocytometer, conducted IgE ELISA, Isolated mast cells, harvested spleens, and identified cells through flow cytometry.
- Summer Intern; Bioinformatics and biotechnology Summer Internship (BBSI) Program
  [June 2010- August 2010]
  Location: Virginia Polytechnic Institute and State University, Blacksburg, VA
  Principle Investigator: Dr. Christopher Lawrence (Doctoral candidate: Ha Dang)

Project: Conducted laboratory based proteomics by annotating allergenic proteins that trigger severe immune responses in asthmatics. Utilized state-of-the-art computational sciences to understanding complex biological systems such as genomics, and proteomics. Advanced analytical tools include NCBI, ClustalW, Swissprot, Ensmbl, and BLAST to identify and annotate allergenic proteins.

Publications

Journal Papers

- Jian Han, Justin Plummer, Lumei Liu, **Aria Byrd**, Michael Aschner & Keith M. Erikson. (2017). The impact of obesity on brain iron levels and α-synuclein expression is regionally dependent. Nutritional Neuroscience, 0,0. PMID: 29034829
- Ji Won Park, **Aria Byrd**, Choon-myung Lee, Edward T. Morgan. (2017). Nitric oxide stimulates cellular degradation of human CYP51A1, the highly conserved lanosterol 14α-demethylase. Biochemical Journal, 747,19. PMID: 28830911
- Liu, L., **Byrd, A.**, Plummer, J., Erikson, K. M., Harrison, S. H., & Han, J. (2016). The Effects of Dietary Fat and Iron Interaction on Brain Regional Iron Contents and Stereotypical Behaviors in Male C57BL/6J Mice. Frontiers in Nutrition, 3, 20. PMID: 29034829
- Fan Chen, Xiulong Song, Tanner J. DuCote, **Aria L. Byrd**, Christine F. Brainson. EZH2 inhibition confers PIK3CA-driven lung tumors enhanced sensitivity to PI3K inhibition. Cancer Letters June 2021.

Published Abstracts/Presentations at Professional Conferences

- Byrd A, Chen F, Zhao Y, Edgin A, Kim C, Brainson C. "Squamous cell cancers and chronic obstructive pulmonary disease share Polycomb Repressive Complex 2 dysregulation".
    - American Association for Cancer Research. Atlanta, GA. March 30-April 4, 2019 (Poster)
    - Experimental Biology Conference. Orlando, FL. April 6-9, 2018 (Poster)
    - UK Toxicology and Cancer Biology Department Retreat. Lexington, KY. August 23, 2019 (Poster)
- Byrd A, Chen F, Zhao Y, Edgin A, Kim C, Brainson C. Loss of Polycomb Repressive Complex 2 impairs lung bronchiolar cell growth and underlies chronic obstructive pulmonary disease. 57th Annual Society of Toxicology Conference. San Antonio, TX. March 11-15, 2018
    - Markey Cancer Center Research Day. Lexington, KY. May 9, 2018 (Poster)
    - International Society for Stem Cell Research Conference. Melbourne, Australia. June 20-23, 2018 (Poster)
    - The Lung Epithelium in Health and Disease Conference. St. Bonaventure, NY. July 29-August 3, 2018 (Poster)
- Byrd A, Park J, Lee C, Morgan E T. Nitric Oxide Stimulates CYP51A1 Down Regulation. 35th Annual Federation of American Societies for Experimental Biology (FASEB). San Diego, CA April 2-6, 2016 (Poster)
    - 11th Annual Great Lakes Drug Metabolism and Disposition Group Meeting. Chicago, IL. May 5-6, 2016 (Oral)
- Byrd A. Plummer J, Erikson K, Han J. Dietary-Induced Obesity Disturbs Iron Homeostasis and Alpha-Synuclein Expression in C57BL/6J Mouse Brains. 34th Annual Federation of American Societies for Experimental Biology (FASEB). Boston, MA. March 28-April 1, 2015 (Poster)
    - 3rd Annual Emory University-Laney Graduate School STEM Research Career Symposium. Atlanta, GA. March 25-26, 2015 (Oral)
- Byrd A, Liu L, Cao W, Erikson K, Han J. Interaction of Dietary Iron and Fat on Glucose Clearance. 33rd Federation of American Societies for Experimental Biology (FASEB). San Diego, CA April 26-30, 2014 (Poster)

- Byrd A, Saleem S, Norton S, Conrad D. Role of Myeloid-Derived Suppressor Cells in Asthma 11th Annual Biomedical Research Conference for Minority Students (ABRCMS). St. Louis, MO, November 9-12, 2011 (Poster)
- Byrd A, Dang H, Babiceanu M, Lawrence C. Unlocking the Alergome of the Airborne Fungus Alternaria Alternata.
    - 24th Annual the Association of Minority Health Professions Schools (AMHPS) symposium. Newport News, VA. March 25-27, 2011 (Poster)
    - 18th Annual Florida-Georgia Louis Stokes Alliance for Minority Participation (FGLSAMP) Conference. Jacksonville, FL. February 3-6, 2011 (Poster)
    - 24th Annual Biomedical Research Conference for Minority Students (ABRCMS). Charlotte, NC. November 10-13, 2010 (Poster)

Enrichment Experiences

- **The University of Kentucky Center for Appalachian Research in Environmental Sciences (UK CARES) Faculty Fellows in Science Communication Auditor**
  [September 2020-May 2021]
  Location: Virtual Program
  Responsibilities: This program is designed to provide faculty with skills training for communicating science to a broader audience, leading to an enhanced capability for outreach and success in research, teaching, and service.
- **American society for biochemistry and Molecular Biology's inaugural (ASBMB) Advocacy Training Program Delegate**
  [June 2018-December 2018]
  Location: Virtual program
  Responsibilities: Received extensive training on how to be effective advocates for science and scientific research, whether that be at a community, state or federal level. I met with congressional staff members to advocate for an amendment of H.R. 5119, also known as the Partnership for Progress and Prosperity (P3) Act, to give special consideration to schools and universities that integrate substantial political literacy education into their STEM curriculum.
- **10th Annual NIH Career Symposium attendee**
  [May 11, 2017]
  Location: Bethesda, Maryland
- **Teaching Assistant**
  [January 2013-May 2013]
  Location: North Carolina Agricultural and Technical State University, Greensboro, NC
  Supervisor: Calisha Petty
  Responsibilities: Conducted and prepared laboratory lectures and experiments, grade exams and presentations, interact with non-biology major, undergraduate students on an academic level.
- **Shadowing Intern**
  [November 2010]
  Location: Center for Disease Control- National Center for HIV/AIDS, Viral Hepatitis, STD, and TB Prevention (NCHHSTP), Atlanta, Georgia
  Epidemiologist: Dr. Madeline Sutton
- **Laboratory Assistant**
  [May 2010]
  Location: Emory University, Atlanta, GA
  Principle Investigator: Dr. Nicole Gerardo

Responsibilities: Executed various laboratory techniques such as preparing aphid DNA for polymerase chain reaction, preparing media, bacterial and fungal in vitro bioassays, and capturing and maturing stink bugs.

- Laboratory Assistant
  [May 09-July 09]
  Location: Albany State University, Albany, GA
  Principle Investigator: Dr. Ashok Jain
  Responsibilities: Sub-cultured rose plants, sterilized lab instruments, successfully executed the procedures in formulating root and stem media
- Dental Assistant
  [June 2005-July 2005]
  Location: Smile Success Dental Center, Bellwood, IL
  Supervisor: Dr. Mimi Johnson
  Responsibilities: Assisted the dentist and hygienist with dental restorations, cleaning impressions, and radiographs, prepared operatories, and sterilized instruments

Honors, Awards, and Scholarships

2021 Southern Regional Education Board Doctoral Scholars Fellowship
2020 National Heart Lung and Blood Institute (NHLBI) F31 Fellowship Award
2019 Women in Medicine and Science (WIMS) Rising Star Award
2019 Experimental Biology "Scientific Highlights" collaborative poster recognition
2019 American Association for Cancer Research (AACR) Minority Scholar in Cancer Research Award
2019 Distinguished Speaker for IdeaFestival Bowling Green at Western Kentucky University
2018 Delegate for American society for biochemistry and Molecular Biology's inaugural (ASBMB) Advocacy Training Program
2018 $500 poster presentation award for FASEB Lung Epithelium in Health and Disease Meeting
2018 T-32 Molecular Mechanisms of Toxicity Training Fellowship
2018;2019 $1000 Center for Graduate and Professional Diversity Initiatives, Student Professional Development Funds
2018 Finger Lakes Environmental Film Festival Diversity Scholars Fellowship (FLEFF)
2016-2019 Lyman T. Johnson Diversity Award
2015-2016 T-32 NIH Diversity grant supplement
2015 Laney Graduate School STEM Research and Career Symposium Travel Award
2014-2015 North Carolina A&T State University tuition waver
2014-2015 T-32 Basic Immune Mechanisms Training Fellowship
2014 FASEB/MARC Travel Award
2013-2014 T-32 Basic Immune Mechanisms Training Fellowship
2013-2015 North Carolina A&T State University tuition waver
2013 Teacher Assistantship at North Carolina Agricultural and Technical State University
2011 1st Place- Poster presentation at Association of Minority Health Professions Schools (AMHPS) conference

2011 3rd Place- Poster presentation at 2011 Florida-Georgia Louis Stokes Alliance for Minority Participation (FGLSAMP) Conference

2010 $1000 South East Alliance for Graduate Education and Professorate (SEAGEP) Undergraduate Research Award

2010 1st place- Outstanding Research Presentation in Albany State University's 2010 STEM Conference

2007 HOPE Scholarship

Community Service

2020 Panelist: *Picture a Scientist: A New Chapter for Women Scientists*

2020 Panelist: *Mentoring Moments; Graduate School 101*

2020 Creator and collaborating coordinator of S*ecure the Bag* project: Initiative aimed at securing funding to enable the University of Kentucky counseling psychology graduate students to receive free counseling services. $2,500 seed money secured!

2020 Collaborating Coordinator of *New Visions for Black Men: From Maleness to Manhood*. Developed the panel session entitled *Melinated Matriculation* which explored black men's unique journey of getting into- and matriculating through grad/professional school.

2020 36th Annual Kentucky American Water District Science Fair Judge

2020 Creator and Coordinator of *The Spectrum:* A forum endeavoring to unpack the nuances of blackness and contextualize those topics through the lens of trying to thrive socially and professionally in the small college town of Lexington

2020 Lead Coordinator/volunteer: Black Graduate and Professional Student Association Valentine's Day fundraising event

2019, 2020 Lead Coordinator/Volunteer for Lexington Regional Science Fair: Mentoring initiative intended to assist the young men of Carter G. Woodson Academy and Henry Clay High School prepare for their science poster presentation. All three placed 1st, 2nd, and 3rd place in their field of study!

2019-2020 Lead Coordinator of 70th Anniversary Celebration Lyman T. Johnson Distinguished Speaker event: Workshop with Austin Channing Brown discussing the disconnect between franchised and disenfranchised communities, the implications that this has in academic settings, and how both communities can contribute to equity in professional (specifically academic) and social settings. Managed $12,000 account.

2019-2020 Lead Coordinator of monthly personal and professional Development Workshops: Informative dialogues with the Universities Graduate Student Congress representatives, the Office of Bias Incident Support Services, James W. Stuckert Career Center, and financial advisors, in an effort to support them in their desire to thrive during their matriculation in graduate/professional school.

2019-2020 Lead Coordinator of Monthly "Networking @ Nite" events: Initiative aimed at providing spaces where marginalized graduate and professional students could come together and network in a relaxed environment.

2019 Ronald McDonald House breakfast preparation for residents

2019 Lead Coordinator of University of Kentucky Graduate Student Congress' Mental Health Awareness Week Keynote address event: Dr. Della Mosley spoke to more than 50 UK faculty, staff and students about self-care strategies for students of color at historically white institutions.

2019 Host of University of Kentucky Graduate Student Congress' Emergency Town Hall Meeting to discuss HR.1044/S.386 "Fairness for High Skilled Immigrants Act of 2019" with the graduate, professional, and post-doctoral community.

2019 Participant in National Association of Graduate-Professional Students (NAGPS) Legislative Action Day to advocate, on behalf of graduate-professional students, to policy makers at the federal level.

2019 Hope Lodge dinner preparation volunteer

2019 4th Annual BioBonanza Volunteer

2019 Panelist: *I'm Not Your Token*; University of Kentucky Center for Graduate and Professional Diversity Initiatives

2019 Panelist: *Building Collaborative Relations*; University of Kentucky Graduate Student Life Summit

2018, 2019 Panelist: *Life as a black graduate student at a Predominantly White Institute*; University of Kentucky graduate school

2018 Minorities in Agriculture Natural Resources and Related Sciences (MANRRS) state competition Oral presentation judge

2017-2019 Summer Undergraduate Research Experience in Environmental Health Sciences (SURES) Near Peer Mentor

2013, 214 Sister's Network Inc. *Gift for Life* Block Walk and Health Fair

2011 Albany State University's Health career fair volunteer

2010 East Albany primary health center's annual health fare volunteer

2009-2010 Girls Inc. volunteer

2009 Albany, Georgia's Daddy Daughter dance volunteer

2006-2007 Helping Our Teen Girls In Real Life Situations (HOTGIRLS) Inc. member

National and International Memberships

2018 American Society for Biochemistry and Molecular Biology (ASBMB)

2018 American Association for Cancer Research (AACR)

2016 American Society for Pharmacology and Experimental Therapeutics (ASPET)

2016 American Physiological Society (APS)

2015 Honor Society of Phi Kappa Phi

2014 Beta Beta Beta National Biological Honor Society

Intramural Memberships

2018, 2019 Black Graduate and Professional Student Association (BGPSA); Secretary, President

2019 Graduate Student Congress; External Affairs Officer

2019 Women in Medicine and Science; Graduate Student Representative

2009-2011 HIV/AIDS Peer Educators; Assistant Secretary

2009-2010 Environmental Science Club; Recycling Committee Chair

2009-2010 Musically Unified Sister In Collaboration (M.U.S.I.C); Sergeant at Arms

2007-2010 Albany State University Marching Ram Show Band; Ms. Classic Touch of Gold